CAPILLARY CHARACTERISTICS IN MICROFLUIDIC EXPERIMENTS AND COMPUTATIONAL SIMULATION

by

Anusuya Das

B.S. E Bioengineering
Arizona State University, 2005

SUBMITTED TO THE DEPARTMENT OF BIOLOGICAL ENGINEERING IN PARTIAL FULFILLMENT OF THE REQUIREMENTS FOR THE DEGREE OF

DOCTOR OF PHILOSOPHY IN BIOLOGICAL ENGINEERING
AT THE
MASSACHUSETTS INSTITUTE OF TECHNOLOGY

FEBRUARY 2011

Signature of Author: _____

Department of Biological Engineering
September 30, 2010

Certified by: _____

Roger D. Kamm
Singapore Research Professor of Biological and Mechanical Engineering
Thesis Supervisor

Accepted by: _____

Dane Wittrup
Chairman, Department Committee on Graduate Students

Committee Members who voted in Favor of Thesis:

Advisor: Roger Kamm

Chair: Doug Lauffenburger

Other Member: Harry Asada

Other Member: Rakesh Jain

Capillary Characteristics in Microfluidic Experiments and Computational Simulation

by

Anusuya Das

Submitted to the Department of Biological Engineering
on September 30, 2010 in Partial Fulfillment of the
Requirements for the Degree of Doctor of Philosophy in
Biological Engineering

Abstract

Angiogenesis is crucial during many physiological processes, and is influenced by various biochemical and biomechanical factors. Models have proven useful in understanding the mechanisms of angiogenesis and the characteristics of the capillaries formed as part of the process. We have developed a 3D hybrid, agent-field model where individual cells are modeled as sprout-forming agents in a matrix field. Cell independence, cell-cell communication and stochastic cell response are integral parts of the model. The model simulations incorporate probabilities of an individual cell to transition into one of four states - quiescence, proliferation, migration and apoptosis. We demonstrate that several features such as continuous sprouts, cell clustering and branching that are observed in microfluidic experiments conducted under controlled conditions using few angiogenic factors can be reproduced by this model. We also identify the transition probabilities that result in specific sprout characteristics such as the length and number of continuous sprouts.

We have used microfluidics to study cell migration and capillary morphogenesis. The experiments were conducted under different concentrations of VEGF and Ang I. We demonstrated that capillaries with distinct characteristics can be grown under different media conditions and that characteristics can be altered by changing these conditions. A two-channel microfluidic device fabricated in PDMS was used for all experiments. The rationale underlying the design of the experiments was twofold: the first goal was to generate reproducible and physiologically relevant results in a microfluidic device, and the second goal was to quantify the capillary characteristics and use them to estimate the transition parameters of the model. We developed stable, well-maintained sprouts by using human microvascular endothelial cells in 2.5 mg/ml dense collagen I gel and by using media supplemented with 40 ng/ml VEGF and 500 ng/ml Ang 1 for two days. It has been shown in many studies that VEGF acts as an angiogenic factor and Ang 1 acts as stabilizing factor. Here we showed that their roles are maintained in the 3D microenvironment, and the sprout characteristics obtained by using this baseline condition could be altered by changing the concentrations of these two growth factors in a systematic way.

Sprout and cell characteristics obtained in the experiments and simulations were analyzed by adapting Decision Tree Analysis. This methodology provides us with a useful tool for discerning the impact of different growth factors on the process of cell migration or proliferation as they alter general sprout morphology. The imprints obtained via experiments and simulations were compared; by choosing appropriate values of the transition probabilities, the model generates capillary characteristics similar to those seen in experiments ($R^2 \sim 0.82$- 0.99). Thus, this model

can be used to cluster sprout morphology as a function of various influencing factors and, within bounds, predict if a certain growth factor will affect migration or proliferation as it impacts sprout morphology. This was demonstrated in the case of anti-angiogenic agent, PF4. We showed that at high concentration of PF4 (~ 1000 ng/ ml), the transition to migration is more profoundly affected while at low concentrations of ~ 10 ng/ ml, PF4 does not have much of an effect on either migration or proliferation.

Thesis Supervisor: Roger D. Kamm
Title: Singapore Research Professor of Biological and Mechanical Engineering

Table of Contents

Dedication

I dedicate this thesis to my parents, Niharika Das and Dr. Bani Prasad Das. Thanks for your all your love and support though the years.

Acknowledgements

First, I would like to thank MIT biological engineering for giving me the opportunity to pursue research in a very collaborative and supportive environment. I am especially grateful to Prof. Roger Kamm for accepting me in his lab, and for providing me with intellectual and financial support. It has been an absolute pleasure to work with him. I would like to thank all my committee members- Prof. Doug Lauffenburger, Prof. Harry Asada and Prof. Rakesh Jain for giving me valuable guidance and setting aside time for all the one on one and committee meetings.

Second, I would like to thank my funding sources: Medtronic first year support, NSF- EFRI and the Singapore-MIT Alliance for Research and Development.

Third, I would like to thank all Kamm lab members, past and present for providing a helpful and encouraging environment. I also want to acknowledge all my friends who have been there through all the trials and tribulations and helped me through the last five years. I would especially like to thank some friends- Nate, Bahar and Andrea. They have been there through all the difficult and good times over the last five years.

Finally and most importantly, I am forever indebted to my relatives and especially my immediate family. I would like to thank Anjan, who came into my life a couple of years ago and was a continuous source of calm and support. I would like to thank my sister, Arundhati, who has been a constant sounding board for me over the last years. Most importantly, my sincere and heartfelt gratitude goes to my parents who have gone through a lot of struggles to send me to the US at the age of seventeen. They supported me through my entire education financially and emotionally. This would not have been possible without their unyielding faith and never ending encouragements

1. Background

i. Angiogenesis: The Process

Angiogenesis is the formation of new blood vessels from a monolayer of cells or by the reorganization of capillaries via morphogenesis. It is crucial during development, healing, and for physiologic processes such as menstrual cycles and reproduction. Two other cases are of particular interest. First, angiogenesis occurs during invasive tumor growth because of the additional nourishment required by the tumor. Second, it is essential for tissue engineering purposes because it is necessary to be able to predict and control capillary development in scaffolds during *in vitro* tissue development. The primary stages of angiogenesis can be categorized as:

(a) endothelial cell activation by chemotactic agents,

(b) secretion of proteases into the matrix,

(c) selection of endothelial cells for sprouting,

(d) capillary growth,

(e) tubulogenesis,

(f) non-angiogenic growth of blood vessels via capillary loop formation and

(g) formation of second generation capillaries (Adams et al., 2007; Figure 1).

ii. Influencing Factors

The process of angiogenesis is regulated by a balance between several pro-angiogenic and anti-angiogenic factors. Over the years, numerous factors - VEGF, PLGF, PDGF, TNFα, TGFβ, α-FGF, β-FGF, ENA/VASP (Folkman and Shing, 1992), Angiopoietin-1 (Ang 1), Angiopoietin-2 (Ang 2) (Davis et. al., 1996) and chemokines like PF4 (Slungaard, 2005) have been shown to

influence the process. Additionally, it has also been demonstrated that mechanical factors such as flow, extra-cellular matrix (ECM) stiffness, and surface shear stress each affects the extent and directionality of capillary formation. Helm et al. (2005) showed that interstitial flow on the order of one micron per second in combination with VEGF induced directionality in capillary structures (in the direction of flow) and caused fibrin-bound VEGF to be released via proteolysis. Yamamura et al. (2007) studied the effect of substrate stiffness on bovine pulmonary microvascular endothelial cells (BPMECs). They demonstrated that BPMECs cultured on flexible collagen gels form networks in three days and show extensive sprouting and formation of complex networks in five days, whereas the cells cultured on stiffer gels tend to form aggregates and thicker networks.

Various matrix and non-matrix derived factors act either as promoters or as inhibitors for angiogenesis. Two such factors: Vascular Endothelial Growth Factor (VEGF) and Angiopoietin-1 (Ang 1) are considered here. VEGF is a hypoxia-inducible 38-46 kDa glycoprotein that is a ligand for EC specific tyrosine kinase receptors Vascular Endothelial Growth Factor Receptor-1 (VEGFR-1/ Flt-1) and Vascular Endothelial Growth Factor Receptor-2 (VEGFR-2/ Flk-1). It functions as a potent permeability-inducing agent, EC chemotactic agent, EC proliferative factor and an anti-apoptotic signal (Brekken & Thorpe, 2001). VEGFA is the most common isoform of the ligand and has an affinity for VEGFR1 that is about an order of magnitude higher than that for VEGFR2. But the tyrosine kinase activity of VEGFR1 is relatively weaker.

Ang 1 stabilizes newly formed vessels and has been identified as the primary activating ligand to Tie2 receptor which is also an EC specific receptor tyrosine kinase. It is constitutively expressed

and undergoes auto-phosphorylation, activating many intracellular pathways leading to endothelial cell migration (Witzenbichler et al., 1998; Jones et al., 1999), tube formation (Hayes et al., 1999; Teichert-Kuliszewska et al., 2001), sprouting (Koblizek et al., 1998) and survival (Kwak et al., 1999; Jones et al., 1999). Some studies have shown that Ang 2 does not activate Tie2 and competitively inhibits Ang I activity, while others have demonstrated that the binding of Ang 2 to Tie2 results in receptor activation (Bogdanovic, et al., 2006). Thus, Ang II is a natural antagonist of Ang 1 and is also a ligand for Tie 2 receptor. It is expressed only at the site of vascular remodeling and is responsible for the destabilization of the vasculature. Both Ang 1 and Ang 2 are known to activate Tie2 in a concentration-dependent manner (Boglanovic et. al., 1999). It was decided to incorporate two pro-angiogenic factors: VEGF and Ang 1 in the first stage of the modeling-to-experiment cross talk. It has also been shown that Ang 1 has an impact on VEGF signaling irrespective of the presence or absence of Ang 2 (Zhu et. al., 2002).

The activation of several signaling pathways downstream from VEGFR-2 mediates cell proliferation and migration. One classical pathway activated is the Ras-dependent signaling cascade. Grb-2 is recruited by VEGFR-2 either by direct interaction or via association with adaptor protein Shc. Phosphorylation of VEGFR-2 leads to the activation of Ras and stimulation of the Raf1/MEK/ERK signaling cascade (Cebe-Suarez et al., 2006). p-ERK, which is activated by many growth factors and is involved in the MAPK pathway, plays an important role in both cell migration and proliferation. p-FAK is required for integrin regulation of the cell cycle and thus plays an important role in mediating the effect of mechanical stresses on the cell. p-PLCγ is important for cell migration and affects the cell membrane dynamics. Hernández Vera et al., (2009) have shown that although the rate of capillary formation and the extent of branching is a

function of the interstitial flow to which the endothelial monolayer is exposed during *in vitro* experiments, the number of capillaries remains constant and the initiation of capillary morphogenesis occurs only in regions of extensive Src phosphorylation. These regions are inherent to the endothelial monolayer itself. However, experiments in our lab have demonstrated that capillary morphogenesis is sheet-like in a softer matrix, while it is sprout-like in stiffer gels. Thus, it is possible that certain mechanical cues may activate some other signaling cascades, causing the difference in capillary morphogenesis.

iii. Motivation

A few decades ago angiogenesis was described as the fourth tenet of cancer treatment after surgery, chemotherapy and radiotherapy. Since then, a lot research has been focused on understanding this process in that context. Its importance in the realm of tissue engineering, while relatively unexplored is equally important. It is crucial to understand and control vessel formation in order to develop artificial organ and bio-machines. The motivation underlying this project is to gain a better understanding of the impact of specific angiogenic and anti-angiogenic factors on the sub-processes of angiogenesis with the goal of implementing the knowledge obtained. To this end, we use a combination of modeling and experimental approaches that will detailed in the following chapters.

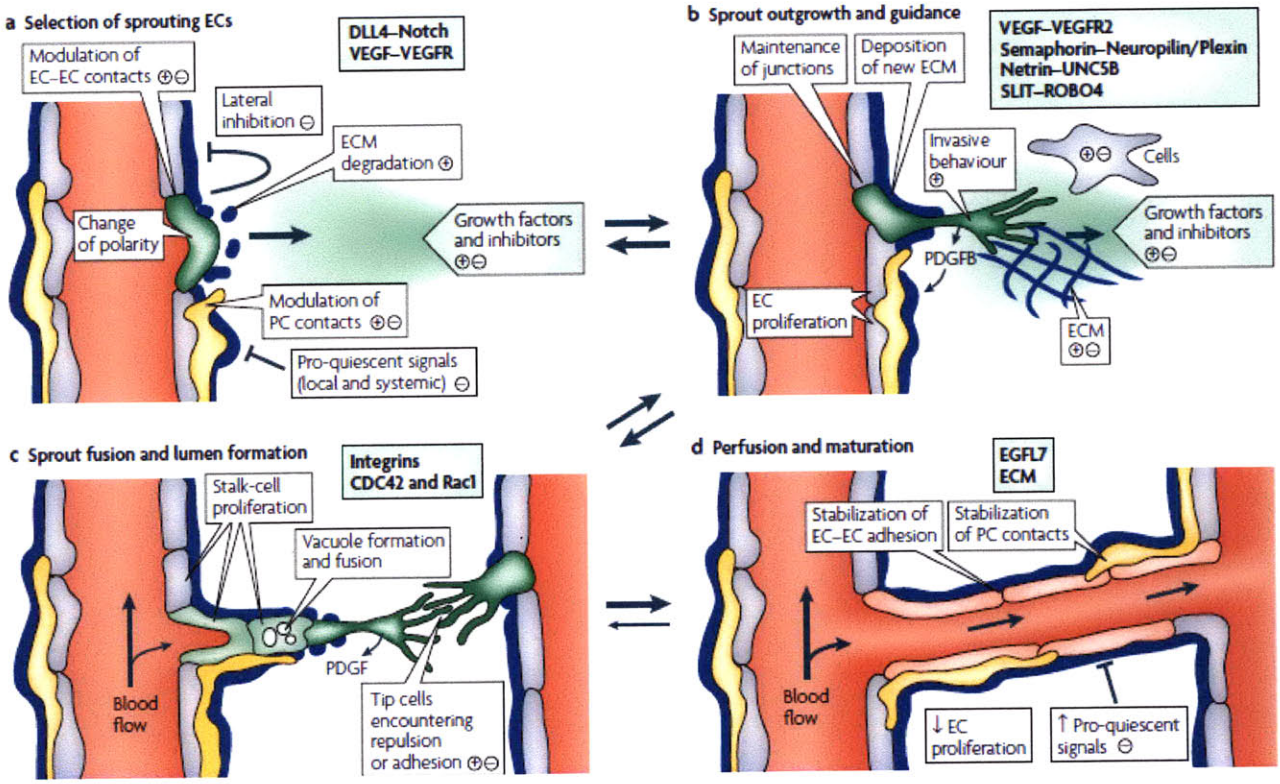

Figure 1: Stages of Angiogenesis (Adams and Alitalo; 2007)

2. Hybrid Continuum-Discrete Model of Angiogenesis

i. Rationale

Computational models and simulations provide meaningful insights into biological processes. There are especially useful in identifying specific mechanistic effects of biological agents and enable a more controlled study or application of the process under consideration. Over the years, mathematical and computational modeling has grown to play an integral role in biology and medicine. As one of the tenets of biological engineering, it is a tool that can be exploited to develop better understanding of many important processes.

ii. Angiogenesis Models

Angiogenesis modeling is a useful tool for understanding the interplay between all the factors that affect it and for the design of experiments of a predictive nature. Over the years various models spanning different scales and focusing on different aspects of angiogenesis have been developed. These can be classified as continuum models (Anderson and Chaplain, 1998; Chaplain et al., 2004; Chaplain et al., 2006; Chaturvedi et al., 2005; Dallon et al., 1997; Levine et al., 2000), and discrete models (Anderson et al., 1998; Chaplain et al., 2006; Stokes et al., 1991; Mantzaris et al., 2004). Some of the model results are shown in figure 2.

The continuum models are based on conservation equations for chemotactic and haptotactic gradients. In one such continuum model the Chaplain group models a 'tissue response unit', which includes an endothelial cell (EC), tumor angiogenic factor (TAF) and a generic matrix molecule. The numerical solution is obtained from a finite difference approximation subject to no flux boundary conditions and a specified initial condition. They have also developed a

discretized version of the continuum model where the motion of the capillary in response to a tumor is governed by the EC at the tip (Anderson and Chaplain, 1998).

The Cellular Potts Model (CPM) is a lattice-based model developed to describe the behavior of cellular structures and their interactions. It could be an agent-based model, which is a computational model that is based on one (or more) specific component(s) and its effect on the individual cells (agents) being modeled. A 2D agent-based model of angiogenesis based on CPM has been developed by Pierce et al. (2004), where they identify multiple cell types and growth factors. Their cell-level rule-based model of network growth in mesenteric tissue predicts new vessel formation, vessel length extensions and recruitment of contractile perivascular cells in response to localized pressure, circumferential strain and focal application of growth factor. The Sherratt group has used an extension of the Potts model to simulate malignant cells and quantified invasion morphology as a function of cell-cell adhesion (Turner and Sherratt, 2002; Figure 3). In a different approach, the Popel group has developed a multi-scale integrative model with specific modules for various growth factor receptor pairs and ECM proteolysis (Qutub et al., 2009). Their model considers oxygen delivery by hemoglobin-based oxygen carriers (Tsoukias et al., 2007), the cellular response to oxygen in skeletal muscles (Ji et al., 2006) and a cell based model which results in angiogenesis via reorganization of existing capillaries (Qutub and Popel, 2009). Other models include a Random Walk Model (Plank and Sleeman, 2004), which is distinguished by the fact that it places no restrictions on the direction of capillary growth, an individual cell-based 2D mathematical model of tumor angiogenesis in response to a diffusible angiogenic factor (Plank and Sleeman, 2004), and a fractal-based model in which the smaller pieces of the system show 'statistical self similarity' to the whole and the anatomical

entities are given a fractal dimension. Random walk models that incorporate biochemical cascades when VEGF binding occurs have also been developed (Levin et al., 2002). Physiological models, for instance a model of corneal angiogenesis, have also been developed. Jackson and Zheng (2010; figure 4) have developed one such model that integrates a mechanical model of elongation with a biochemical model of cell phenotype variation. Despite the wide variety in modeling approach, most of the models focus on tumor angiogenesis instead of *in vitro* capillary growth, and may lack one of the following: stochasticity, a 3D framework or simplified binding kinetics, and are therefore difficult to apply in practice for tissue engineering applications. A combination of these characteristics in a model used for tissue engineering applications would be very useful. Finally, model validation in many of the existing models is a challenge due to the difficulty in controlling all important factors *in vivo* combined with limited capability of most *in vitro* systems to replicate angiogenesis.

The complex biological processes leading to capillary morphogenesis are a consequence of cell-level decisions that are based on global broadcast signals, limited near-neighbor communication, and stochastic decision-making with feedback control. Integrating these factors, a cell becomes programmed to follow one of several state trajectories that could be characterized as quiescence, division, apoptosis or migration. We have developed a model to address the needs for greater understanding of the process and for a practical tool with predictive capabilities.

iii. Proposed Model Framework

This is a 3D coarse-grained multi-scale hybrid model in which each cell is modeled as an individual decision-making entity and cell-cell interactions are incorporated via the combined

effect of cells on the matrix and the effect of the surrounding matrix in the individual cell decision-making process. Thus, this model demonstrates the phenomenon that when individual cells are modeled independently according to a set of rules and when cell-cell communication is embedded, the cell ensemble results in capillaries with features that can be attained experimentally in bioreactors for controlled tissue engineering purposes. It also provides a platform for bracketing these cell ensemble results into clusters with different sprout characteristics and identifying the factors that affect them. Most importantly, this study presents a model framework designed alongside experimental constraints and one that can simulate capillaries like the ones generated in an *in vitro* microfluidic system. This model-experiment cross talk is crucial in identifying the effect of individual influential factors on angiogenesis.

A major driving force in this model is its usefulness in predicting the angiogenic response in a closely regulated experimental platform, with the objective of providing validation and of implementing feedback control over a prototypical biological process. One such experimental platform is the microfluidic system recently developed by our group (Vickerman et al., 2008). The first step in analyzing model predictions is to identify a set of relevant sprout characteristics that would be useful in measuring the effect of different conditions and that could be easily measured in real time during an experiment. These features are then compared to the simulation results.

The model is discrete and can be divided into two distinct parts or modules; one is stochastic and the other is deterministic. These modules communicate with each other to predict capillary formation as a function of the local microenvironment, including the effects of growth factors

and matrix properties. This interplay is depicted in Figure 5. This is a 3D lattice model based on Markov processes, where at any time point each lattice point can be occupied by a cell, the matrix or remain empty. A cell can be in one of three states: quiescent, migrating or proliferating. It can also undergo apoptosis, at which point that lattice point becomes empty. Every lattice point that is occupied by matrix is referred to as the 'field' and has associated with it concentrations of the various growth factors and matrix properties. In its current form, the model only includes VEGF, Ang 1 and MMP concentrations and matrix stiffness. However, this can be easily extended to include any number of growth factors and is modular in nature. Capillary features successfully depicted in this 3D model are continuous sprouts, secondary and tertiary branches, and cell clusters – all of which are observed in experiments. 3D modeling enables capillary surface area and protrusion volume calculations in the simulations and their comparison to experiments conducted in microfluidic devices. It also enables the proper representation of the factors in the surrounding matrix and their effects on individual cell responses. The deterministic component of the model includes the diffusion-convection-reaction equations that govern these growth factor concentrations.

A cell can exist in four main states: Migrating (M), Proliferating (P), Quiescent (Q) and Apoptotic (A). Its transition between states is depicted in Figure 6. Once it undergoes transition to either a migratory or proliferating state, it subsequently passes through a series of sub-states. The number of these sub-states is determined by the time of persistence of migration and the average cell cycle of an individual cell, thereby enabling us to account for differences in the time scales of these processes. Consequently, if a cell can exist in 'm' migratory sub-states and 'p' dividing sub-states, a transition probability matrix is established. Transition probabilities,

e.g., $p_{Q\to Q}$, $p_{Q\to M(1)}$, $p_{Q\to P(1)}$, $p_{Q\to A}$ where *M(1)* and *P(1)* are the first steps of the respective processes, depend on the global (g) and local (l) conditions such as growth factor concentration and matrix properties in a manner described below.

The transition of each cell from one state at time t to another at time $t+\Delta t$ is stochastic and is a function of its current state, the condition of the surrounding matrix and external governing factors such as the presence or absence of flow, the growth factors present in neighboring matrix and initial matrix stiffness. That is, transition from state X^t to $X^{t+\Delta t}$ is described as $X^{t+\Delta t} = f(X^t, U^t(g), U^t(l))$, where $U^t(g)$ are the global or external factors and $U^t(l)$ are the local factors or the characteristic of the surrounding matrix and measured by the output Y^t. Certain variables like growth factor concentrations only affect the local environment while other factors like flow and pressure gradients have a global effect. The difference being, in the case of global influence, the same function is applied at all spatial locations, while in the case of local variables, the changes are calculated at each lattice point. This function is represented in the model as a transition probability.

iv. Model Characteristics

a) Assumptions

Some of the basic assumptions underlying the model are:

1. A Hidden Markov Model is applicable to cell decision processes in angiogenesis.
2. Cells can be modeled as independent Markov processes: The cell state at time t+Δt is independent of its states prior to the one at time t. This is reflective of the assumption that

cell state effects are additive and whatever the cell underwent in prior states has affected its outcome in the penultimate state.

3. A four state transition matrix provides enough information for process evolution: The states used in this model are quiescence, migration, proliferation and apoptosis. It is assumed that these are the most relevant transitions that cells undergo as they form capillaries. Future experiments might support or negate this assumption. It is possible that some other cell state may be important to gain a complete understanding of the process, however, the use of these four states certainly provides enough information to obtain valuable insights.
4. The states of a cell are independent of each other: A cell can either be in migratory or proliferative states. It is also assumed that certain growth factors can independently impact a cell's decision to transition either into proliferation or migration.

b) Stability

The time step ($t+\Delta t$) for the numerical solution of the diffusion equations is equal to 0.1 second in order to preserve stability of the solution as the equations are calculated explicitly. In order to determine the effect of the size of the time step on the accuracy of the numerical solution of the diffusion equations, we decided to run the simulations by reducing Δt to half the time. After 20 hours, at any given lattice point the concentration of soluble VEGF (C_{vegf_s}) differed by less than 0.03%.

c) Sampling Frequency

The sampling frequency of the 'cellular' time step is the frequency with which the cell is allowed to change its step. It should be noted that once a cell decides to go into the migrating or proliferating state, it remains in that state for different lengths of time. It was decided to select a 'cellular' time step of one hour for two primary reasons. A) Initially, this code was designed to make it compatible with time lapse imaging and one hour was the lowest limit of the frequency with which live imaging could be done without dire photo-bleaching effects. B) This is shorter than the time scale of events (migration / cell division) occurring. In order to determine the effect of the size of the 'cellular' time step on the accuracy of the concentrations being calculated, we decided to run the simulations by reducing the time by half. Cells were allowed to make decisions every 30 minutes instead of every hour. When making these comparisons, the number of time steps during which a cell stayed in the migrating / proliferating stage were modified accordingly. At any given lattice point the concentration of soluble VEGF (C_{vegf_s}) differed by an average of 0.78% near sprouts of similar lengths.

v. Field Equations

The field equations in this model are presented below and can be simplified when required to provide feedback control. The field equations are written in this instance to include one growth factor, VEGF, and one protease, MMP. Similar equations for other factors can be easily incorporated. C_{vegf_s}, C_{vegf_b}, C_{vegf_r}, C_{MMP}, M and M_{cl} are the concentrations of soluble VEGF, VEGF bound to matrix, VEGF bound to receptor, MMP, matrix binding sites available for binding to MMP and cleaved matrix, respectively.

The following governing equations describe C_{vegf_s}, C_{vegf_b}, C_{MMP} and M, where D_{vegf} is the diffusion coefficient of soluble VEGF, D_{MMP} is the diffusion coefficient of MMP, and v is the interstitial flow velocity causing convective transport of VEGF. k_{on_m} and k_{off_m} are the binding constants for the reaction between soluble VEGF and binding motifs in the matrix. k_{on_c} and k_{off_c} are the binding constants for the reaction between soluble VEGF and VEGF receptors on the endothelial cells. ϕ is the density of cells and C_{vegf_rec} is the number of VEGF receptors per unit volume, equal to the number of receptors on a single cell times ϕ. Pr_{vegf} and Pr_{MMP} are the rate of production of VEGF and MMP by a single cell, respectively. ϕ will be set equal to one for those grid points containing a cell (since we assume here a density of one cell per unit volume), and $\phi = 0$ for matrix. k_{c_m} is the rate at which the matrix is cleaved by MMP.

The kinetic reactions for the VEGF, MMP and matrix binding sites (M) are:

$$C_{vegf\_s} + C_{vegf\_r} \square \quad C_{vegf\_r} \tag{1}$$

rate constants- k_{on_c} and k_{off_c}

$$\varphi \rightarrow C_{MMP} \tag{2}$$

production rate- Pr_{MMP}

$$C_{MMP} M \rightarrow M_{cl} \tag{3}$$

rate constant- k_{c_m}

The governing conservation equations are those for soluble VEGF:

$$\frac{\partial C_{vegf\_s}}{\partial t} = -\vec{v} \cdot \nabla C_{vegf\_s} + D_{vegf} \nabla^2 C_{vegf\_s} + R_{vegf\_s}, \tag{4}$$

where

$$R_{vegf\_s} = -k_{on\_m} C_{vegf\_s} M + k_{off\_m} C_{vegf\_b} - k_{on\_c} C_{vegf\_s} C_{vegf\_rec} + k_{off\_c} C_{vegf\_r} + \mathrm{Pr}_{vegf}\, \phi$$

for bound VEGF:

$$\frac{\partial C_{vegf\_b}}{\partial t} = R_{vegf\_b} \tag{5}$$

where

$$R_{vegf\_b} = k_{on\_m} C_{vegf\_s} M - k_{off\_m} C_{vegf\_b} - k_{c\_m} C_{MMP} V_{vegf\_b}$$

for MMP:

$$\frac{\partial C_{MMP}}{\partial t} = -\vec{v}.\nabla C_{MMP} + D_{MMP} \nabla^2 C_{MMP} + R_{MMP} \tag{6}$$

where

$$R_{MMP} = \mathrm{Pr}_{MMP}\, \varphi$$

and for the concentration of matrix binding sites:

$$\frac{\partial M}{\partial t} = R_M \tag{7}$$

where

$$R_M = -k_{c\_m} C_{MMP} M$$

Assuming local chemical equilibrium, and given the fact that VEGF (VEGF-165 Isoform) binding to the matrix (collagen I) at pH 7.4 is negligible (Adrienne et al., 2004), the equations simplify further. Also, there is no convective transport due to interstitial flow, but this can be added to the model easily.

The first two equations are simplified as follows:

$$\frac{\partial C_{vegf\_s}}{\partial t} = D_{vegf} \nabla^2 C_{vegf\_s} + R_{vegf\_s} \tag{8}$$

where

$$R_{vegf\_s} = -k_{on\_c} C_{vegf\_s} C_{vegf\_rec} + k_{off\_c} C_{vegf\_r} + \mathrm{Pr}_{vegf} \phi$$

and

$$\frac{\partial C_{vegf\_b}}{\partial t} \sim 0 \tag{9}$$

These equations are discretized and used in instances where all the parameters are known. While most have been experimentally derived, some of the parameter values would still be subject to considerable uncertainty. In those cases, an approximation was made.

The diffusion term in equations (8) is discretized spatially as follows:

$$\begin{aligned}(D_{vegf}\nabla^2 C_{vegf\_s})_{x,y,z,t} = D_{vegf} * [(C_{vegf\_s})_{x,y,z+1,t} - 2*(C_{vegf\_s})_{x,y,z,t} + (C_{vegf\_s})_{x,y,z-1,t}]/[\Delta z^2] + \\ D_{vegf} * [(C_{vegf\_s})_{x+1,y,z,t} - 2*(C_{vegf\_s})_{x,y,z,t} + (C_{vegf\_s})_{x-1,y,z,t}]/[\Delta x^2] + \\ D_{vegf} * [(C_{vegf\_s})_{x,y+1,z,t} - 2*(C_{vegf\_s})_{x,y,z,t} + (C_{vegf\_s})_{x,y-1,z,t}]/[\Delta y^2]\end{aligned} \tag{10}$$

where Δx, Δy and Δz are the spacings of the computational grid in x, y, and z, respectively, and are equal to 10 μm.

The diffusion term in equation (6) is discretized similarly.

For the reaction terms, the following methodology is used. The concentration of the biomolecules being modeled will locally change in a single time step by an amount that is dictated by local conditions. This change in the concentration is a sum of the local consumption and production of that molecule and expressed as:

$$R = \Delta C_{i,P,j} - \Delta C_{i,C,j} \tag{11}$$

and where

$$\Delta C_{i,C,j} = (C_{i,C,j})_{t+\Delta t} - (C_{i,C,j})_t$$
$$\Delta C_{i,P,j} = (C_{i,P,j})_{t+\Delta t} - (C_{i,P,j})_t$$

These could potentially be experimentally determined by measuring changes in concentration of signaling molecules, MMP and matrix around a single cell. This can be done by using fluorescent collagen and measuring the matrix properties around individual cells. However, as such experimental data for individual cells are not available, these ΔC values can be empirically established relative to the rates of production and degradation of these substances by quantifying the qualitative effects on individual cells. When those are being ascertained, $\Delta C_{i,Cj}$ and $\Delta C_{i,Pj}$ represent step functions associated with this change at the j^{th} level in the concentration of the i^{th} biomolecule included in the model due to consumption and production by the cells, respectively. In the simulation results included in this study, we have used a two-level change for the biomolecules being considered, i.e. high production/consumption or low production/consumption. These changes depend on the cell state and the surrounding matrix characteristics. One can imagine that instead of having only a high and low value (e.g., where j = 1 or 2) for each of these reactions, we can have finer increments where each element is dependent on the different permutations and combinations of other factors in the field. The existing model framework allows for such expansion depending on the different pro- and anti-angiogenic factors being considered.

The equations are discretized over time and the spatial derivatives are calculated at time t. Equation (8) is discretized as:

$$\frac{\Delta(C_{vegf\_s})_{x,y,z}}{\Delta t} = D_{vegf}\nabla^2 C_{vegf\_s} + (R_{vegf\_s})_{x,y,z} \quad (12)$$

where

$$(R_{vegf\_s})_{x,y,z} = \Delta C_{vegf\_s,P,j} - \Delta C_{vegf\_s,C,j}$$

and where

$$\Delta C_{vegf\_s,C,j} = (C_{vegf\_s,C,j})_{t+\Delta t} - (C_{vegf\_s,C,j})_t$$
$$\Delta C_{vegf\_s,P,j} = (C_{vegf\_s,P,j})_{t+\Delta t} - (C_{vegf\_s,P,j})_t$$

At a time t, the amount of VEGF produced and consumed via binding to the cells is a function of the cell state and the state of the surrounding matrix concentration of soluble VEGF, i.e. C_{vegf_s} in the lattice. Thus, the reaction terms are evaluated based on the cell state. k_{on_c} and k_{off_c} values were obtained from literature (Gabhann and Popel, 2007). Hence, the amount of VEGF consumed ($\Delta C_{vegf\_s,C,i}$) is determined by the rate equation. However, as it is difficult to obtain the amount of VEGF produced by an individual cell, it was approximated by the following method. If there is a migrating cell at a given lattice point, we assume it produces a certain amount of VEGF ($\Delta C_{vegf\_s,P,1}$) if the surrounding VEGF concentration is below a certain threshold and a different amount ($\Delta C_{vegf\_s,P,2}$) when it is above a threshold. This threshold of the surrounding VEGF is 12 units (or 24 ng/ml normalized to the minimum concentration of VEGF i.e. 2 ng/ml). This was chosen because it has been shown that VEGF induces its own expression

in microvascular endothelial cells in a STAT3-dependent fashion when the cells are treated with 25 ng/ml VEGF (Bartoli et al., 2003).

Assuming negligible interstitial flow, equation (6) is discretized as:

$$\frac{\Delta(C_{MMP})_{x,y,z}}{\Delta t} = D_{MMP}\nabla^2 C_{MMP} + (R_{MMP})_{x,y,z} \tag{13}$$

The change in MMP concentration due to production in equation (13) was approximated by assuming that the change around a migrating cell ($\Delta C_{MMP,P,1}$) and that around a quiescent or proliferating cell ($\Delta C_{MMP,P,2}$) are different.

Equation (7) is discretized as:

$$\frac{\Delta(C_M)_{x,y,z}}{\Delta t} = (R_M)_{x,y,z} \tag{14}$$

The value of k_{c_m} is obtained from literature (Karagiannis and Popel, 2004). The amount of matrix consumed $\Delta C_{M,C,i}$ is determined by the rate equation and the state of the cell, as a migrating cell tends to release more MMP that cleaves the matrix.

The field also includes a stabilizing agent i.e. Ang 1. Ang 1 acts on the Tie-2 receptor in endothelial cells and the range of effective activity on Tie-2 receptor has been shown to be 80ng/ml – 800ng/ml [Bogdanovic *et al.,* 2006]. Several reports document robust Tie-2 phosphorylation at greater than 100 ng/ml concentrations [Kim *et al.,* 2000; Papapetropoulos *et*

al., 2000; Du *et al.,* 2000]. Ang-1 inhibits endothelial cell apoptosis through several pathways, which include PI-3 kinase/AKT activation, inhibition of Smac release from the mitochondria, and upregulation of Survivin protein [Harfouche *et al.,* 2002]. Thus, the graded stabilizing effect of Ang 1 is included in the model. This is discretized and included as an effect on cell connectivity and discussed in section vi.

vi. Cell Transitions

The transition probability of a cell from one state to another is dependent on the initial conditions, such as growth factor concentrations in the medium and matrix stiffness. Cell decisions are made once every hour or every 'cellular' time step. Thus, during each hour, a certain number of cells migrate, proliferate, become quiescent and die. These probabilities are empirically derived. We have explored the range of probabilities and identified combinations that depict sprout characteristics seen under certain experimental conditions. The transitional probability to a particular state at time $t+1$ can be written as:

$$p_{M,t+1} = p_{Q,t} \cdot p_{Q \to M,t} + p_{M,1,t} + \ldots + p_{M,m-1,t} - p_{M,m,t}$$

$$= p_{Q,t} \cdot p_{Q \to M,t} + p_{M,t} - p_{M,m,t} \qquad (15)$$

$$p_{Q,t+1} = p_{Q,t} \cdot p_{Q \to Q,t} + p_{M_m,t} + p_{Pp,t} - p_{Q,t} \cdot p_{Q \to M} - p_{Q,t} \cdot p_{Q \to P} - p_{Q \to A,t} \qquad (16)$$

$$p_{P,t+1} = p_{Q,t} \cdot p_{Q \to P,t} + p_{P,1,t} + \ldots + p_{P,p-1,t} - p_{P,p,t}$$

$$= p_{Q,t} \cdot p_{Q \to P,t} + p_{P,t} - p_{P,p,t} \tag{17}$$

$$p_{A,t+1} = p_{Q,t} \cdot p_{Q \to A,t} \tag{18}$$

where $p_{M,t+1}$, $p_{Q,t+1}$, $p_{P,t+1}$ and $p_{A,t+1}$ are the probabilities that the cell state at time t+1 becomes M, Q, P or A respectively.

$p_{Q,t}$, $p_{M_m,t}$ and $p_{Pp,t}$ are the probabilities defined as:

$$p_{Q,t} = p(X_t = Q) \tag{19}$$

$$p_{M,t} = \sum_{i=1}^{m} p_{Mi,t} \tag{20}$$

$$p_{P,t} = \sum_{i=1}^{p} p_{Pi,t} \tag{21}$$

and $p_{Q \to M,t}$, $p_{Q \to Q,t}$, $p_{Q \to P,t}$ and $p_{Q \to A,t}$ are the transition probabilities to migration, quiescence, proliferation and apoptosis, respectively, under the instantaneous global and local conditions. These are expressed as a probability distribution of percentages of transition (equations 22-25). These probabilities are to be experimentally determined. Alternatively, they could be specified functions of the activation of relevant intracellular signaling pathways.

$$p_{Q \to M,t} = p(X_{t+1} = M \mid X_t = Q) \tag{22}$$

$$p_{Q \to Q,t} = p(X_{t+1} = Q \mid X_t = Q) \tag{23}$$

$$p_{Q \to P,t} = p(X_{t+1} = P \mid X_t = Q) \tag{24}$$

$$p_{Q \to A,t} = p(X_{t+1} = A \mid X_t = Q) \tag{25}$$

vii. Cell Communication

Cell communication is achieved via the cell-cell connectivity factor, MMP release and lateral inhibition.

a. Cell- cell connectivity

Cell- cell connectivity is maintained under two different scenarios:

1. During individual cell migration: as a cell cannot change shape in this model, a temporary or 'temp' cell is used during cell migration to ensure connectivity and remove any bias during lattice evaluation. This ensures that the impact of transition will not affect other cells in the same time step. When a cell migrates from one lattice point to another, its former location is identified as a 'temp' position and for the remainder of that time step the cell occupies both locations.

2. During sprout formation because of cell adhesion and stabilization: to incorporate cell adhesion and stabilization, cell connectivity between two cells is enforced as a field function that is dependent on the states of the two cells being considered and the local field conditions. All cell-cell communication occurs via the field, i.e. the surrounding matrix. Direct cell-cell interactions were avoided to support the independence of each cell. Otherwise, the model would have to deal with joint probabilities of multiple cells, which are quite complex. On the other hand, by making this assumption, we are still ensuring that the essence of cell-cell interactions is included while minimizing model complexity. This is done by a field variable termed the 'connectivity factor'. Anything the cell 'gives' or 'receives' from a nearby cell is done via this field-associated factor.

The local Ang I concentration is directly proportional to the cell connectivity. The probability of a cell to break away and migrate individually is inversely proportional to the connectivity factor.

The connectivity factor is a discrete number that is dependent on cell states and neighboring Ang I concentration. It is classified into three scales: low, medium, high.

The connectivity rules are as follow:

- If a cell is quiescent, the connectivity factor increases by 2, if it is dividing, it increases by 1 and if is migrating, it increases by 3.
- The average Ang 1 concentration, $Ang1_{average}$ is defined as

$$Ang1_{average} = \sum_{i=1}^{14} [Ang1]_i / 14$$

where i =1…14 are all the neighboring lattice points

If the average concentration is below 100 $ngml^{-1}$, the connectivity factor increases by 1; if it is between 100 $ngml^{-1}$ to 500 $ngml^{-1}$, the connectivity factor increases by 2; and, if the average concentration in greater than 500 $ngml^{-1}$, it increases by 3.

The connectivity factor has an impact on the time steps the cell tends to stay in the migratory state. Though the default is three time steps, a connectivity factor of 5 or 6 keeps it in that sub-state for a longer time, and a connectivity factor of less that three makes it evaluate its state sooner. It also impacts cell adhesion in the following way. If a cell adjacent to a migrating cell has a relatively low connectivity factor compared to that of its neighbor, it will tend to stay quiescent, resulting in capillary breakage or individual migrating cells.

b. MMP Release:

The other tool for cell communication is the release of MMP into the field. The surrounding MMP concentration affects the directionality of migration for neighboring cells. Thus, an individual cell has an impact on its neighbors. It is possible to increase the impact of this tool by involving other molecules released by cells in addition to MMP. Figure 7 demonstrates the effect of migrating cells on the matrix via the MMPs as a change in their concentrations is observed in the region surrounding a developed sprout.

c. Lateral Inhibition:

DL4/ Notch signaling: An important aspect of angiogenesis is lateral inhibition, which is enforced via DL4/ Notch signaling. In order to include this characteristic of the process, cell communication is very important. When a cell at the monolayer is evaluating its state transition, it examines a certain radius of influence. For the current version of the simulation, this has been fixed to a one cell distance. If any of its neighboring cells are in the process of sprout formation, the cell in question has a high probability of staying in the quiescent state.

viii. Rules and Parameters

a) Rules

. Certain 'rules' for cell transitions that are incorporated in the mode are outlined below:

1. Initially, a uniform monolayer of cells is assumed to exist on the surface of the matrix. New sprouts are allowed to be initiated for the first four hours. This is implemented to prevent multiple sprout formation and also depicts the biological state when only certain cells in the monolayer sprout and act as 'inhibitors' on nearby cells. This lateral inhibition is enforced via the field.

2. Each cell undergoes a 'decision-making' process, where it can decide to migrate, divide, die or stay quiescent.
3. If a cell has 'decided' to migrate, the direction of migration is stochastic, though it is biased toward the lattice position occupied by matrix that is associated with the highest concentration of chemoattractants and MMP by giving the cell a higher probability to migrate towards that lattice point. It has a lower probability to migrate into any of the other matrix-occupied lattice positions.
4. If a cell has 'decided' to divide, the new cell occupies the matrix-occupied lattice position that is associated with the highest concentration of MMP, as it causes local degradation of the matrix.
5. If a cell dies, its position is occupied by empty space.
6. A cell can migrate only into a lattice position occupied by matrix but can divide into either empty space or matrix.
7. If two cells choose the same lattice point into which to divide or migrate, a tie-breaking rule is applied.
8. A migrating or dividing cell releases MMP into each of the adjacent matrix elements, thus influencing the migration of itself and of neighboring cells. The amount released depends on the state of the cell and can be classified as 'low' or 'high' - the values of which are recorded in Table 1.
9. VEGF is both released and consumed by the cells according to the state of the cell and the surrounding VEGF concentration. As explained earlier and recorded in Table 1, the surrounding local concentration above which VEGF production is 'high' is 12 and that above which VEGF consumption by a cell is 'high' is 10 units.

10. Cells are allowed to divide both at the monolayer and in the stalks.
11. In the current simulations, the number of migration sub-states (m) is three and the number of proliferation sub-states (p) is twenty, where each 'cellular' time step corresponds to approximately one hour.
12. VEGF influences endothelial 'decision-making' via both paracrine and autocrine signaling. Therefore, the deterministic model accounts for the diffusion, consumption and production of VEGF and MMP by the cells.
13. While the sample simulations included in this study account for change in concentration of VEGF and MMP, as well as initial addition of VEGF (40 $ngml^{-1}$or 20 $ngml^{-1}$) and/or Ang 1 (500 $ngml^{-1}$) to the 'field', the module-based algorithm and signaling molecules interacting with the cells in a modular array format ensures that additional molecules can be included easily.
14. In the simulations, the 3D lattice is normalized to the characteristic length of an endothelial cell: ~10 μm. The concentration of the different growth factors and MMP are normalized to the maximum concentration in every simulation.
15. All simulations are recorded 50 hours after the monolayer is established. All experimental images are documented two days after cell seeding.

b) Parameters

Several parameters have been used in the development of the model. They can be broadly classified into simulation parameters, field parameters and cell parameters.

1. *Simulation parameters:*

- ***Grid size:*** Dependent on the simulation volume. For all model behavior experiments, the grid size was 20x20x20, and for all experimental matching simulations referred to in chapter 4, the grid size was 10x10x10. This is user-specified and can be changed to any size.
- ***Simulation time:*** For all simulations this was limited to 48 time steps, implying 48 hours. This is user-specified and can be changed to any length of time.
- ***Simulation frequency:*** This is a design specification and was chosen to be one hour for reasons mentioned in section iii.c (Model Characteristics).
- ***Location of monolayer:*** The monolayer was specified at z=1, at one end of the matrix. This is user-specified.

2. *Field Parameters:*

The parameters associated with the production and consumption of VEGF and MMP were discussed in section iv (Field Equations) and are recorded in the table 1.

	High	In Model	Condition at which the 'high' values are used	Low	In Model
VEGF Consumption	$\Delta C_{vegf\_s,C,1}$ Change in VEGF due to consumption by a single cell	$-k_{on\_c}C_{vegf\_s}C_{vegf\_rec} + k_{off\_c}C_{vegf\_r}$	VEGF concentration > 12	$\Delta C_{vegf\_s,C,2}$	0
VEGF Production	$\Delta C_{vegf\_s,P,1}$ Change in VEGF due to production by a single cell	0.05 ± 0.025	VEGF concentration > 10	$\Delta C_{vegf\_s,P,2}$	0.04 ± 0.02
MMP Production	$\Delta C_{MMP,P,1}$ Change in MMP due to production by a single cell	0.6 ± 0.2	Cell is migrating	$\Delta C_{MMP,P,2}$	0.2 ± 0.1
Matrix Binding Sites	$\Delta C_{M,C,1}$ Change in MMP binding sites due to MMP	$-k_{c\_m}C_{MMP}M$	High release of MMP	$\Delta C_{M,C,2}$	0

Table 1: The variables used in the four different rate equations described above have two different activities: 'high' and 'low'. These are normalized by the starting concentrations and are therefore dimensionless.

3. *Cell Parameters:*

- ***Transition probabilities:***

These are parameters that can be varied and be user-specified.

Q→Q: This is an input variable that is user-specified. Systematic variations of this parameter have been done and the results are included in section viii (Model Behavior).

Q→M: This is an input variable that is user-specified. Systematic variations of this parameter have been done and the results are included in section viii (Model Behavior).

Q→P: This is an input variable that is user-specified. Systematic variations of this parameter have been done and the results are included in section viii (Model Behavior).

Q→A: This is a fixed variable that could be varied if required. This has been fixed because experiments demonstrated that the growth factors being used did not alter the cell transition to apoptosis. So, this can be fixed at zero and be changed into a cell age dependent factor, or can be changed if a factor that affects cell apoptosis is used.

- ***Direction transitions:***

For migrating: A migrating cell samples all neighboring grid values of MMP and VEGF and identifies the location that has the highest values associated with itself. It then has a 72% probability to move to that location. It has an equal (but comparatively lower; 2%) probability to move to any other lattice point. These values are arbitrary and selected based on the qualitative fact that the cells tend to move towards a higher concentration of chemoattractants and MMP-cleaved matrix.

For dividing: A dividing cell samples all neighboring grid values of MMP and identifies the location that has the higher values associated with itself. It then has a 72% probability to

move to that location. It has an equal (but comparatively lower; 2%) probability to move to any other lattice point. These values are arbitrary and selected based on the qualitative fact that the cells tend to sprout along MMP-cleaved gels and regions with larger pore size.

- ***Temporal parameters:***

Time in migratory state: The default time in migratory state is fixed to be three time steps. This can be changed depending on surrounding Ang 1 concentration, as explained in section vi (Cell Communication).

Time in proliferative state: The default time in proliferative state is fixed to be twenty time steps. This is in congruence with the dividing time of an endothelial cell.

- ***Others:***

Radius of Influence: One cell sphere. This is used to enforce lateral inhibition via DL4/ Notch signaling.

Cell age and apoptosis: There is 5% chance of a cell undergoing apoptosis after 24 hours.

The cell parameters, the transition probabilities will be determined in chapter 4.

ix. Model Behavior

a) Characteristics being measured

Various morphological characteristics can be measured by running the model under different input conditions. In order to exploit the capabilities of the model, we decided to evaluate certain characteristics that could be easily measured in experiments. All simulations were performed in a

20x20x20 grid. The characteristics evaluated were those that most reflect cell population behavior:

1. Average number of sprouts per simulation region
2. Average number of branches per simulation region
3. Average number of anastomoses per simulation region
4. Average length of sprouts
5. Average number of individual migrating cells

The capillaries in the model can be represented either in the form of individual cells, as shown in figure 10d or more commonly as tubular structures, as shown in figure 8. Figure 8 shows the effect of increasing probability of a cell to transition into migration on the number and length of capillaries.

b) Discussion of Results

The model can be used to explore how specific features depend on the imposed conditions, as shown in the following examples. Consider first the average protrusion length of cells into the matrix (Figure 9). This is determined by calculating the depth to which cells penetrate at each lattice point in the monolayer in the z direction and assuming unit volume occupied by each cell. Corresponding sets of transitional probabilities are listed in the figure. In the first three transitional sets, the probabilities to migrate and die are held constant, the probability to divide decreases and that to remain quiescent increases. In the next three transitional probabilities sets, the probabilities to divide and die are held constant, the probability to migrate decreases and that to remain quiescent increases. As expected, certain transition probabilities result in higher cell

protrusion into the matrix. As the probability of the cell to remain in the quiescent state increases in the first data set, the protrusion distance increases because of the lower proliferation rate. Thus, fewer sprouts are initiated, and the ones that are formed grow longer. This implies that while proliferation occurs both in the monolayer and in the sprouts, addition of any proliferating agent impacts the proliferation rate in the monolayer more significantly. Hence, the addition of growth factors that stimulate proliferation should result in a larger network of sprouts and/or more cell clusters. In the second data cluster, with higher migration probability, longer sprouts are formed. While the difference in sprout length is not significant with small changes in migration probability, the trends observed are very significant. It provides an insight into the conditions that would give rise to network-like vs. single-sprout-like capillary structures.

1. Continuous Sprouts vs. Cell Clustering

In order to understand the effect of each of the different transition probabilities, the number of different morphologies are recorded when two of the four transitions are kept constant and the other two are systematically varied. Figure 10 shows an average of thirty simulations for each of these conditions.

To determine the effect of increasing specific transitional probabilities, we varied specific ratios (migration (M) to quiescence (Q); proliferation (P) to quiescence (Q); and migration (M) to proliferation (P)) systematically by keeping the other two constant in each case. The results observed for each of the variations mentioned above are depicted in Figures 10 and 11. As the M/Q ratio increases (Figure 10a), the number of individual migrating cells increases and the number of cell clusters at the monolayer decreases. This is because at a certain fixed transition

probability of proliferation, as the tendency of cells to migrate increases, cluster formation decreases. However, discontinuous sprouts or clusters formed away from the monolayer show a bimodal response. At the first peak, these clusters tend to be broader, and at the second peak (when the tendency to migrate is higher than that to proliferate), these clusters tend to be longer. This behavior is clearly seen when capillaries are plotted as an aggregate of individual cells and not tubular structures as shown in all other simulation representations. Figure 10d shows the distinction between the optima for discontinuous sprouts clearly. At lower M/Q ratios, these clusters tend to aggregate more than at higher ratios. When the ratio of migration to quiescence nears one, the number of such 'floating clusters' decreases. This is also the condition that causes an increase in the number of continuous cell sprouts. This shows that these two morphologies lie in two distinct areas in the space map of the different transition probabilities.

A crucial element in capillary morphology prediction is identifying the balance between the transition probabilities of migration and proliferation. Figure 10b shows the effect of varying these two transition probabilities, keeping the transition to quiescence and transition to apoptosis rates fixed at 15% and 5%, respectively. The most relevant prediction is that the number of continuous probabilities peak when this ratio nears one. Though the number of cell clusters in the matrix does not change much, these clusters, like the clusters at the monolayer, tend to become larger as this ratio increases.

The simulations in Figure 10c were generated while keeping the transition probability of migration fixed at 15% and the transition probability of apoptosis fixed at 5%. While the number of continuous sprouts and discontinuous sprouts or cell clusters in the matrix remains unchanged

as the ratio increases, it is also important to note that at this fixed transition rate for migration, very few continuous sprouts are formed. Since this lies in the first half of the curve that determines the effect of migration on sprout formation as shown in Figure 10a, it is verified that sprout formation is optimal at a higher migration transition probability. The number of single migrating cells decreases and the number of clusters at the monolayer increases as the P/Q ratio increases.

The customary capillary morphology found *in vivo* is continuous sprouts, and its ratio to each of the other morphologies as a function of the ratio of the transition probabilities between migration and quiescence, proliferation and migration, and proliferation and quiescence are shown in Figure 11. As expected, the curves peak when there is a balance between migration and quiescence, which translates into effective capillary induction and stabilization (Figure 11a). The model predicts that the ratio between proliferation and quiescence should be increased in order to increase the number of continuous sprouts in comparison to individual migrating cells (Figure 11c). Again, as expected after observing Figure 10b, the number of continuous sprouts is maximized in comparison to any other capillary morphology when the ratio of transition : proliferation to that of transition : migration tends towards one (Figure 11b).

Figures 12, 13 and 14 are contour graphs that plot the change in M/Q ratio on the y axis and the change in P/Q ratio on the x axis. They help identify the 2D space where there is maximum likelihood of obtaining a higher number of continuous sprouts (Figure 12), discontinuous sprouts / cell clusters (Figure 13) and cell clusters at the monolayer (Figure 14). It is observed that the peak of the continuous sprouts contour graph lies in one of the troughs of the discontinuous

sprouts / cell clusters contour graphs. Thus, this provides a transition space where one can probably obtain sprouts without significant cell clustering. Another prominent observation is that high P/Q and M/Q rations result in a peak in the discontinuous sprouts / cell clusters contours and high values even in the contour graph for cell clusters at the monolayer. Thus, this is definitely a space to avoid if one is interested in long sprouts. On the other hand, if the goal is to populate a gel region with short cluster-like capillaries, one may want to explore the space in the lower left of the contour graphs i.e. high P/Q and low M/Q regions. While this space has a high value in figure 14, it has a low value in figure 13. Thus, it represents a region of cluster-like sprouts at the monolayer with the absence of cell clusters or discontinuous sprouts.

2. Branching

This model is also a useful tool for studying and analyzing branching patters in capillary formation. Very little is known about the characteristics of capillary networks and the factors that influence them. In order to use this model to study such patterns, we first need to identify certain significant characteristics. We limited these to number of sprouts, number of total branches, number of branches per sprout and number of anastomoses per simulation. These were analyzed as a function of changing transition probabilities, based on the expectation that most growth factors will impact migration, proliferation, apoptosis and quiescence and hence will fall in the transition data space being analyzed. The results shown in figure 15 can be used to narrow down the transition probabilities that provide the desired network characteristics.

3. *Intracellular Signaling*

An advantage of this model is that it allows for the incorporation of an intracellular signaling model. Though it has not been included in the current version, the model can call intracellular modules during the different states: migration, division and quiescence. These functions will predict the signaling pathway that will be used by the different growth factors and the cellular responses to them in a probabilistic manner. The output of these functions (cellular responses) will act as the input for the next step of cell ensemble response.

4. *Limitations*

The simplifications made in the algorithm of this model may make it difficult to identify factors that affect the sprout characteristics in small gradients. Additionally, the usage of the 'field' as the cell communication medium is primarily used for modulation of endothelial cell-cell contact, connectivity in the sprout and lateral inhibition due to notch signaling. Since the cells cannot change shapes in the current format of the model, such communication restricts the ability to maintain the cell junction. This limitation of the model can be overcome by allowing the cells to change shape in future versions. Additionally, cell polarity and intercellular communication, which is a function of cell polarity, is ignored in the current form of the model. It can be foreseen that this can be incorporated when cells are allowed to change shape. In that event, the cell communication function will have to evolve to account for that complexity.

5. *Advantages*

The advantage of the 3D agent based coarse-grain stochastic angiogenesis model outlined here is that several angiogenic factors can be included and that it can function both as a stand-alone

model and inside the control framework mentioned above. Most importantly, all simulations can be compared in-house to experiments conducted in the microfluidic devices described. By modeling cell populations via the application of global controls that are collectively modified by the aggregate cell population, cell-cell interactions are introduced into this model in an explicit manner. Several previous works have modeled capillary growth as a function of the leading cell or developed models that involve distinct zones of capillaries. For example, Balding & McElwain (1985) modeled two regions of endothelial cell density: the sprout proper and the tip; however, they neglected dynamics of the cells remaining on the monolayer. Such cell-cell interactions are crucial for developing a model that reflects the impact of cellular signaling molecules and the extra-cellular matrix because of the feedback loop that exists between the aggregate effect of cells on the matrix and the impact of the matrix on each individual cell. Since then, as mentioned in the introduction, several types of models which provide crucial insights into the process have been developed. However, the model we present is unique in its ability to cross talk with experimental results and thus, provides a platform for predicting non tumor angiogenesis in *in vitro* bioreactors.

By developing a model based on the influence of global and local conditions, the coarse-grain combined impact of various biochemical and biomechanical factors on angiogenesis can be determined. The model can be extended to include any number of biomolecules that are either being added to the bioreactor (affecting global conditions) or being secreted/consumed by migrating/dividing cells (affecting local conditions) because the 'molecular matrix', i.e. the components associated with each lattice in the 'field,' can be of any size. Such a methodology is

essential in order to develop a systems-based, experimentally verifiable approach to the process of capillary formation.

This model enables us to simulate individual cell behavior and compare cell population behavior at the end of the simulation. Certain basic characteristics observed in these simulations that reflect experimental observations are the presence of continuous sprouts, their differential formation as a function of added growth factors, horizontal and vertical migration and cell clustering. Different transitional probabilities reflect these experimental observations, and future work will explore the predictive nature of such a model.

x. Conclusion

In conclusion, we demonstrate here the successful implementation of a 3D agent-field model for capillary formation that can generate sprouts with characteristics similar to those observed in 3D *in vitro* experiments. This is a hybrid stochastic-deterministic model where individual cells are modeled independently and their communication via cell-cell interactions is included in a mathematically simplified manner that captures the importance of that action but does not complicate the implementation. The simulation results obtained are characteristically similar to experimental observations as shown, indicating that this model can be used for various demonstrative and predictive applications.

a

$$\frac{\partial n}{\partial t} = \overbrace{D_n \nabla^2 n}^{\text{random motility}} - \overbrace{\chi_0 \nabla \cdot (n \nabla c)}^{\text{chemotaxis}} - \overbrace{\rho_0 \nabla \cdot (n \nabla f)}^{\text{haptotaxis}},$$

$$\frac{\partial f}{\partial t} = \overbrace{\omega n}^{\text{production}} - \overbrace{\mu n f}^{\text{binding/degradation}},$$

$$\frac{\partial c}{\partial t} = - \overbrace{\lambda n c}^{\text{uptake/binding}}.$$

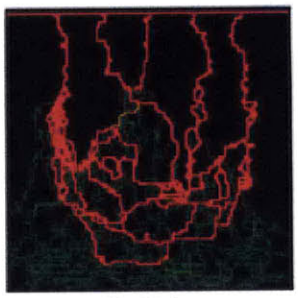

$\tilde{t} = 30.0$

Tumor (TAF source)

b

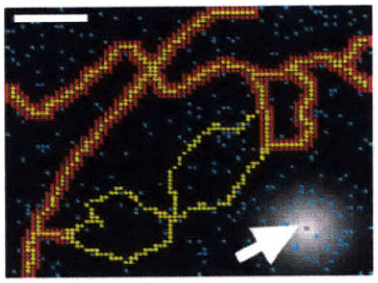

c

Figure 2: Examples of existing angiogenesis models [(a) deterministic model; Anderson and Chaplain (1998); (b) CPM model, Pierce et al. (2004); (c) random walk model, Plank and Sleeman (2004)]

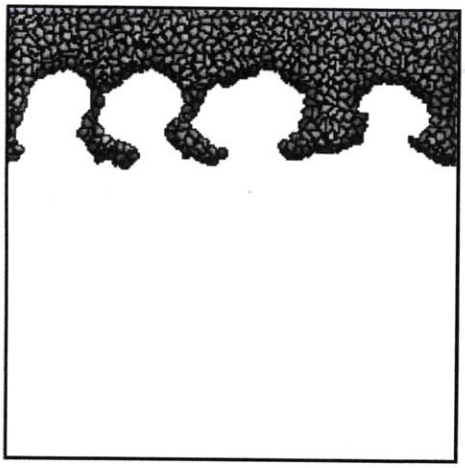

Figure 3: An extension of the Potts model to simulate malignant cells and quantify invasion morphology as a function of cell-cell adhesion (Turner and Sherratt, 2002).

Showing the characteristic appearance of the simulated tumour after 1500 Monte-Carlo time steps.

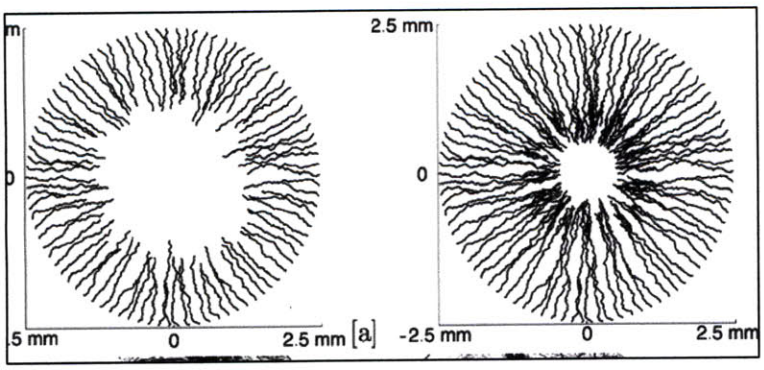

Figure 4: Physiological model of corneal angiogenesis that integrates a mechanical model of elongation with a biochemical model of cell phenotype (Jackson and Zheng, 2010).

Simulations of normal growth after days 4 and 7

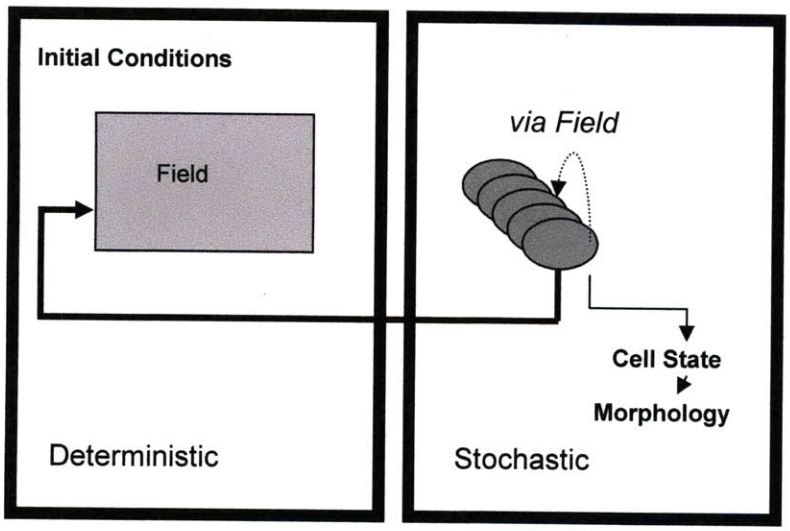

Figure 5: The two components of the model: Deterministic Field and Stochastic Cell Population Behavior

The 'field' represents the set of deterministic equations that specify the local microenvironment. Variables that specify the state of the field act locally on the cells, determining their state and morphology governed by probability distributions. Feedback occurs by the virtue of the factors secreted by the cells such as growth factors and degradative enzymes (Das et. al., 2010).

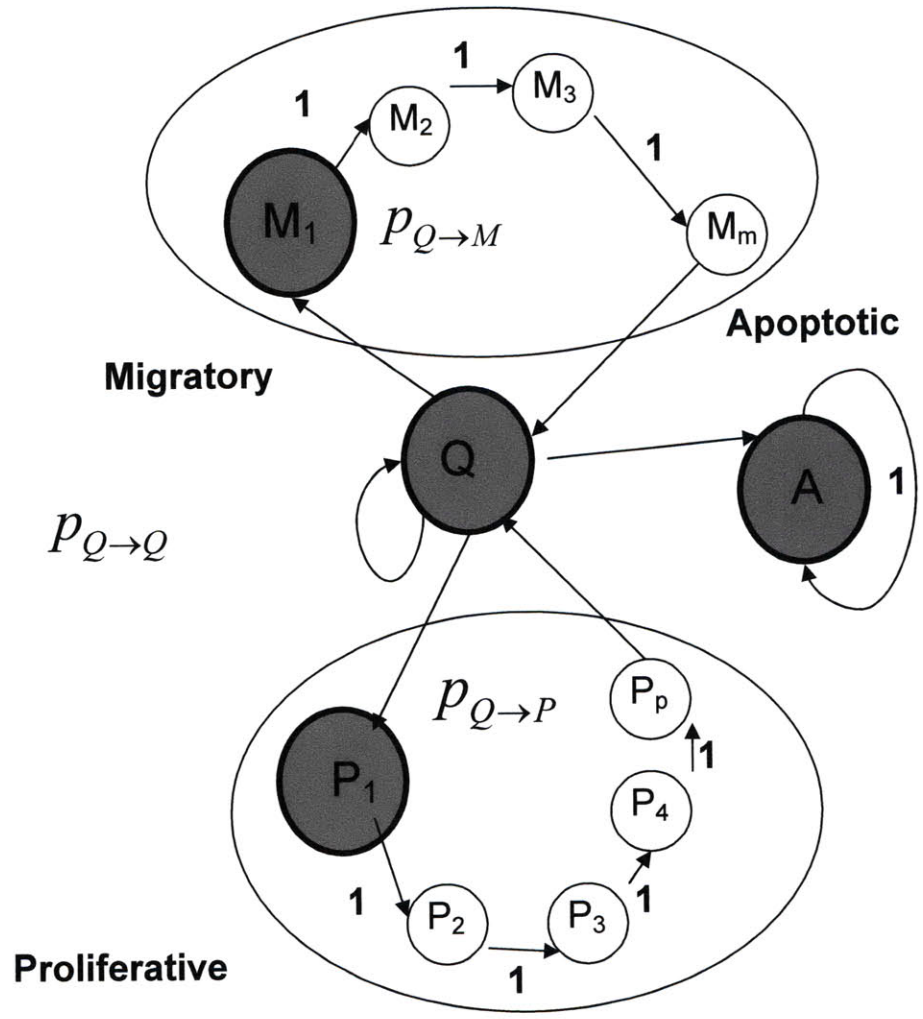

Figure 6: States in the Markov process

The state of a single cell can evolve from quiescent (Q), to proliferative (P), migratory (M), or apoptotic (A). Once in the migratory or proliferative states, the cell remains there for "m" or "p" sequential sub-states, respectively, before returning to quiescence. From the apoptotic state, the cell dies after a specified period and cannot again become quiescent (Das et. al., 2010).

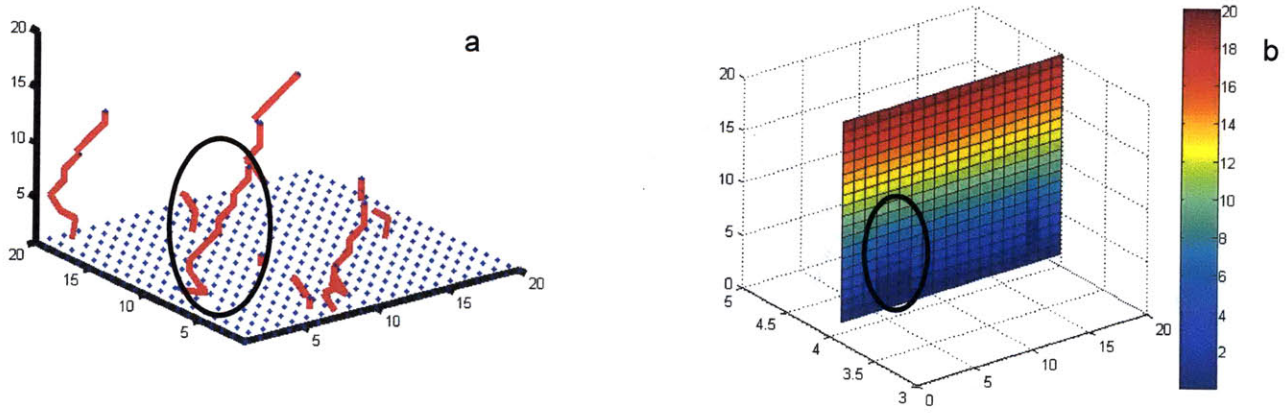

Figure 7: Occurrence of cell-cell communication occurs via the 'field'.

(a) The simulation shows a sprout growing a 3D lattice normalized to the characteristic length of a cell (10μm). (b) The field evolution shows the change in the free matrix binding sites normalized to the maximum concentration in three spatial coordinates. This demonstrates the effect of migrating cells on the matrix via the MMPs as a change in their concentrations is observed in the region surrounding a developed sprout. (Das et. al., 2010)

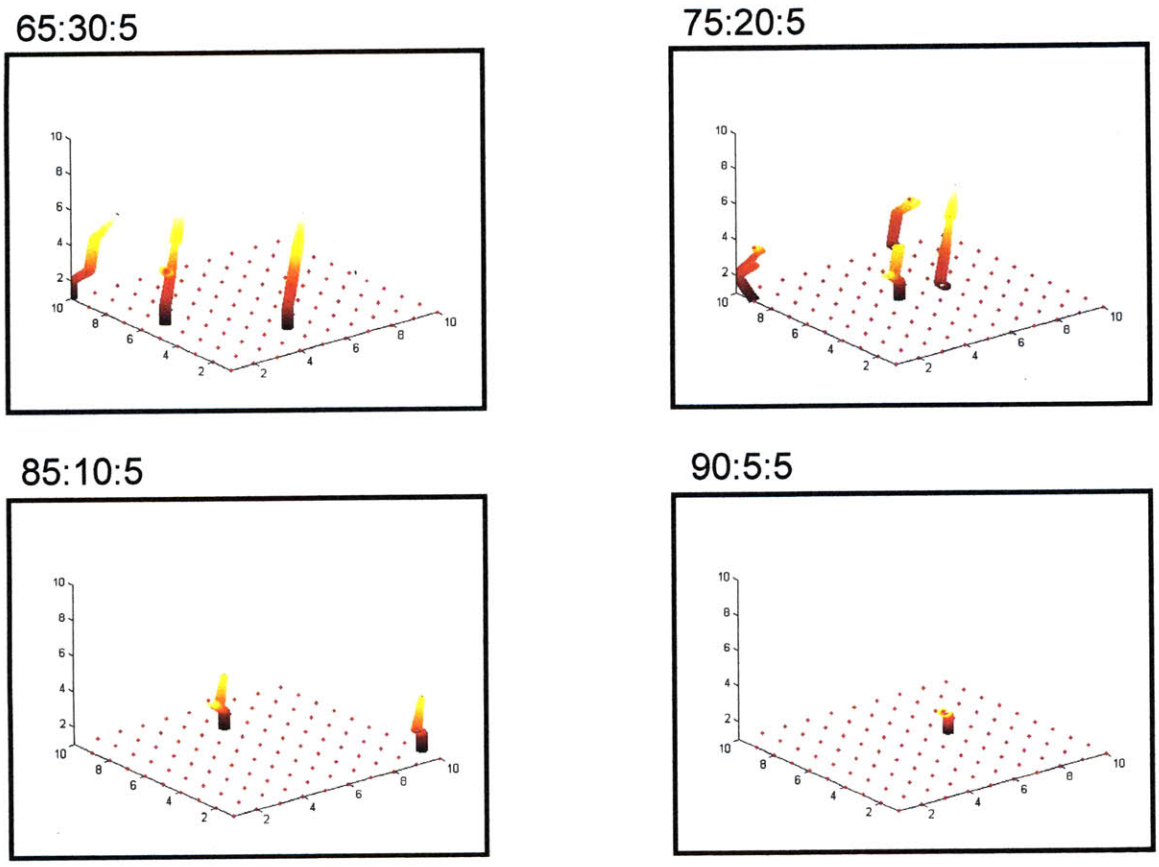

Figure 8: Representation of the effect of increasing M/Q ratio on the length and number of sprouts in simulations.

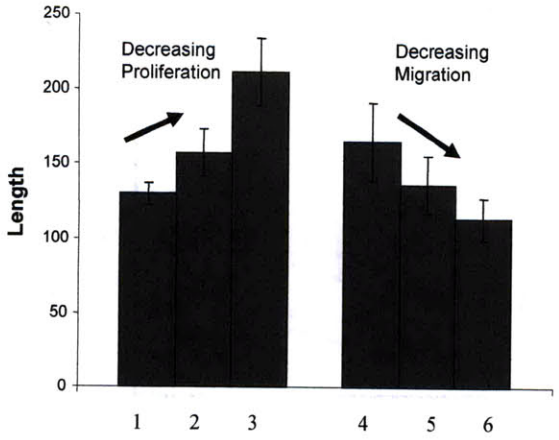

	$p_{Q \to Q}$	$p_{Q \to M}$	$p_{Q \to P}$	$p_{Q \to A}$
1	0.05	0.6	0.3	0.05
2	0.15	0.6	0.2	0.05
3	0.25	0.6	0.1	0.05
4	0.3	0.55	0.1	0.05
5	0.45	0.4	0.1	0.05
6	0.55	0.3	0.1	0.05

Figure 9: Average protrusion length of capillaries into matrix as a function of transition probability trends. The numbers in the x axis of the graph represent transition probability sets described in the accompanying table (Das et. al., 2010).

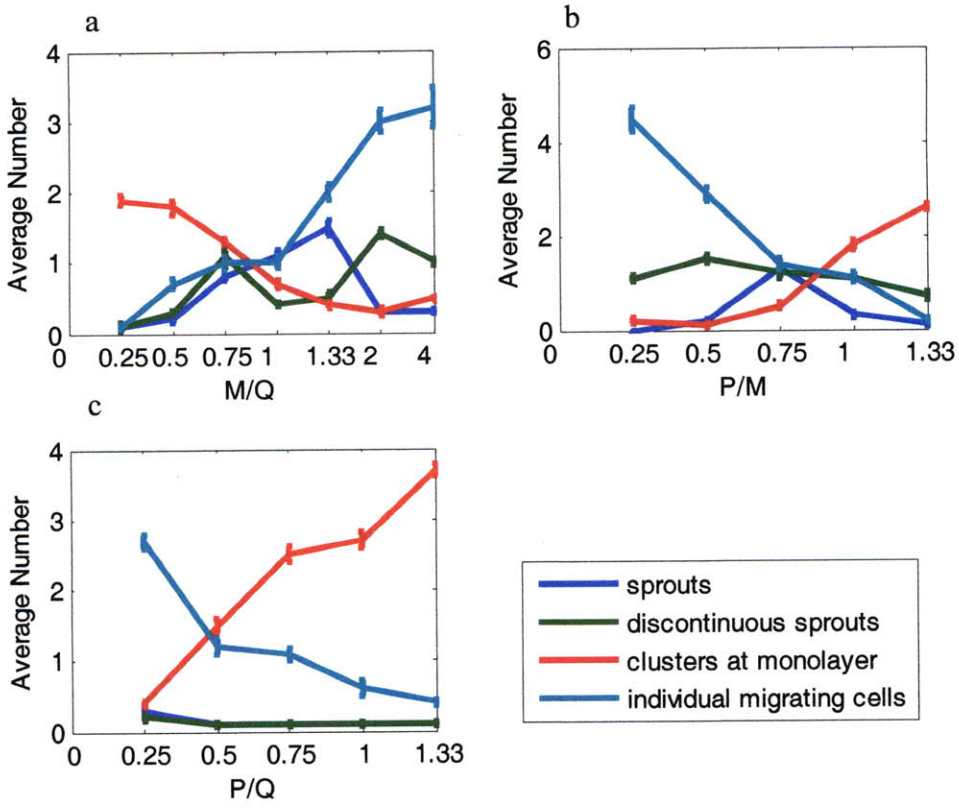

Figure 10: Average number of different capillary morphologies as a function of different transition probabilities.

(a) *M/Q* ratios (keeping transition to *P* and to *A* constant); (b) *P/M* ratios (keeping transition to *Q* and to *A* constant); (c) *P/Q* ratios (keeping transition to *M* and to *A* constant). Adapted from Das et al., 2010.

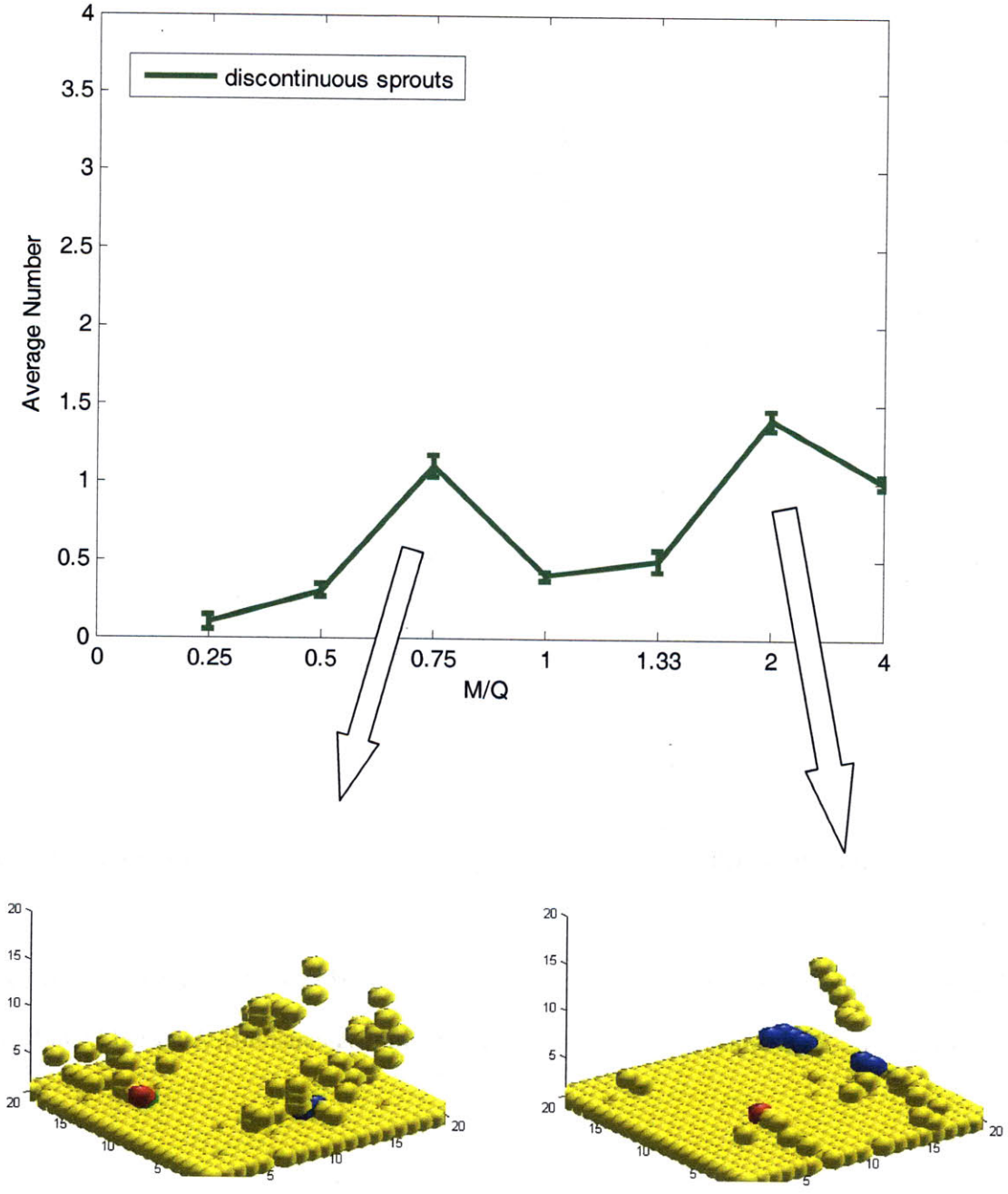

Figure 10d: The two local optima observed in the number of discontinuous sprouts with increasing M/Q ratio represent two different types of morphologies.

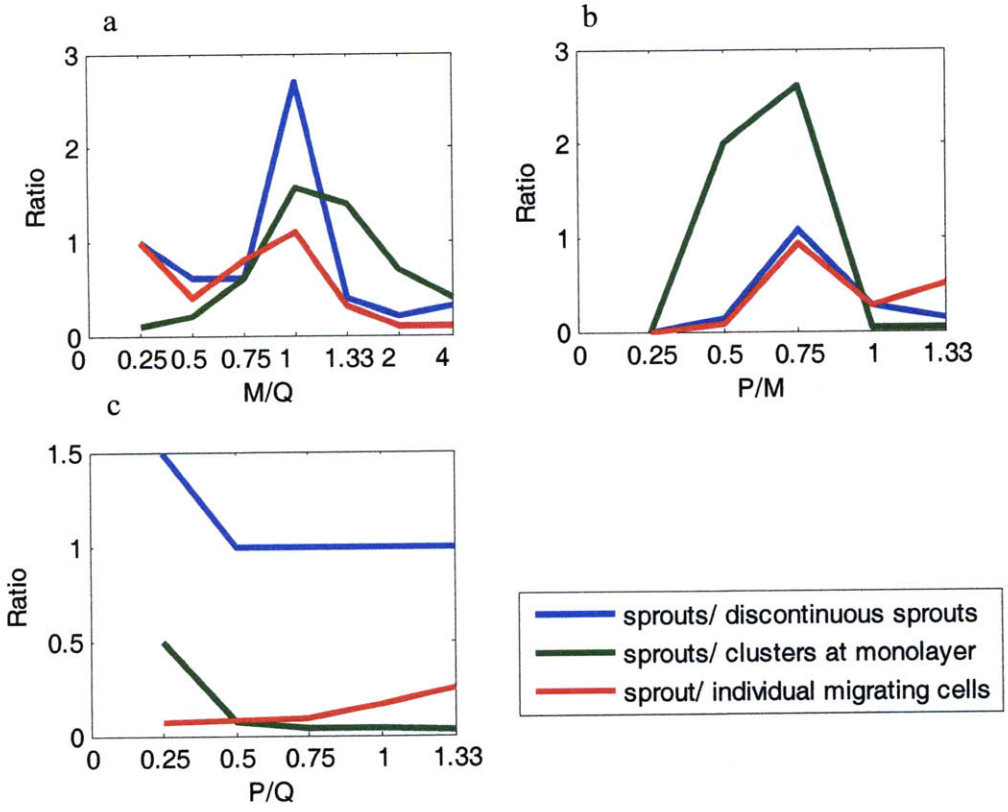

Figure 11: Ratio of continuous sprouts to other morphologies as a function of increasing transition ratios

(a) as a function of increasing *M/Q* values (keeping transition to *P* and to *A* constant); (b) as a function of increasing *P/M* values (keeping transition to *Q* and to *A* constant); (c) as a function of increasing *P/Q* ratios (keeping transition to *M* and to *A* constant). Adapted from Das et al., 2010.

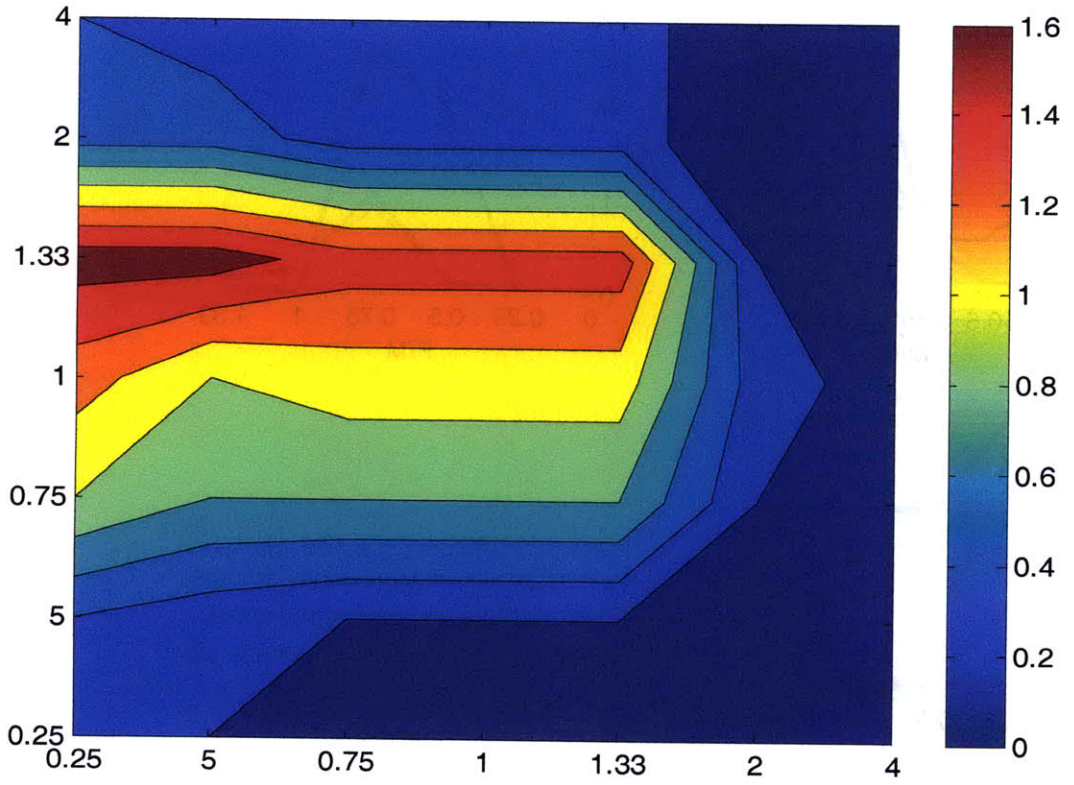

Figure 12: Contour map of average number of sprouts as a function of increasing M/Q and P/Q ratios.

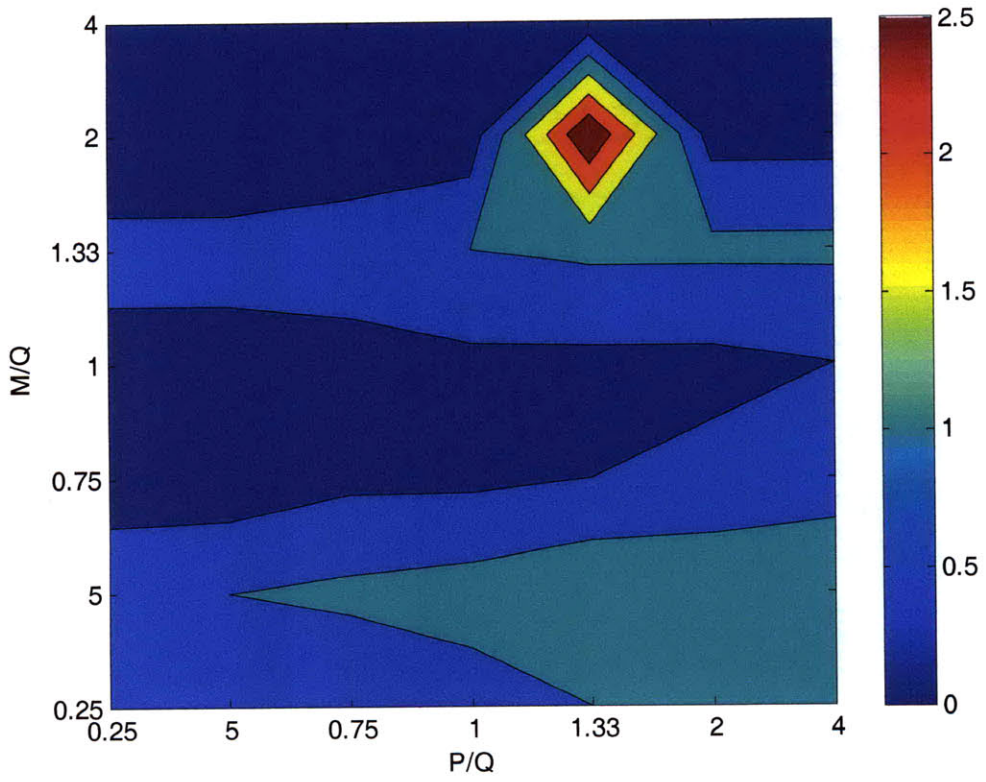

Figure 13: Contour map of the average number of discontinuous sprouts as a function of increasing M/Q and P/Q ratios.

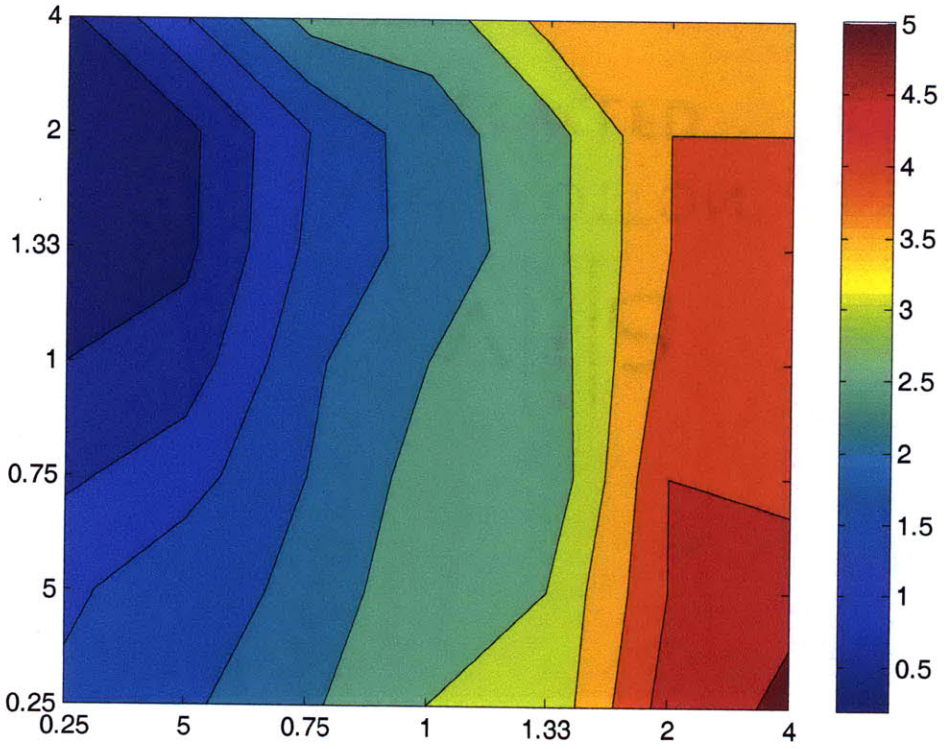

Figure 14: Contour map of average number of cell clusters at the monolayer as a function of increasing M/Q and P/Q ratios.

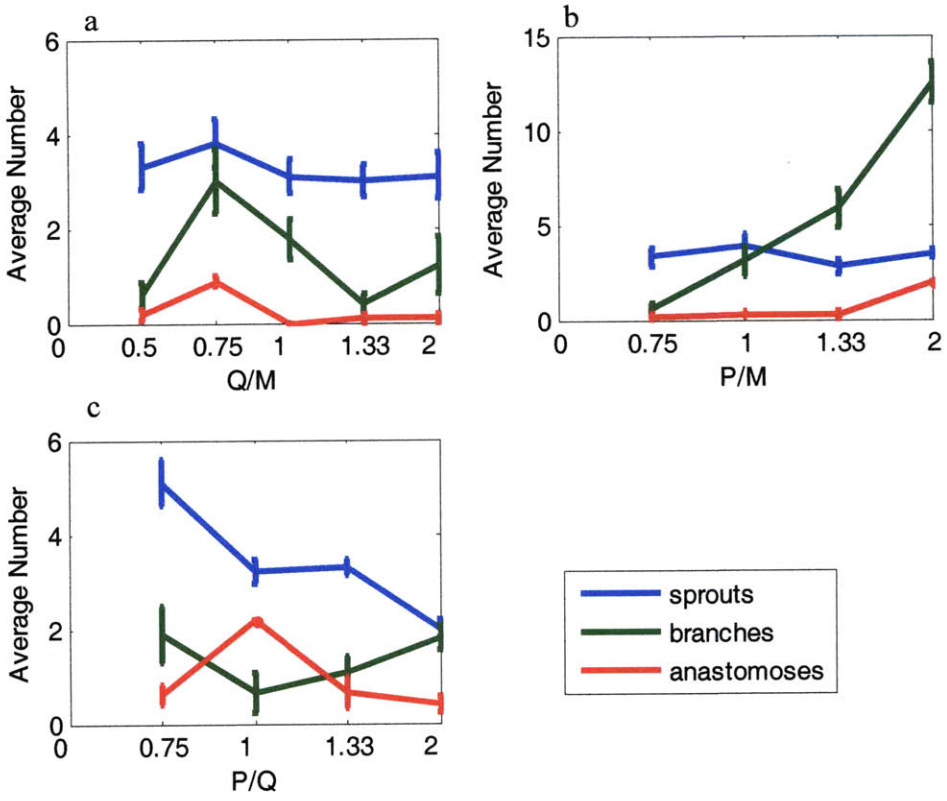

Figure 15: Branching patterns as a function of increasing transition probabilities.

(a) Increasing *Q/M* transition; (b) Increasing *P/M* transition; (c) Increasing *P/Q* transition.

Adapted from Das et al., 2010.

3. Microfluidic Experiments

i. Rationale

In this chapter, experiments are designed to provide estimates for the parameters of the model described in chapter 2. We chose to use a microfluidic system for this purpose since it provides the capability of exerting precise control over the inputs to the *in vitro* sprouting assay while imaging the sprout growth during the course of an experiment or at its completion. The objective here is to observe and quantify sprouting under several distinct biochemical conditions, and then use the experimental results as inputs for our computational model. The first set of experiments were designed to determine if the model and experiments were "compatible" with one another, in the sense that the networks generated in the model, for certain ranges of parameters, could be made to resemble the experimental data (comparative study). Then, having confirmed that, a second set of experiments were designed in which we systematically varied the experimental conditions (characterizing study), and adapted decision tree analysis (DTA) to back out the parameter values. The extraction of the parameters is described in the following chapter. This chapter focuses on the experimental methodology and results.

ii. Background

Several *in vitro* platforms have been adapted for angiogenesis experiments in the last two decades. These can be broadly classified into proliferation, migration and differentiation assays. The cell proliferation assays described here primarily rely on determining the net cell number. Cells are seeded at a fixed confluence percentage, and the cell number is determined after 18-24 hours of being subject to different media conditions. The increase in the cell number is measured by a cell counting device such as a haemocytometer, a coulter counter or a Vi-cell counter

(Staton et al., 2009). DNA synthesis is an alternative measure of cell proliferation and is assayed by measuring the incorporation of [^{3}H] Thymidine into the DNA of the cell using scintillation counting, where the amount of radioactivity is proportional to the neosynthesis of DNA (Staton et.al., 2009; Yu et al. 2004).

Migration assays are usually some form of a Boyden chamber assay. A summary of the different Boyden assays is provided by Staton et al. (2009) in their review of angiogenesis assays. There are 3D assays which allow the passage of active cells towards an attractant (test angiogenic factor) placed in the lower chamber (Alessandri et al. 1983) with or without the filter being coated with single ECM proteins such as collagen or fibronectin, or complex matrices, such as matrigel (Albini et al. 2004). Though very useful, these assays have some disadvantages in that imaging through the filter is difficult: the pores and cells cannot always be distinguished, the cell microenvironment is not always preserved, and the pore size tends to alter sprout formation characteristics.

Assays that simulate the formation of capillary-like tubules are regarded as representative of the later stages of angiogenesis known as differentiation. They are used extensively to assay novel compounds for pro- or anti-angiogenic effects (Staton et al., 2009). Differentiation assays are useful in determining the tube formation behavior of endothelial cells. They could be 3D assays where beads coated with endothelial cells are dispersed in a matrix and allowed to form tubules. Nakatsu et al. (2007) coated beads that were layered on top of the gel, where they provide necessary soluble factors that promote EC sprouting from the surface of the beads. In this assay, while the cells are exposed to a 3D environment, they do not have the same microenvironment,

as the bead and the gel have different material characteristics. A spherical localization exposes the cells to a different concentration profile than what they would encounter *in vivo*. Moreover, these vessels cannot be perfused after formation and in some instances the spherical carriers sink to the bottom of the gel. In other instances, cells are coated on a gel matrix (collagen, matrigel or fibronectin), exposed to various angiogenic agents, and allowed to form capillaries into the gel (Lawley & Kubota, 1989; Kanzawa et al., 1993). While this is very similar to the *in vivo* layout, cells usually see a different microenvironment as the precise environment around them cannot be controlled and most measurements are made based on bulk profiles. A further limitation common to all the 3D macro assays is that the gel has to be relatively thin to allow the diffusion of oxygen and nutrients (Staton et al., 2009).

To balance the pros and cons of the various assays described above, and because we are interested in forming well-developed capillaries, we decided to use a gel-based assay in a microfluidic environment that overcomes the limitations of these previous assays, as described below.

iii. Device design

a) Background

Microfluidic devices have been used extensively to study various biological processes. In addition to providing a cell microenvironment that replicates *in vivo* conditions better than macro-assays, they may also enable 3D controlled experiments with a minimal number of agents. Unlike experiments conducted on the macro scale, like those in well plates, we can exert better control on the concentration and flow profiles in microfluidic devices. Thus, the results obtained

can be correlated to the input conditions in a more precise manner. The amount of expensive reagents required for each experiment is reduced and most devices also allow for better imaging of the experiments. While assays conducted in Boyden chambers cannot be easily imaged using a confocal microscope in 3D, experiments conducted in microfluidic devices can be. Many micro-fabricated devices have also been developed to induce and monitor cell migration in the channel in response to either biochemical gradients or biomechanical forces (Jeon et al., 2002; Chung et al., 2005; Tourovskaia et al., 2005; Gomez-Sjoberg et al., 2007; Gu et al., 2004). These methods have been used to apply well-defined biochemical gradients to either cells plated on a gel surface comprising the walls of a microfluidic channel (Jeon et al., 2002; Chung et al., 2005) or within gel scaffolds (Frisk et al., 2007; Saadi et al., 2007). These techniques demonstrate the potential to be versatile tools for analyzing cellular responses under biochemical gradients.

In our own laboratory, we have used microfluidic devices that replicate a realistic 3D environment in combination with gradient and flow control to study cell migration and capillary morphogenesis (Chung et al., 2009). Sudo et al. used microfluidic devices to culture hepatocytes and studied the impact of flow by using phase-contrast images (2009). They cultured liver and vascular cells on each sidewall of a collagen gel scaffold between two microfluidic channels under static or flow conditions and found that the morphogenesis of 3D hepatocyte cultures was dependent on diffusion and convection across the nascent tissue. Chung et al. studied responses of endothelial cells when they were placed in co-culture with physiologically relevant cell types such as cancer cells (2009). Kothapalli et al. studied axonal growth and chemo-attractant

gradients orthogonal to axon growth in 3D matrices using similar microfluidic devices (In review).

We are using one such microfluidic device (developed by Farhat, W) to grow capillaries in a controlled and predictive manner. We demonstrate that capillaries with distinct characteristics can be grown under different media conditions and that characteristics can be altered by changing these conditions. A two-channel multiple gel surface microfluidic device (Figure 16) fabricated in PDMS was used for all experiments. The main advantage of a device of this type is that the network growth can be easily visualized as they grow on a horizontal plane. The device used here has four ports for media, two for each channel, and two gel-filling ports. It is similar to one described in Vickerman et al. (2008), but has multiple gel surfaces along the channel.

iv. Experiment Design

The rationale underlying the design of the experiments was two fold: the first goal was to be able to generate reproducible and physiologically relevant results in a microfluidic device, and the second goal was to quantify the capillary characteristics and determine certain input parameters to the model by comparing them to simulation results. The experimental time was an important design factor. Based on previous experiments, it was decided that two biochemical factors would be varied, VEGF and Ang 1. VEGF was chosen because it is the most common and researched angiogenic factor. Various experiments conducted in the microfluidic device in our lab have demonstrated that capillary stabilization is achieved when Ang 1 is used in the media along with VEGF. Hence, it was decided to incorporate these two pro-angiogenic factors in the first stage of the experiments.

v. Device Making Protocol

a) PDMS Substrates

PDMS was used as the substrate for the devices that, after patterning the channels and gel regions, were formed into closed channels and chambers by bonding to a glass coverslip. For this purpose, PDMS and the curing agent mixture was used in a 10:1 ratio and thoroughly mixed. The mixture was degassed in a vacuum chamber to remove all bubbles. It was then poured onto the wafer and allowed to bake for 24 hours at 80°C, after ensuring that no bubbles formed on the wafer. After this, holes were punched into the devices to make media reservoirs and gel-filling ports, and then wet/dry (20/10) autoclaved to make them sterile. After being dry autoclaved, they were allowed to dry in the oven overnight. Autoclaved and punched devices were plasma-bonded to thin glass cover slips. Within five minutes of bonding, the devices were filled with PDL and kept in the incubator at 5% CO2 and 37°C for four hours, after which, each device was washed thoroughly with DI water twice and then left to dry overnight in the oven at 80°C overnight.

b) Gel Filling

Type I collagen gel was used in all experiments, based on the success of previous experiments in angiogenic sprouting (Vickerman et al., 2008). 2.5 mg/ml collagen (pH 7.4) was prepared by mixing 10 parts of 10X phosphate buffered saline (PBS), 17.2 parts of sterile water, 2.6 parts of 0.5 N NaOH and 70.2 parts of 3.56 mg/ml collagen (upstate) and titrated with minimal amount of 0.5 N NaOH. 2 mg/ml collagen gel was prepared in a similar manner.

After being dried overnight, the devices were filled with 2.5 mg/ml collagen I (or 2 mg/ml collagen I) (BD Biosciences) and the gel was allowed to polymerize in humidified incubators

maintained at 37°C under 5% CO2 and 95% air for an hour. They were then filled with basic media without growth factors (EBM-2, Lonza) and allowed to equilibrate overnight. A bubble was incorporated between the two media channels (Figure 1) in order to enable cell seeding only in one of them. Twenty-four hours after gel filling, human microvascular endothelial cells (HMVECs) (Lonza, CC-0207, Batch #0000097428) were seeded as a monolayer on the collagen I gel. The devices were tipped for the first one hour so that the cells seeded onto the gel surface and then a monolayer was observed within 24 hours.

vi. Cell Culture

a) Method

All cell cultures were maintained in a humidified incubator at 5% CO_2 and 37°C. HMVECs were propagated in EGM-2MV growth media (Cambrex, USA) in 250 ml flasks coated with 50 μg/ml collagen I solution. Collagen I solution was prepared by adding 3.56 mg/ml collagen I to the required volumes of the 0.02 N acetic acid solution that was filtered and sterilized. This was stored at 4°C. Cell culture plates were coated with this solution and incubated at 37°C for one hour.

b) Conditions

VEGF (Invitrogen, USA) and Ang 1 (Invitrogen, USA) were used in different concentrations for both sets of experiments (comparative and characterizing studies). For the first set of experiments (comparative study), the assays were conducted under the following conditions (recorded in table 2). 20 ng/ml VEGF + 500 ng/ml Ang 1 in 2 mg/ml collagen I gel, 40 ng/ml VEGF in 2 mg/ml collagen I gel; 500 ng/ml Ang 1 in 2mg/ml collagen I gel; 40 ng/ml VEGF in 2.5 mg/ml collagen I gel and 20 ng/ml VEGF + 500 ng/ml Ang 1 in 2.5 mg/ml collagen I gel.

Condition #	VEGF	Ang 1	Collagen Density
A	20 ng/ml	500 ng/ml	2 ng/ml
B	40 ng/ml		2 mg/ml
C		500 ng/ml	2 mg/ml
D	40 ng/ml		2.5 mg/ml
E	20 ng/ml	500 ng/ml	2.5 mg/ml

Table 2: Experimental conditions used for all assays in the characterizing study

For the characterizing study, seven conditions were used (recorded in table 3) : (1) 40 ng/ml VEGF , (2) 40 ng/ml VEGF + 100 ng/ml Ang 1; (3) 40 ng/ml VEGF + 500 ng/ml Ang 1; (4) 10 ng/ml VEGF + 100 ng/ml Ang 1; (5) 10 ng/ml VEGF + 500 ng/ml Ang 1; (6) complete media with no VEGF or Ang 1; (7) basic media with 500 ng/ml Ang 1; and (7) 40 ng/ml VEGF. These conditions will henceforth be referred to as 1-7, respectively.

Condition #	VEGF	Ang 1
1	40 ng/ml	-
2	40 ng/ml	100 ng/ml
3	40 ng/ml	500 ng/ml
4	10 ng/ml	100 ng/ml
5	10 ng/ml	500 ng/ml
6	-	-
7	-	500 ng/ml

Table 3: Experimental conditions used for all assays in the characterizing study

vii. Cell Seeding

Cell seeding density of 2 x 10^6 cells per ml was used for every device. One hour after seeding the cells in complete media, the media in the channel opposite the channel with cells was changed to the condition media and the media in the channel with cells was changed to basal media EGM-2MV growth media (Cambrex, USA). This process ensured that all unattached cells were washed away. This was recorded as time point 0. At 24 hours, the condition media was changed, and at time 48 hours, the cells were fixed using 4% PFA (for 30 minutes). Our preliminary experiments showed that under certain conditions capillaries formed within a span of 24 hours. This result, and given the need for a large number of experiments, led us to select an experimental duration of 48 hours long. Phase contrast and confocal microscopy were used to monitor capillary development under different treatment conditions.

viii. Imaging

a) Confocal vs. Phase Contrast

Time lapse confocal imaging enables a better understanding of the three dimensional structure of the capillaries as they evolve in space and time. While this tool is very useful, it does bring to light some concerns like the effect of dyes and photobleaching on cells. Nevertheless, through careful design of experiments and controls, it can be used to exploit cell population behaviors like angiogenesis. It also enables one to distinguish between a capillary growing in 3D in the gel and one growing along the coverslip surface. Also, by doing some confocal imaging we had established that most of the capillaries were growing in the gel and not along the glass, as is demonstrated in figure 17. The imaging protocols are listed below and the method used for the different experiments is listed in the next section.

Confocal Imaging

All time lapse imaging and some end point imaging was done using an Olympus point scanning confocal microscope.

Dyeing Cells for Live Imaging

In some cases, time lapse, live cell imaging was performed to gain insight into the overall experimental process. For these tests, cells are first grown in 250 ml flasks. Sufficient amounts of EGM2MV medium and 1X PBS are warmed in a water bath. 15 mL tube wrapped with aluminum foil is prepared for the dye-containing medium. Once the medium and PBS are warmed, the dye is diluted in the medium to the desired working concentration (stock: 10 mM; working concentration: 20 μM). Cells are washed with ~ 2 ml/flask PBS, then ~ 2ml dye-containing medium is added to each flask. The flasks are then covered with aluminum foil. The cells are incubated at 37°C for 30 minutes. After 30 minutes of incubation with dyed medium, the dye-containing medium is replaced with regular medium. The flasks are put back in the incubator at 37°C for another 30 minutes, after which they are washed with regular medium. The cells are then ready for seeding.

Phase Contrast Imaging

For most endpoint experiments, phase contrast microscopy was used. All phase contrast images were taken with a 20X or a 40X lens on a Nikon Eclipse Ti-U scope.

Procedure

1. Comparative Study

Device-making, cell-seeding and experimental procedures were carried out as outlined above. The experimental conditions used for this study are recorded in table 2. To image during the 48 hour experiments, cells were stained with 0.01μM Hoestch nuclear dye and 20μM CMFDA (CellTracker™ Green CMFDA (5-chloromethylfluorescein diacetate); Molecular Probes, Invitrogen, C7025) cytoplasmic dye before seeding. Confocal microscopy was used to monitor capillary development under different treatment conditions (see figure 17).

2. Characterizing Study

Three devices were used for each condition (see table 3). Five gel regions from each device were randomly chosen for all of the analyses. Phase contrast microscopy was used for this study. Most of the imaging was done with out focusing on a single plane in order to identify the extent of the sprouts in the 3D gel region. Number of sprouts per gel region was calculated manually. ImageJ (NIH, Bethesda, MD, USA) was used for sprout length analysis. The lengths in all images were calibrated to the distance between the posts ~100 um. This was used as the inherent scale. Individual migrating cells and active cells (identified via morphology) were also enumerated for the different conditions. Tukey's range test with a family confidence of 95% was used to identify the statistical relevance of the different conditions on the sprout metrics.

Protocol for f-actin staining:

Several samples were fixed and stained to visualize actin and nuclei and thereby to identify the different cell characteristics. F-actin and nuclear staining was performed after fixing samples

with 4.0 % PFA (30 minutes). The fixed samples were rinsed twice with 1X phosphate buffered saline (PBS), treated with 0.1 % Triton-X (1-2 minutes), rinsed with 1X PBS, followed by the infusion of a mixture of DAPI and rhodamine phalloidin (30 minutes) and a final wash step with 1X PBS. Cells without any neighboring connecting cells were identified as 'individual migrating cells,' and cells with multiple extended processes were identified as 'active cells'. Figure 18a shows an example of end point actin/DAPI staining that was done to identify cell characteristics.

ix. Results

a) Comparative Study

The first set of results show that the likelihood of obtaining sprouts is similar to those in experiments in our simulations for certain ranges of the parameters. The goal of this study was to determine if the types of morphologies found in the microfluidic devices could be reproduced in the simulations. These probabilities are selected based on a trail and error approach, and intended simply to see if comparable morphologies could be obtained. We have explored the range of probabilities and identified combinations that depict sprout characteristics seen under certain experimental conditions (see table 2). These combinations are shown in Figure 19. Later in this chapter, a more rigorous method for obtaining parameter values is presented.

1. Sprout Morphology

In all the simulations, cells were seeded as a monolayer and a VEGF gradient was established from z=20 before the simulations were started. Simulations were run with different transition probabilities for $p_{Q\to Q}$, $p_{Q\to M(1)}$, $p_{Q\to P(1)}$, $p_{Q\to A}$ transitions.

Figures (19a,-e) are generated for five such sets of transition probabilities and include a pictorial representation of sprout formation under different conditions and phase contrast images of experimental conditions that give rise to similar sprout formation characteristics. The experiments were conducted in the microfluidic devices referred to above, with or without two important growth factors: VEGF and Ang 1. Various experiments conducted in the microfluidic device in our lab have demonstrated that capillary stabilization is achieved when Ang 1 is used in the media along with VEGF. Since the experiments in our lab have been limited to VEGF and Ang 1, it was decided to incorporate these two pro-angiogenic factors in the first stage of the modeling. It has also been shown that Ang 1 has an impact on VEGF signaling regardless of the presence or absence of Ang 2 (Zhu et. al., 2002). Ang 2 is a natural antagonist and disrupts blood vessel formation. As the primary goal of the study is to determine conditions that will result in the evolution of well-developed capillaries, it was decided to first focus on such factors. In our experience, high transition probability of migration and proliferation correspond to high concentrations of growth factors and matrix of optimal stiffness, while low probabilities correspond to lower concentration of growth factors and a softer or stiffer matrix. High concentration of Ang 1 implies a lower rate of regression due to capillary stabilization. These figures are included here to demonstrate that certain experimental conditions can be reproduced by some combination of transition probabilities. The exact matching of these probabilities to specific conditions will require further experimentation.

When the transition probabilities represent extreme states such as 85% migration / 5% proliferation / 5% quiescence / 5% proliferation, many migratory cells are seen that protrude far into the matrix. Under a different extreme state, e.g., 85% proliferation / 5% migration / 5%

quiescence / 5% proliferation, the entire monolayer starts to proliferate and forms large cell clusters. These extreme cases are not representative of any physiological condition but were conducted to demonstrate the range of applicability of the model. As observed in the figures below, longer sprouts are observed with higher migration probabilities, and almost no sprouts are observed when the cells have a higher probability to remain quiescent.

Sprout formation under conditions of VEGF (20 ng/ml) and high Ang 1 (500 ng/ml), which act as sprout-stimulating and sprout-stabilizing agents, respectively, in a collagen I gel made with concentration 2 mg/ml, as well as a simulation generated with transition probabilities that result in similar morphology to the above mentioned condition are shown in Figure 19a. The branching network is well-developed under such conditions. Simply by removing Ang 1 and increasing VEGF concentration, so that there is a high concentration of sprout-stimulating agent (VEGF 40 ng/ml) but no sprout-stabilizing agent, cell clusters and short branches are prevalent (Figure 19b). With only Ang 1 (500 ng/ml) present and no VEGF, the absence of a sprout-stimulating agent leads to relatively less sprout formation. Very few stable capillaries are observed relative to small sprouts and single migrating cells (Figure 19c). With only VEGF (40 ng/ml) and no Ang 1 in a stiffer collagen I gel (2.5 mg/ml) there is a sprout-stimulating agent but no sprout-stabilizing agent. But due to the stiffer gels, the cells find it harder to migrate; hence they cannot form many branches (Figure 19d). When both VEGF (20 ng/ml) and Ang 1 (500 ng/ml) are present in a stiffer gel (2.5 mg/ml collagen I) some capillary-like structures are observed, but fewer and longer branches and more cell clusters are observed at the monolayer than would be seen in a less stiff matrix under the same conditions (Figure 19e). In this case the branches have fewer cells per branch compared to the same growth factor combination in a softer matrix. These

sample results demonstrate that by proper adjustments of the parameters, the model can produce a variety of morphologies.

b) Characterizing Study

The phase contrast images obtained provide both a qualitative and quantitative understanding of sprout morphology as a function of media conditions. As observed in figures 20 and 21, the number and the length of sprouts are directly proportional to VEGF concentration. The sprouts appear better developed with increasing concentration of Ang 1. Tukey's range test with family confidence interval of 95% was used to identify conditions that are significantly different from each other.

1. Sprout and Cell Characteristics

Phase contrast images from fifteen gel regions from each of the seven conditions were processed for sprout characteristics (sprout number, branch number, number of anastomoses), sprout length, and cell characteristics (active cells, individual migrating cells). Here, an anastomosis is defined as the fusion of two sprouts. A caveat in all the measurement is that these are all 2D projections of 3D sprouting. For the conditions used in this study, the length of the sprout increases with increasing VEGF concentration. Thus, the longest sprouts are 72 μm (standard error of mean - 2.84 μm; standard deviation – 10.99 μm) and are observed with 40 ng/ml VEGF in the media. This length decreases by the addition of Ang 1, to 61 μm (standard error of mean - 3.64 um; standard deviation – 14.1 μm) with 100 ng/ml Ang 1 and to 56 μm (standard error of mean - 3.75 μm; standard deviation – 14.52 μm) with 500 ng/ml Ang 1. The sprouts formed with a high concentration of VEGF are not only longer but also form with a higher frequency. When

the VEGF concentration is decreased to 10 ng/ml, the sprouts are observed to be 42.19 μm (standard error of mean - 2.2 μm, standard deviation 8.52 μm) and 24.05 μm (standard error of mean - 1.53 μm, standard deviation – 9.8 μm) with 100 ng/ml and 500 ng/ml Ang 1 respectively. Ang 1, thus, appears to have a stabilizing effect on the endothelial cells, resulting in better developed but shorter sprouts.

For the conditions used in this study, the number of sprouts per gel region is proportional to VEGF concentration and is inversely proportional to Ang 1 concentration. While sprout number and sprout length are statistically different for the different conditions tested, branch number and number of anastomoses do not show any identifiable trend. All these experiments were analyzed with 2D phase contrast imaging and hence the anastomoses that have been identified could be a caveat of the methodology. An example of an anastomosis identified via phase contrast imaging is shown in figure 18b. One way of identifying possible trends in the future is to maintain the experiments for a longer time period and doing 3D confocal imaging. It is hypothesized that proliferation has a bigger impact on branching, as discerned from the agent-field model (Das et al., 2010). Hence, having an extended time course for the microfluidic experiments would better reflect the effects of the different factors on cell division and branching.

Ang 1 acts as stabilizing factor in many studies (Nakatsu et al., 2003) and in this instance increases individual cell stability as well. The number of cells that are identified as 'active' based on morphology (i.e. extended cellular processes) increases with increasing VEGF concentration and decreases with increasing Ang 1 concentration. Figure 22 shows the relationship of active and individual migrating cells on VEGF and Ang 1 concentration. VEGF, which is known to

increase cell permeability (Joško et al., 2000), also causes more individual migrating cells and active cells in the sprouts. An increase in the number of active cells correlates with the length of the sprouts, suggesting a direct relationship with cell activity (migrations and sprout development).

x. Conclusion

The generation of well-developed sprouts and understanding the conditions that result in such sprouts is very crucial to the field of tissue engineering. We have developed stable, well-maintained sprouts by using human microvascular endothelial cells in 2.5 mg/ml collagen I gel and by using media supplemented with 40 ng/ml VEGF and 500 ng/ml Ang 1 for two days. It has been shown that VEGF acts as an angiogenic factor and Ang 1 acts as stabilizing factor here as in previous studies (Nakatsu et al., 2003). Here we show that their roles are maintained in the 3D microenvironment, and the sprout characteristics obtained by using this baseline condition can be altered by changing the concentrations of these two growth factors in a systematic way.

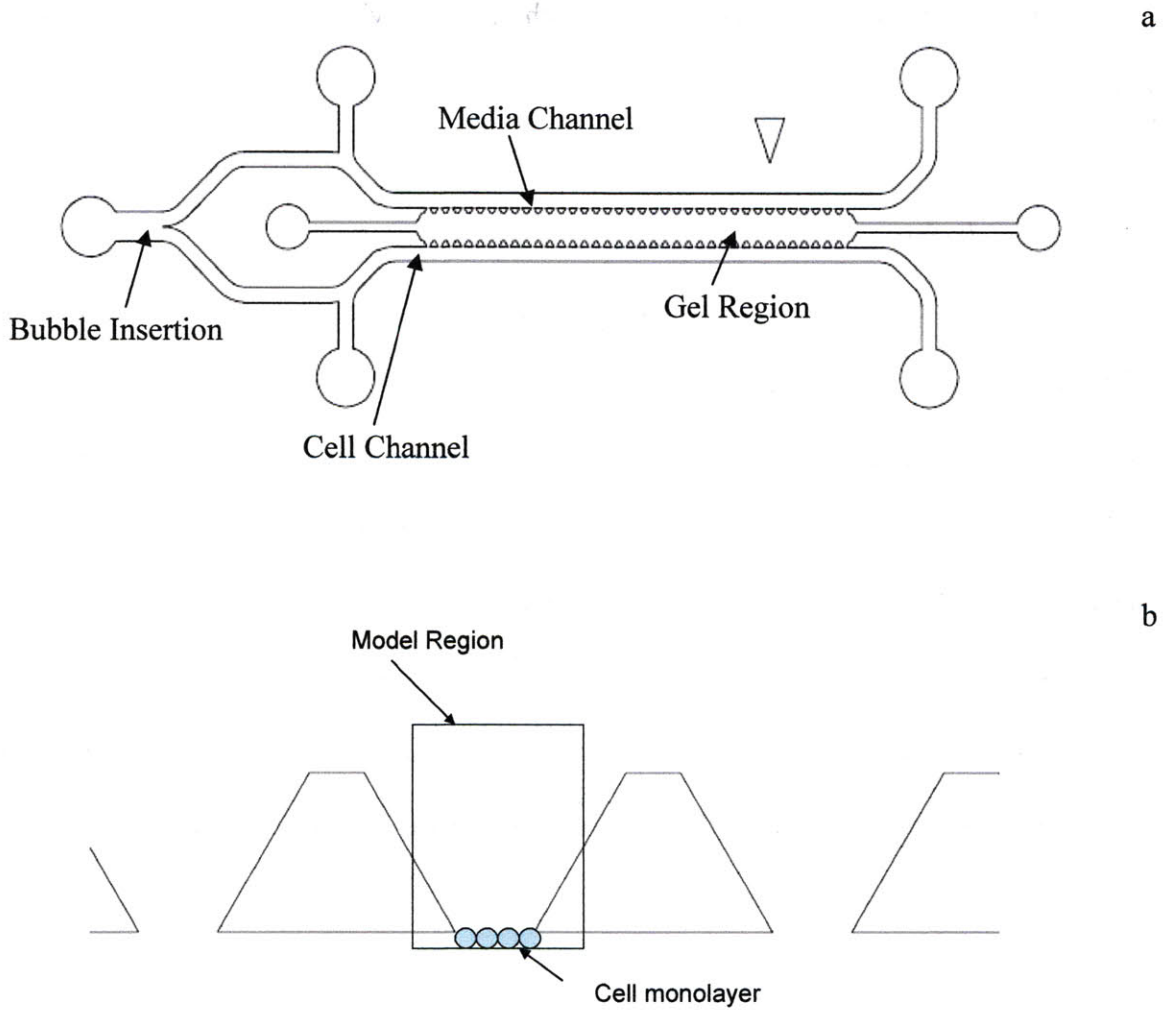

Figure 16: (a) Schematic of the microfluidic device used for the experiments showing the various regions. (b) The region of the device modeled during the simulations. Capillaries are formed from the monolayer seeded onto one surface of the gel.

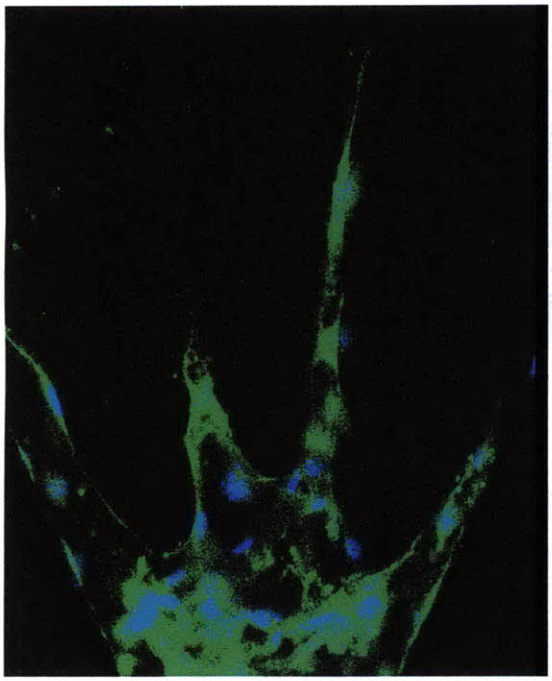

Figure 17: Confocal image showing the 3D nature of sprouts. This image was taken with live cell confocal microscopy under the experimental condition of 20 ng/ml VEGF + 500 ng/ ml Ang 1 in a 2 mg/ml collagen I gel. Cells were labeled with cytoplasm dye, 20μM CMFDA (green) and nuclear stain, 0.01 μM Hoescht (blue).

a

b

Figure 18: (a) End point actin (red) and nuclear (green) staining showing existing sprouts and individually migrating cells. The cells are seeded on the gel below with media channel above. This shows two neighboring gel regions with a post in the middle. The image was taken 48 hours under the experimental condition of 40 ng/ml VEGF in a 2.5 mg/ml collagen I gel. (b) An example of an anastomosis obtained by using phase contrast imaging. The image was taken 48 hours under the experimental condition of 40 ng/ml VEGF + 100 ng/ml Ang 1 in a 2.5 mg/ml collagen I gel.

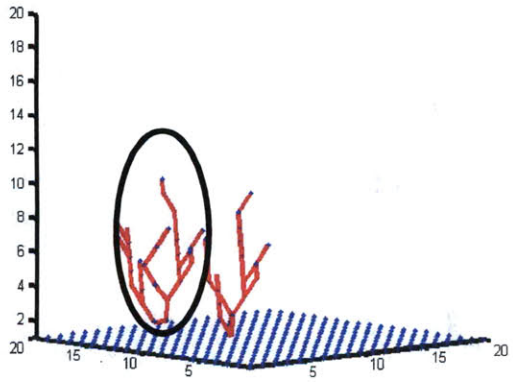
20
18
16
14
12
10
8
6
4
2
20
15
10
5
5
10
15
20

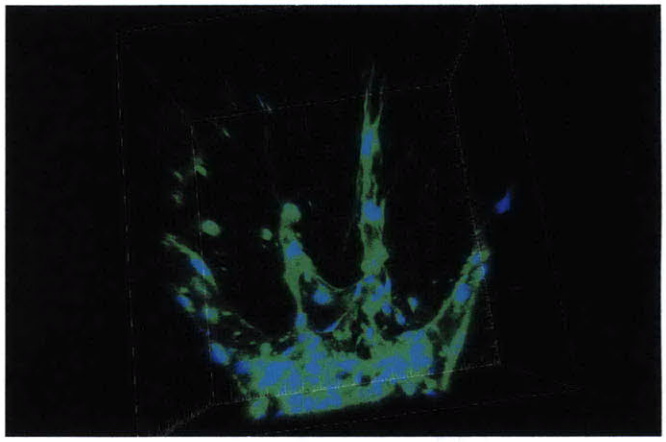

a

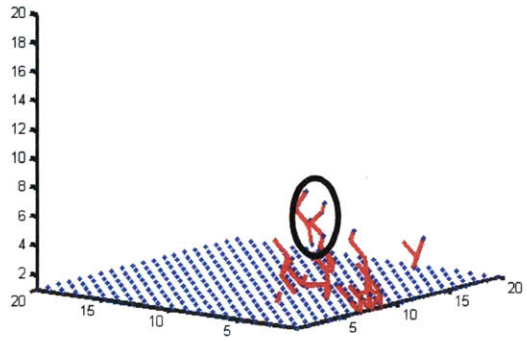
20
18
16
14
12
10
8
6
4
2
20
15
10
5
5
10
15
20

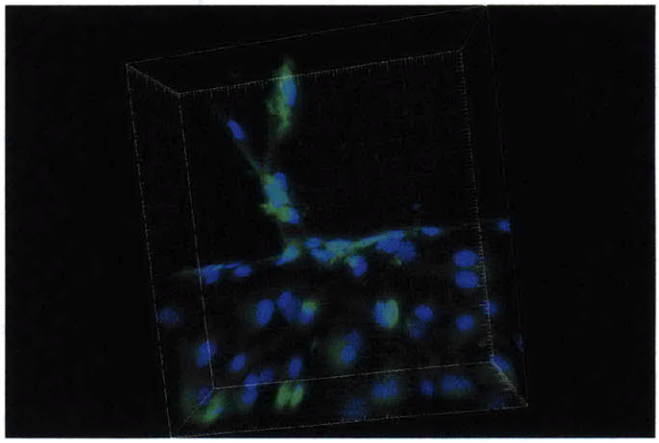

b

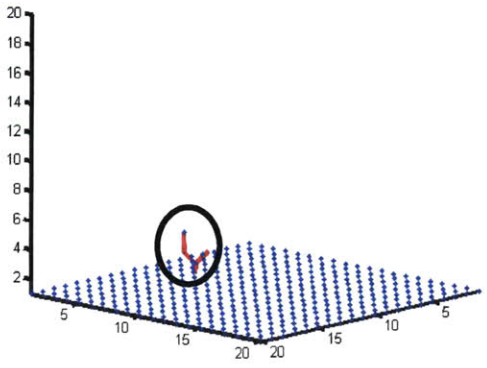
20
18
16
14
12
10
8
6
4
2
5
10
15
20
20
15
10
5

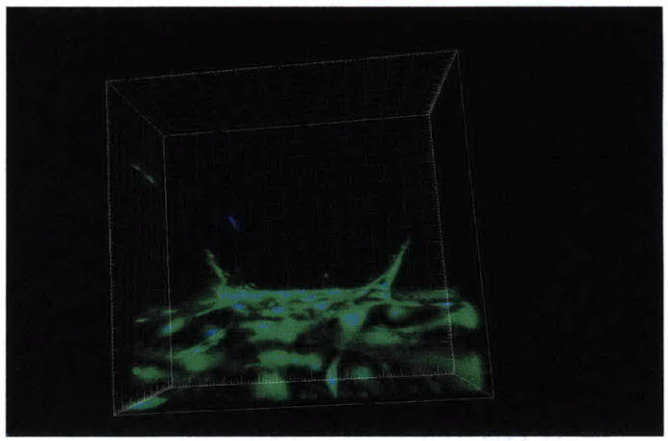

c

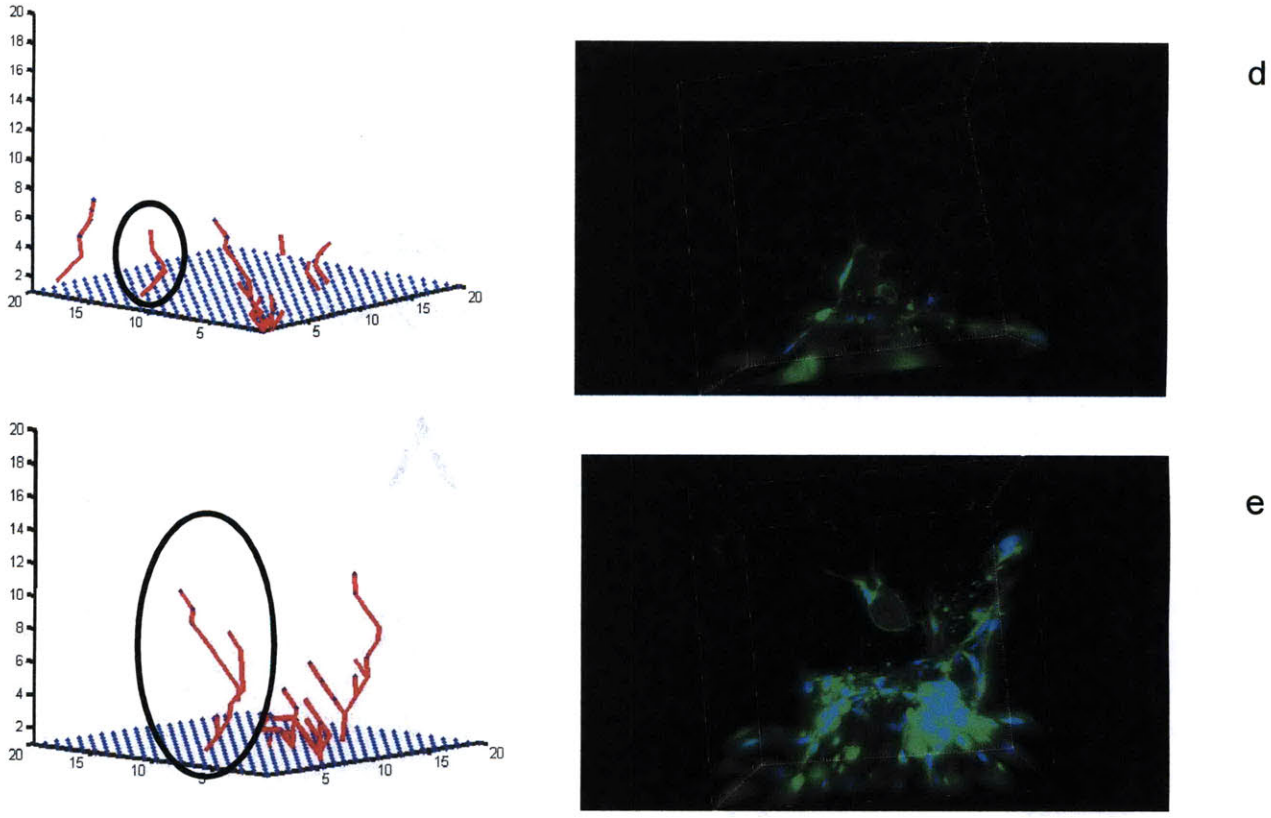

Figure 19: Simulation and experimental results for five transition probability sets -- [$p_{Q\to Q}$, $p_{Q\to M(1)}$, $p_{Q\to M(1)}$, $p_{Q\to A}$]

The x, y and z axes show the spatial coordinates of the device, which are normalized to the characteristic length of a cell (10 μm). The cell network grows upwards from a monolayer. (a) Transition probabilities = [0.5, 0.1, 0.35, 0.05] and an initial condition of uniform VEGF (20ng/ ml) and Ang 1 (500 ng/ml) in less stiff gel (collagen I concentration =2 mg/ml); (b) Transition probabilities = [0.7, 0.15, 0.1, 0.05] and an initial condition of VEGF (40 ng/ml) in less stiff gel (collagen I concentration = 2 mg/ml); (c) Transition probabilities = [0.85, 0.05, 0.05, 0.05] and an initial condition of Ang 1 (500 ng/ml) in less stiff gel (collagen I concentration = 2 mg/ml); (d) Transition probabilities = [0.80, 0.1, 0.05, 0.05] and an initial condition of VEGF (40 ng/ml) in stiffer gels (collagen I concentration = 2.5 mg/ml); (e) Transition probabilities = [0.7, 0.2, 0.05, 0.05] and an initial condition of VEGF (20ng/ ml) and Ang 1 (500 ng/ ml) in stiffer gels (collagen I concentration = 2.5 mg/ml).

(Das et al., 2010)

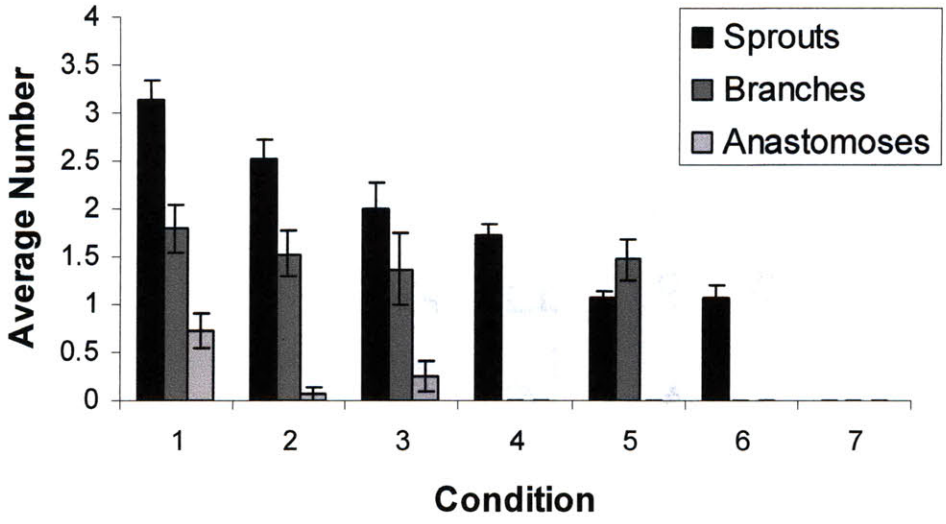

Figure 20: Average number of different sprout characteristics observed in microfluidic device under different experimental conditions. The experimental conditions are (1) 40 ng/ml VEGF; (2) 40 ng/ml VEGF + 100 ng/ml Ang 1; (3) 40 ng/ml VEGF + 500 ng/ml Ang 1; (4) 10 ng/ml VEGF+ 100 ng/ml Ang 1; (5) 10 ng/ml VEGF + 500 ng/ml Ang 1; (6) complete media with no VEGF or Ang 1; (7) basic media with 500 ng/ml Ang 1; (n =15 for each condition).

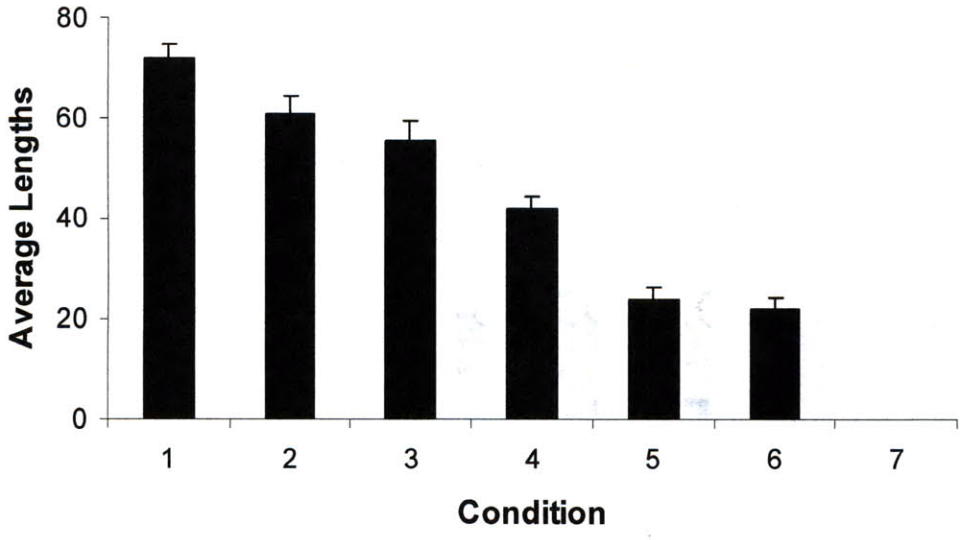

Figure 21: Average sprout lengths observed in microfluidic device observed under different experimental conditions. The experimental conditions are (1) 40 ng/ml VEGF; (2) 40 ng/ml VEGF + 100 ng/ml Ang 1; (3) 40 ng/ml VEGF + 500 ng/ml Ang 1; (4) 10 ng/ml VEGF+ 100 ng/ml Ang 1; (5) 10 ng/ml VEGF + 500 ng/ml Ang 1; (6) complete media with no VEGF or Ang 1; (7) basic media with 500 ng/ml Ang 1; (n =15 for each condition).

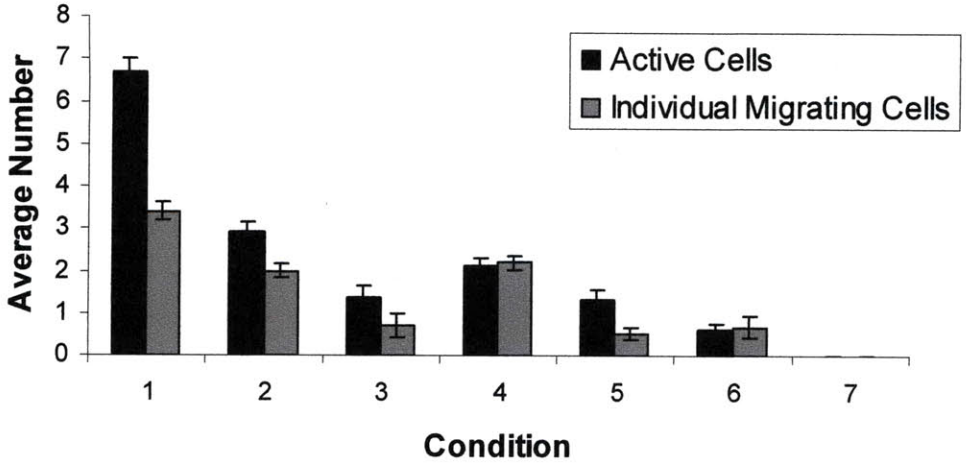

Figure 22: Cell characteristics observed in microfluidic device under different experimental conditions. The experimental conditions are (1) 40 ng/ml VEGF; (2) 40 ng/ml VEGF + 100 ng/ml Ang 1; (3) 40 ng/ml VEGF + 500 ng/ml Ang 1; (4) 10 ng/ml VEGF + 100 ng/ml Ang 1; (5) 10 ng/ml VEGF + 500 ng/ml Ang 1; (6) complete media with no VEGF or Ang 1; (7) basic media with 500 ng/ml Ang 1; (n =15 for each condition).

4. Experiment - Simulation Matching

i. Rationale

Models have been used to identify mechanisms and causes for the observations made in experimental settings for various biological processes. As detailed in chapter 2, many angiogenesis models have been developed with the ultimate goal of better understanding this process. The model proposed in this study provides insight into the relevant impact of various biomolecules on two main sub-processes: migration and proliferation. In chapter 3, we demonstrated that the model is capable of generating sprouts similar to those observed in experiments. We also showed that different sprout characteristics were observed when we systematically varied two angiogenic factors- VEGF and Ang 1.

In this chapter we will use the experimental data to calculate specific values for the transition probabilities in the model. We employ a form of Decision Tree Analysis (DTA) to achieve this. The methodology, assumptions and results of this process are explained in the next few sections (iii and iv). Finally, we use the model to predict the relative impact of a different agent on sprout formation by using the model and matching methodology described below. We decided to use an anti- angiogenic agent, PF4 for this. The signaling of PF4 is relatively unexplored and in an effort to support the ongoing work in the laboratory, we chose PF4 as the anti-angiogenic agent in our experiments. The results obtained are recorded in section v.

ii. Assumptions

Some specific assumptions were made in this study aimed at relating model morphologies to experimentally derived ones.

- A two day time period for simulations and experiments would be sufficient for obtaining insightful data and making substantiated conclusions.
- End point data would be sufficient to make important observations and draw valid conclusions.
- The information lost due to the binning method adopted will not be crucial to identifying trends from the data.

iii. Adapted Decision Tree Analysis

a) Background

Various modeling techniques have been used to understand the relationships between different external cues, signaling molecules and phenotypic responses observed in cells. They range from the very deterministic ordinary differential equation type modeling to fuzzy logic, partial least square regression (PLSR), Boolean and Monte Carlos methods (Aldridge et al., 2009; Kumar et al., 2007; Whitman et al., 2009; Yoon et al., 2009). While some of these methods are very mechanistic and need a great deal of biological information, others are more data-driven. In the context of the current problem, a data-driven model is more appropriate because of the lack of knowledge regarding detailed mechanistic pathways and the inherent stochasticity in the process. Since many growth factors and mechanical forces cause similar phenotypic behaviors in cells via different signaling cascades, it is important to determine which responses are affected by the different cues when certain phenotypes are observed. Huang and Ingber (2000) used boolean modeling to process cellular information in order to show certain growth factors and mechanical forces that affect shape distortion as well as cell growth, differentiation and apoptosis via certain signaling molecules.

Decision Tree Analysis (DTA) is similar to boolean modeling, but quantitatively accounts for all possible combinations of input and all outputs that can be expected from them. Different paths along DTA may have different concentrations of these cues. This is useful when molecules in different concentration ranges cause different outcomes. Hua et al. (2006) used DTA to analyze the Fas apoptotic pathway by clustering and classifying cellular outputs and determining which combination of input signals (molecule concentrations) would lead to a specific output cluster.

b) DTA Applied to Experimental Data

For the purposes of comparing experimental results to simulation predictions, we decided to select the two most robust sprout characteristics obtained from microfluidic experiments – sprout number and sprout length. We have adapted a part of the DTA methodology to classify sprout behavior as a function of different input conditions. We used it to identify the different groups of classification and then developed a probability distribution graph of the experimental observations. The built-in Matlab function *classregtree* was used to identify the different nodes, and then the nodes were grouped into three or four buckets to account for the variability in experimentation. Sprout lengths were classified as either (a) less than 30 μm, (b) 30-60 μm, or (c) greater than 60 μm (see figure 24). Sprout numbers were classified as either (a) zero, (b) one, (c) two, or (d) greater than two sprouts (see figure 23). We then plotted experimental observations under these three (or four) categories and obtained an imprint of sprout length distribution for all different input conditions by plotting histograms of their relative distribution in the different categories. Experimental imprints are obtained under various conditions for sprout number and sprout length, respectively (Figures 23-25).

The cost functions were ascribed values of either 1 or 2 depending on whether the histograms were a result of a change in only Ang 1 concentration, or a change in both VEGF and Ang 1 concentrations, respectively. Thus, in figures 23-25, the cost function of going from imprint I to imprint III is 1 while that of going form imprint I to imprint V is 2. If we consider those imprints with the cost function 1, i.e. those with the same VEGF concentration, and plot the changes in the histograms, figures 23b and 24b are obtained for sprout number and sprout length. This shows that the cost function affects the trends of the observations in a similar manner. When the VEGF concentration is kept constant and Ang 1 concentration is increased, both the number of sprouts and sprout length tend to decrease.

The use of DTA in this case was possible because the use of two factors (VEGF and Ang 1) ensured that identifying the different brackets was feasible. However, if the number of conditions increases, then the results will be resemble a continuous function more than a discrete function and in that case DTA will no longer be useful. However, the exact number of factors at which DTA will break down depends on the data obtained and can only be ascertained after observing them.

c) Applied to Simulation

The agent-field model presented in chapter 2 (Das et al., 2010) was used to understand the effect of these different conditions on migration and proliferation. The simulation results were obtained by systematically varying the transitional probabilities. For each set of transitional probabilities, the sprout length and number were classified into the groups identified above and a probability distribution graph was generated for each of them. The best R^2 fit of the simulation to

experiment for each of the six conditions (no sprouts were observed in condition 7, implying a 100% transition to quiescence) are shown in figure 26. The best simulation condition was identified as the one that had the highest average R^2 value for both the length and the number of sprouts.

iv. Statistics- R squared matching

The imprints of sprout number and sprout length obtained from each experimental condition were matched with the corresponding ones from all the simulations. The R^2 was calculated for every pair, and the transition probabilities in the simulation with the highest average R^2 value for sprout length and sprout number were selected as the best match. This process will be useful in identifying the effect different conditions have on the probability to migrate and proliferate and give an insight into the complicated process of capillary formation.

The transition probabilities identified as a function of changing concentrations of VEGF and Ang 1 are shown in figure 28 ($R^2 \sim 0.82$- 0.99). Ang 1 affects both, the transition to migrate and the transition to proliferate. However, its effect on the transition to proliferation appears to be more pronounced at higher VEGF concentrations. It is possible that minimum a VEGF concentration is required i.e. there is a VEGF threshold for positive Ang 1 activity. While VEGF has a definite impact on the transition to migrate, it does not seem to have a relative effect on proliferation. Thus, it appears that the impact of VEGF on the morphology of the sprouts is via cell migration instead of cell proliferation. One can imagine the probability distribution to be altered when the cells are seeded on a collagen gel of different density. These results suggest that the effect of

certain angiogenic factors on migration and proliferation is dependent not only on their concentration but also the relative concentration of any other factor present in the media.

v. Understanding Impact of Anti-angiogenic Factors

a) Rationale

The process of angiogenesis is a balance between pro and anti angiogenic factors. Sprout characteristics are a function of the relevant concentration of these biochemical factors in addition to biomechanical factors such as matrix stiffness, presence or absence of flow and matrix composition. Since all previous experiments were conducted using pro-angiogenic factors, we decided to apply the model to test a different class of growth factors. Several anti-angiogenic factors are known to have a significant impact on sprout formation. The next few sub-sections will outline the details of the one we chose- Platelet Factor 4 (PF4), the methodology and results obtained from the experiments. Our objective is to test the hypothesis that the computational model as developed can be used to identify the mechanism of action of new pro- and anti-angiogenic factors.

b) Background

Many anti-angiogenic factors have been studied for the past several decades. The relative levels of pro- and anti-angiogenic factors results in different capillary morphologies. Some of the common anti-angiogenic factors are endostatin, thrombospondin 1 (TSP 1), thrombospondin 2 (TSP 2), vasostatin, angiostatin, osteopontin and platelet growth factor 4.

Endostatin, an inhibitor, is a 20 kDa COOH-terminal proteolytic fragment (183 amino acid) of collagen XVIII (O' Reilly et al., 1997). It is a specific endogenous inhibitor of endothelial cell

proliferation, migration (Eriksson et al., 2003), and vascular permeability (Takahashi et al., 2003; Celik et al., 2005). *In vitro* inhibition of endothelial cell (HUVEC) migration by endostatin has been previously demonstrated and the maximum inhibitory effect was obtained using 0.2 μg/mL of endostatin. Lower and higher concentrations led to a decrease in inhibition activity (Celik et al., 2005). The possible cell biological mechanisms underlying the anti-angiogenic effects of endostatin include inhibition of endothelial cell migration, induction of cell cycle arrest, and promotion of apoptosis. Vasostatin is known to inhibit cell proliferation of endothelial cells while angiostatin inhibits cellular proliferation and induces apoptosis. TSP 1 and TSP 2 affect cell migration, cellular proliferation and cellular adhesion and osteopontin inhibits integrin signaling.

Platelet-derived chemokines have been found to modulate several processes in the vasculature, such as atherosclerosis and angiogenesis (Slungaard, 2005; Hundelshausen, 2007). PF4 is a chemokine that has been shown to have an anti-angiogenic effect *in vitro* and *in vivo* (Gengrinovitch et al, 1995; Maione et al., 1990). It is released in high quantities during inflammation but highly purified PF4 lacks chemotactic activity for neutrophils, monocytes, T cells, or any cell population tested so far (Hundelshausen, 2007).

Literature has shown that PF4 impacts both migration and proliferation, but its relative impact on these sub-processes at different concentrations is not well known. Additionally the cell type we are working with, highly express PF4 receptors. This model can be used to understand the relative impact of PF4 at different concentrations on the process of angiogenesis and, more specifically, its relative effect on the sub processes: migration and proliferation. This is made

possible by matching the sprout morphologies obtained in experiments to those obtained in simulations in a manner similar to the description in section iv. Our hypothesis is that by identifying the transition probabilities that give the best fit for morphologies obtained with different PF4 concentrations, we can determine its relative impact on migration and proliferation.

c) Experiments

1. Rationale

The same microfluidic device (see figure 16) was used to assess the effect of PF4 on sprout morphology. The underlying reasoning is that *in vitro* experiments can be conducted in a controlled manner, and every addition to the cell growth media will be accounted for.

2. Methods

The microfluidic experiments were conducted as outlined in chapter 3. We then added two different concentrations of PF4, either 10 ng/ml or 1000 ng/ml, to the media along with 40 ng/ml VEGF and let the cell grow for two days. The devices were fixed and imaged as detailed in chapter 3. The number and average length of sprouts per gel region was quantified, and the imprints were obtained like those for the other conditions.

3. Analysis

Phase contrast images were obtained for fifteen gel regions from three microfluidic devices for each condition. Number of sprouts per gel region was quantified, and ImageJ (NIH, Bethesda, MD, USA) was used to measure sprout lengths.

d) Simulation Matching

The best R^2 value match was determined for the imprint database created by varying the transitional probabilities in the model. Figure 27 shows the best matches. As before, two variables were used for determining the best experiment- simulation fit- sprout number per gel region and sprout length. Figure 27 was made by plotting the distribution of these two variables obtained experimentally in the previously determined discrete bins and finding the best R^2 match from the simulations. The transition probabilities that relate to the experimental condition with 40 ng/ml VEGF + 10 ng/ml PF4 are the same as those that relate to the experimental condition 40 ng/ml VEGF from the previous experiments, as expected. In contrast, the transition probabilities that relate to the experimental condition 40 ng/ml VEGF + 1000ng/ml PF4 show a decrease in the transition to migration as compared to those that relate to the experimental condition 40 ng/ ml VEGF.

As shown in figure 28, PF4 does not exhibit a very effective anti-angiogenic characteristic at a low concentrations in the range of 10 ng/ml. However, at higher concentrations of 1000 ng/ml, it has a relatively large effect on migration of cells and prevents the formation of long capillaries and high number. This is apparent in a change in the M:Q transition probability from 20:75 to 10:85. The value of P:Q remains unchanged at this concentration change suggesting that PF4 has little effect on proliferation rates. It should be noted that all transition probabilities remain unchanged when only 10 ng/ml PF4 is used in the media. Thus, PF4 could also be an effective anti-angiogenic factor at a concentration above a certain threshold. This does not imply that it has no effect on proliferation. It just indicates that its effect on migration is relatively more pronounced as it is reflected by a 50% reduction in transition to migrate in the simulations.

vi. Conclusion

A major driving force in this study is the use of the model-experiment interplay in understanding the angiogenic response in a closely regulated platform. Much can be learned by using an *in vitro* model in collaboration with a computational model, with the objective of providing validation and of implementing feedback control over a prototypical biological process. While various models have been developed over the last few decades, none are designed alongside *in vitro* experimental assays. This gives us the ability to exert tight control over a small number of influencing factors.

This methodology provides us with a useful tool for discerning the impact of different growth factors on the process of cell migration or proliferation as they alter general sprout morphology. Addition of a different growth factor to the medium during the course of the two-day microfluidic experiment will change the sprout morphology imprint obtained in the end. By finding the best matching simulation imprint from the agent-field model, we can identify the impact of this specific growth factor on both migration and proliferation.

This was demonstrated in the case of PF4. The initial hypothesis based on literature survey was that PF4 affects both migration and proliferation, but to different extents and at different concentrations. To test this hypothesis and to extract additional information, we decided to use the model we have developed in conjunction with the microfluidic experiments described in chapter 3. As shown in figures # 12-14, the sprouts with different characteristics can be grouped as a function of different M/Q and P/Q ratios. In the case of the experiments with PF4, we want

to identify the change in the transition probabilities as a result of different chemokine concentrations. This will help us to identify the impact on PF4 on the sub-processes of angiogenesis. Once we have this information, we can direct the focus of future signaling experiments to focus on either the migrating nodes or the proliferating nodes.

As shown in figures # 27 and 28, we identify that at small concentrations, this chemokine has a negligible effect on sprout characteristics. However, at higher concentrations and in the presence of high VEGF, it acts as an anti-angiogenic agent by negating the effect of VEGF and hampering cell migration. The fact that the transition to migration was decreased while the transition to proliferation was not affected at high PF4 concentrations enabled us to gain this insight. Thus, the future signaling experiments should focus on the migration pathway nodes, especially to identify the mechanism of PF4 impact at high concentrations.

While such experiments and simulation matching algorithm was only done for PF4, one can adapt this process to various other molecules and possibly identify the effect of different pro and anti-angiogenic factors on angiogenesis. This can be useful to gain a first round insight into possible mechanisms of newly identified factors and drugs and also in the design of future exploratory experiments.

It should be noted that these results pertain to the specific microfluidic device we use and the very controlled experimental conditions practiced in the lab. Their generality and adaptability to other platforms remains to be validated. Nevertheless, they provide an insight in to emergent behavior observed under controlled conditions.

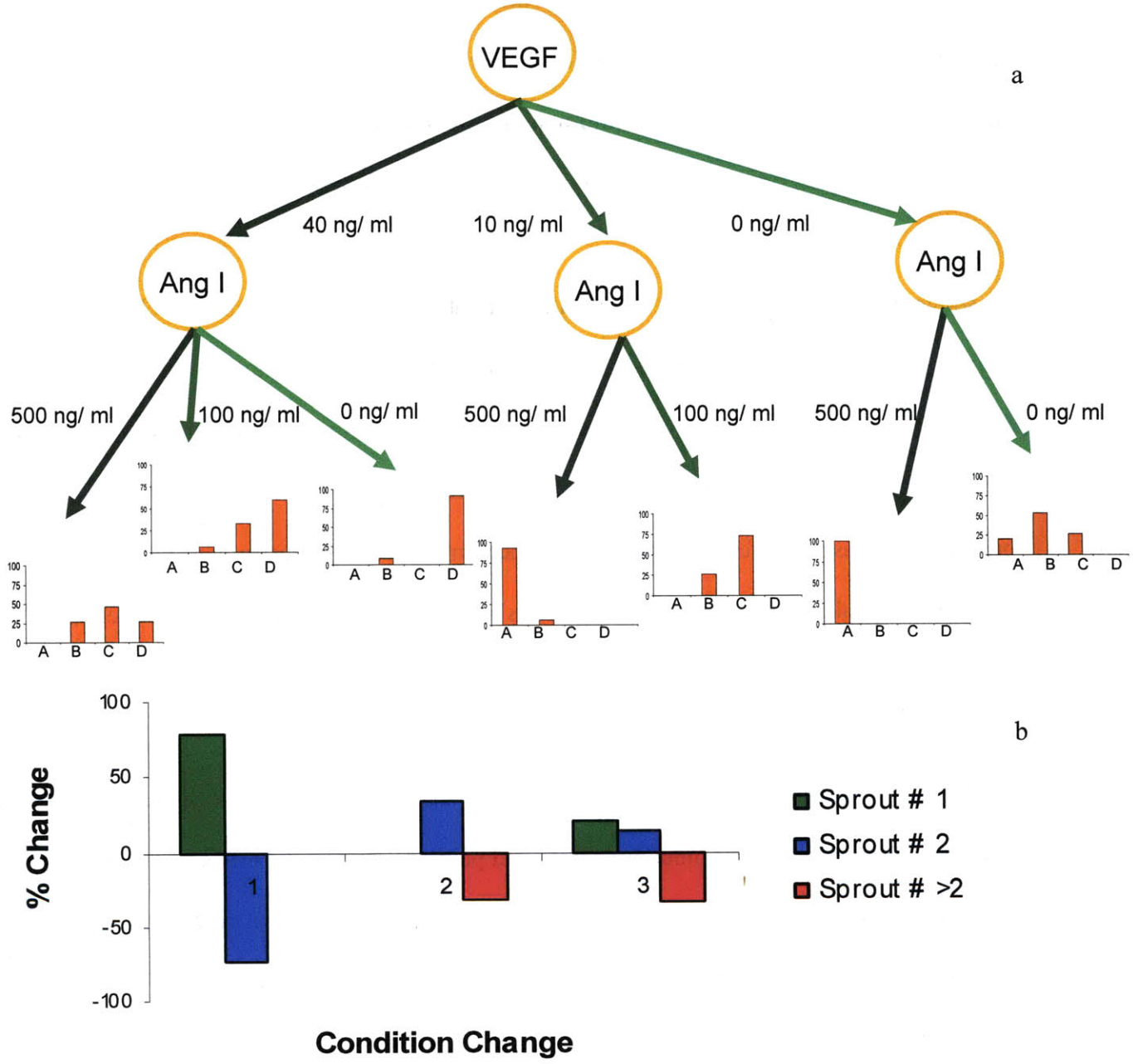

Figure 23: (a) Imprints of the distribution of sprout number per gel region [(A) zero, (B) one, (C) two, (D) greater than 2] as a function of different concetrations of VEGF and Ang 1. (b) Change in the percentatge of sprout number per gel region when cost function is one i.e. the VEGF concentration is fixed and the Ang 1 conetration increases. 1: VEGF 10 ng/ ml and Ang I changed from 100 ng/ ml to 500 ng/ ml; 2: VEGF 40 ng/ ml and Ang I changed from 0 ng/ ml to 100 ng/ ml; 3: VEGF 40 ng/ ml and Ang I changed from 100 ng/ ml to 500 ng/ ml.

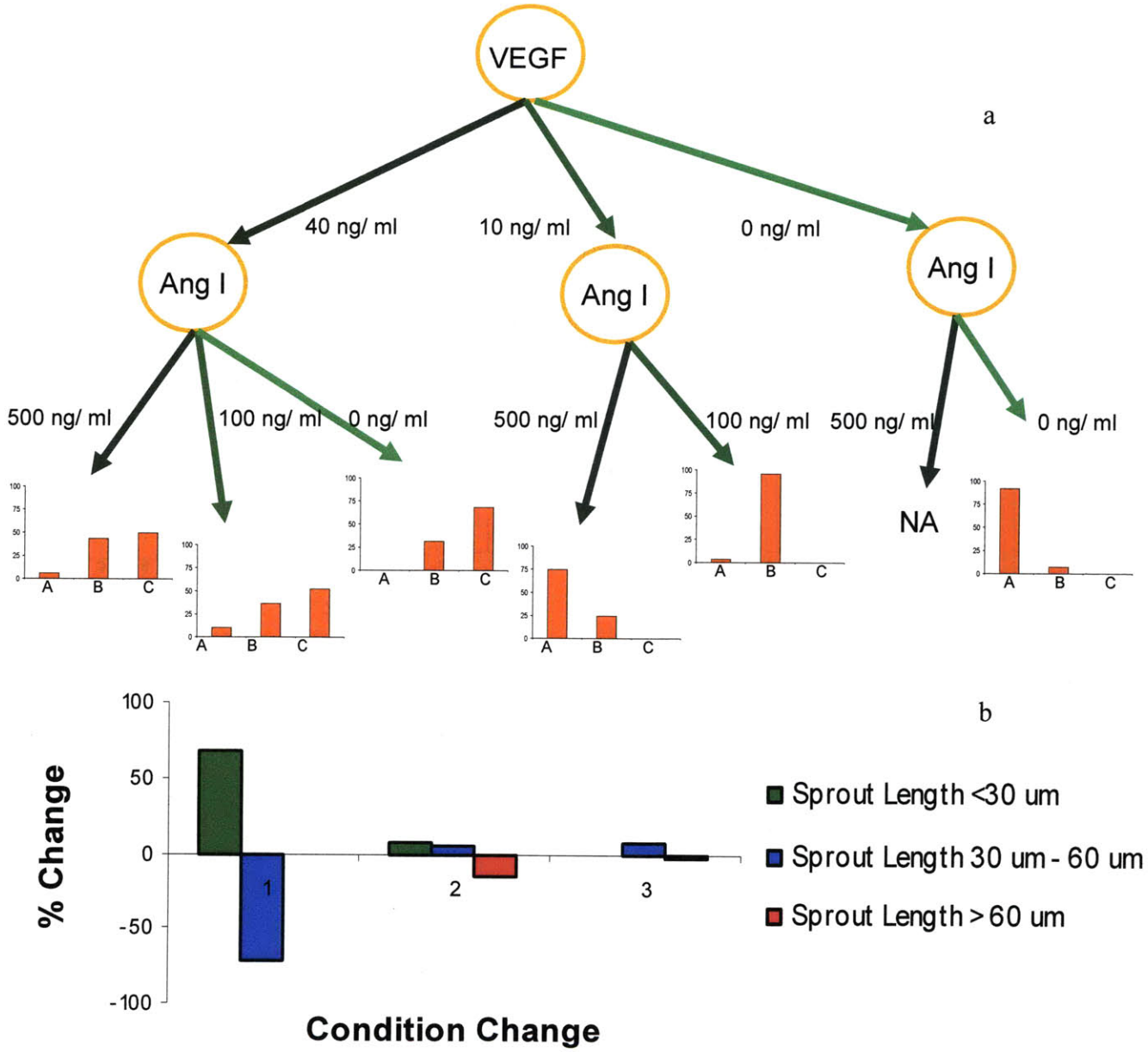

Figure 24: (a) Imprints of the distribution of sprout lengths [(A) < 30 μm (B) 30-60 μm , (C) > 90 μm] as a function of different concetrations of VEGF and Ang 1. (b) Change in the percentatge of sprout lengths when cost function is 1, i.e. the VEGF concentration is fixed and the Ang 1 concentration increases. 1: VEGF 10 ng/ml and Ang I changed from 100 ng/ml to 500 ng/ml; 2: VEGF 40 ng/ml and Ang I changed from 0 ng/ml to 100 ng/ml; 3: VEGF 40 ng/ml and Ang I changed from 100 ng/ml to 500 ng/ml.

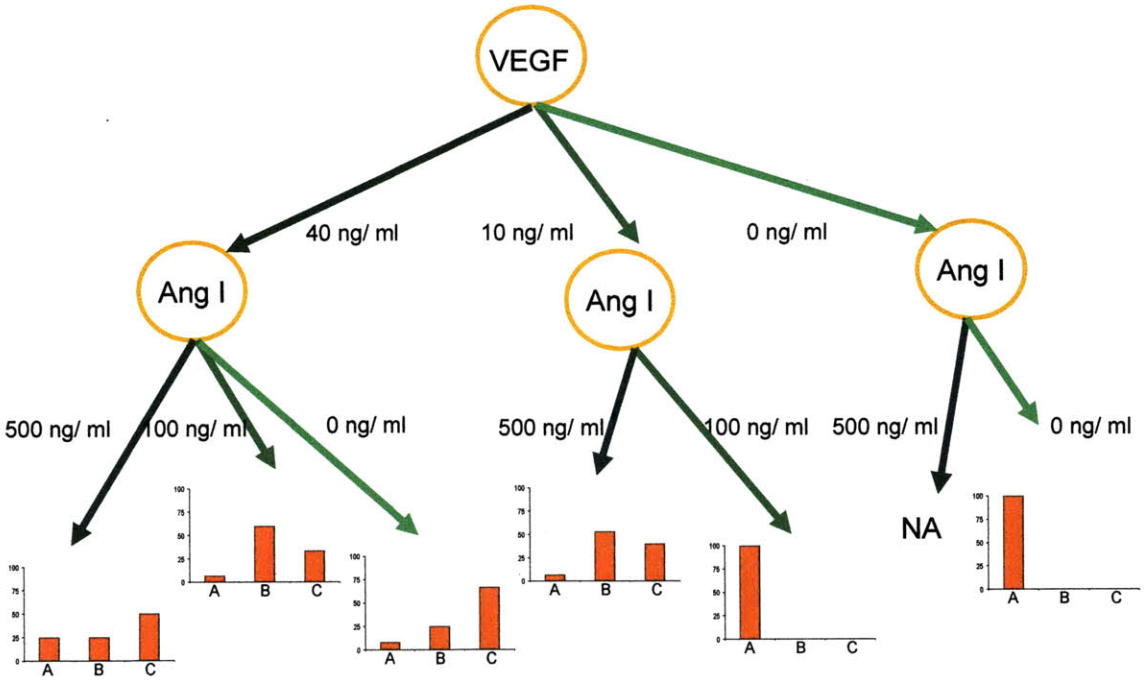
VEGF
40 ng/ ml
10 ng/ ml
0 ng/ ml
Ang I
Ang I
Ang I
500 ng/ ml
100 ng/ ml
0 ng/ ml
500 ng/ ml
100 ng/ ml
500 ng/ ml
0 ng/ ml
NA
A
B
C

a

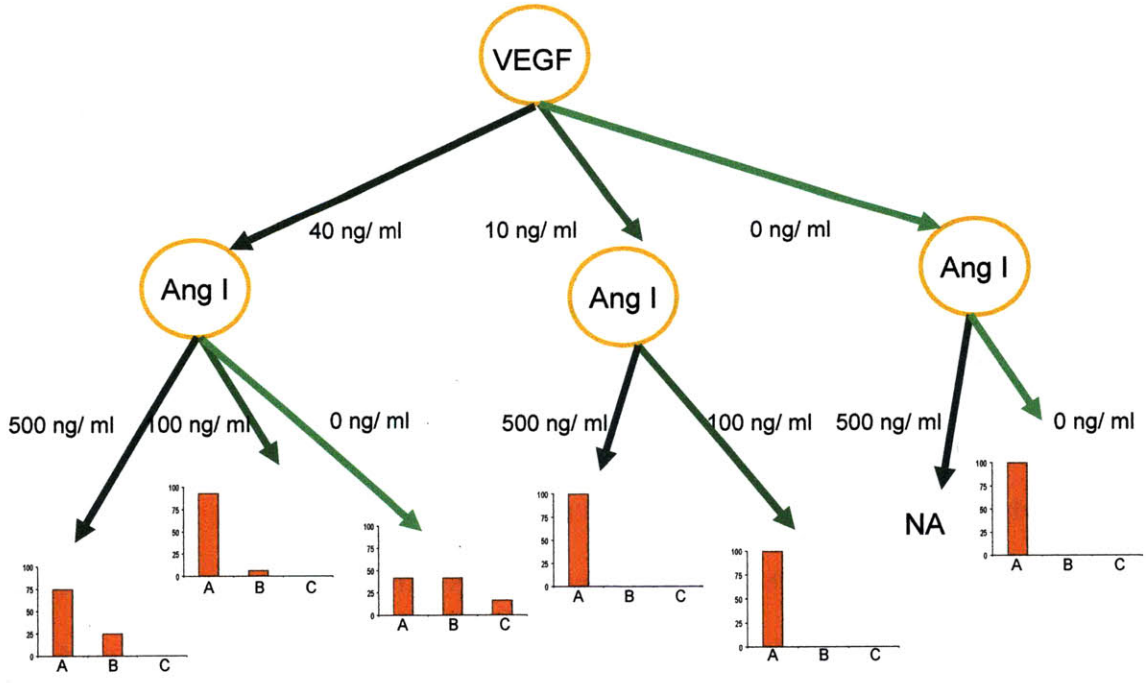
VEGF
40 ng/ ml
10 ng/ ml
0 ng/ ml
Ang I
Ang I
Ang I
500 ng/ ml
100 ng/ ml
0 ng/ ml
500 ng/ ml
100 ng/ ml
500 ng/ ml
0 ng/ ml
NA
A
B
C

b

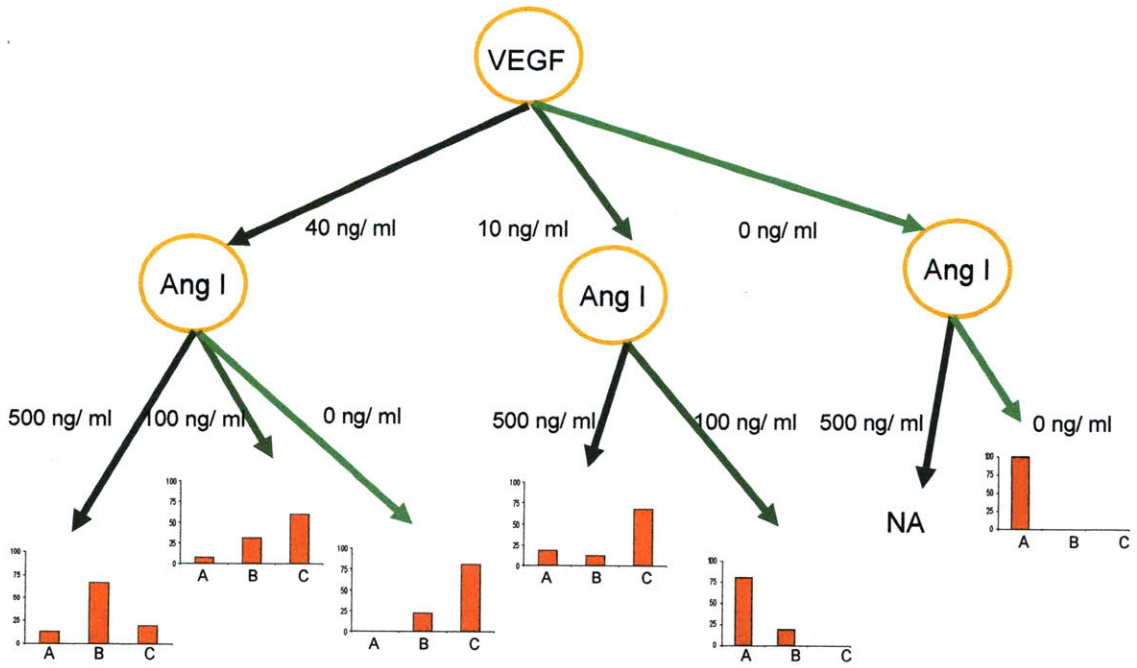

c

Figure 25: (a) Imprints of the distribution of branch number per gel region [(A) zero (B) one , (C) greater than one] as a function of different concetrations of VEGF and Ang 1. (b) Distribution of anastomoses per gel region [(A) zero (B) one , (C) greater than one] as a function of different concetrations of VEGF and Ang 1. (c) Distribution of sprout angles [(A) 60 degrees (along the posts) (B) 90 degrees , (C) < 90 degrees to the monolayer] as a function of different concetrations of VEGF and Ang 1.

a

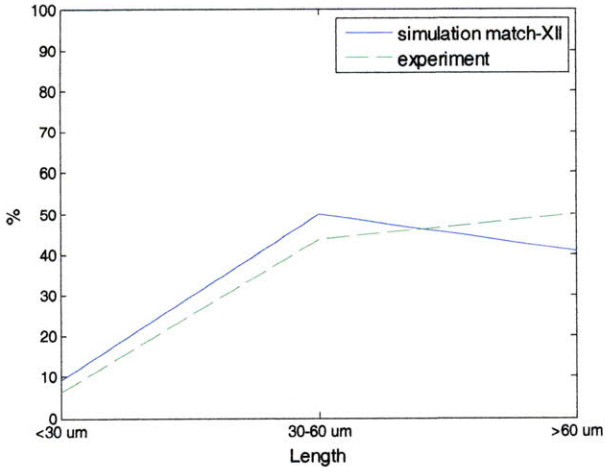
simulation match-XII
experiment
%
<30 um
30-60 um
>60 um
Length

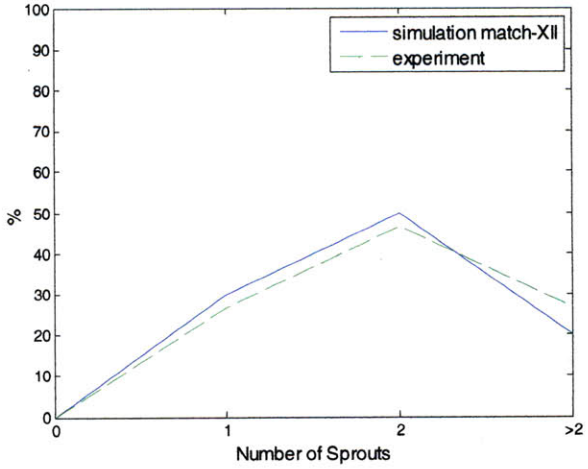
simulation match-XII
experiment
%
Number of Sprouts

b

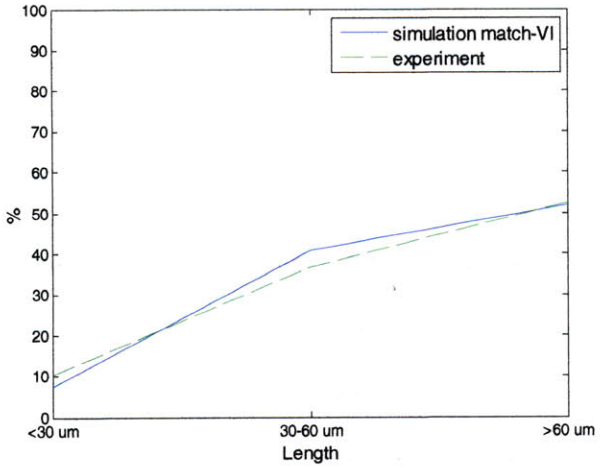
simulation match-VI
experiment
%
<30 um
30-60 um
>60 um
Length

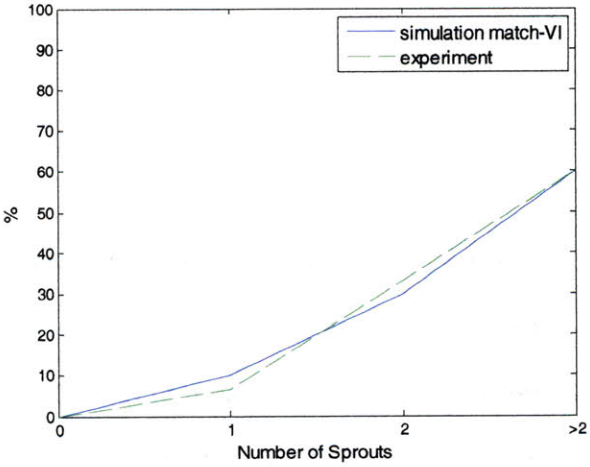
simulation match-VI
experiment
%
Number of Sprouts

c

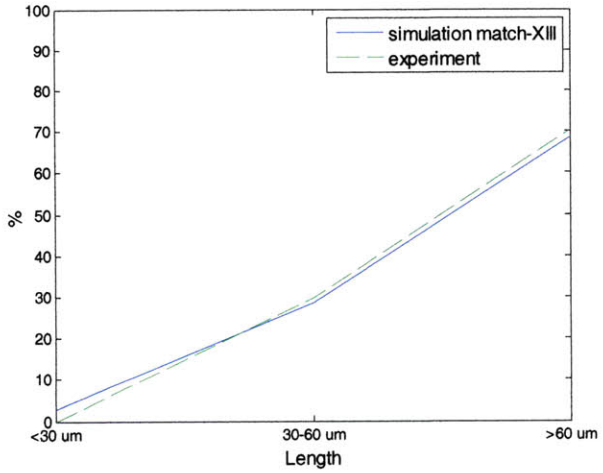
simulation match-XIII
experiment
%
<30 um
30-60 um
>60 um
Length

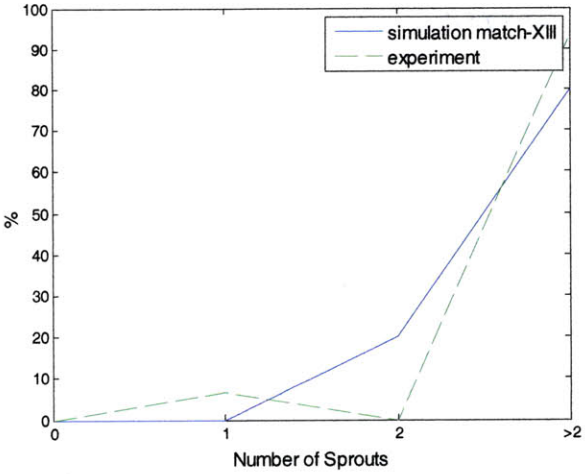
simulation match-XIII
experiment
%
Number of Sprouts

d

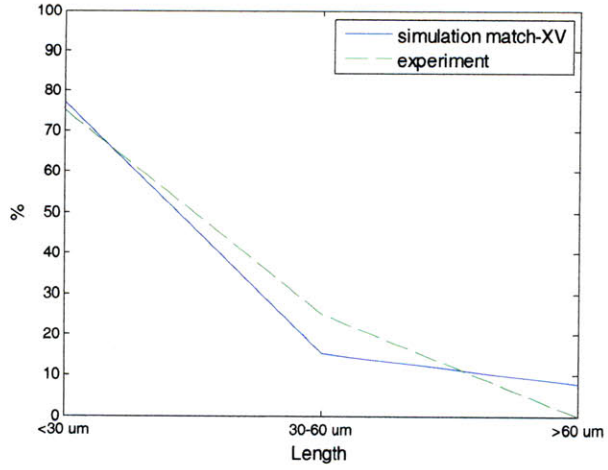
simulation match-XV
experiment
%
<30 um
30-60 um
>60 um
Length

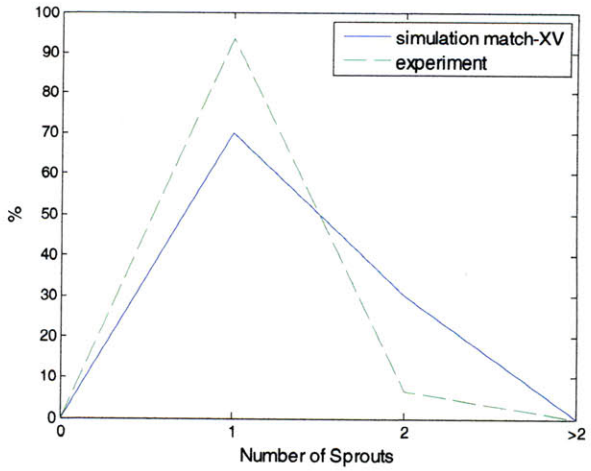
simulation match-XV
experiment
%
0
1
2
>2
Number of Sprouts

e

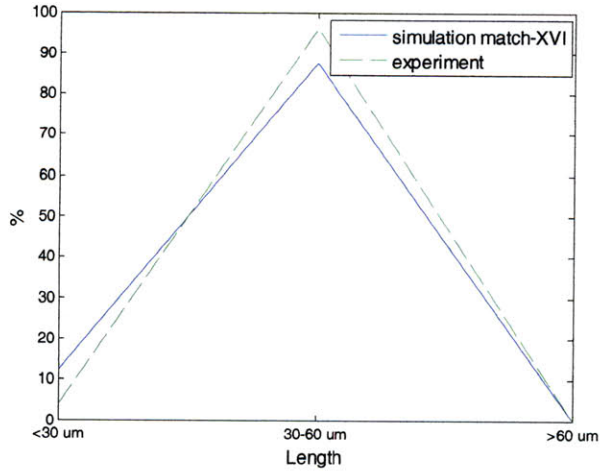
simulation match-XVI
experiment
%
<30 um
30-60 um
>60 um
Length

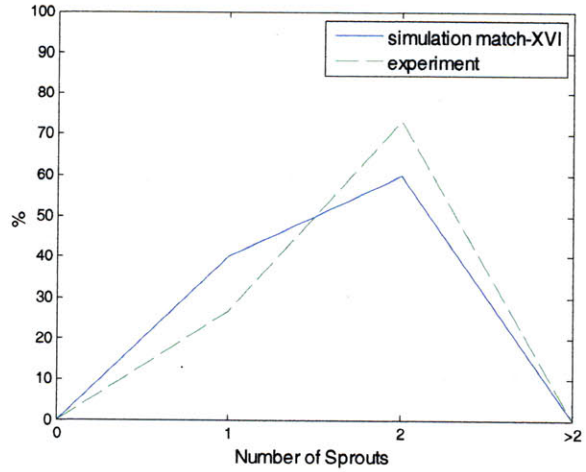
simulation match-XVI
experiment
%
0
1
2
>2
Number of Sprouts

f

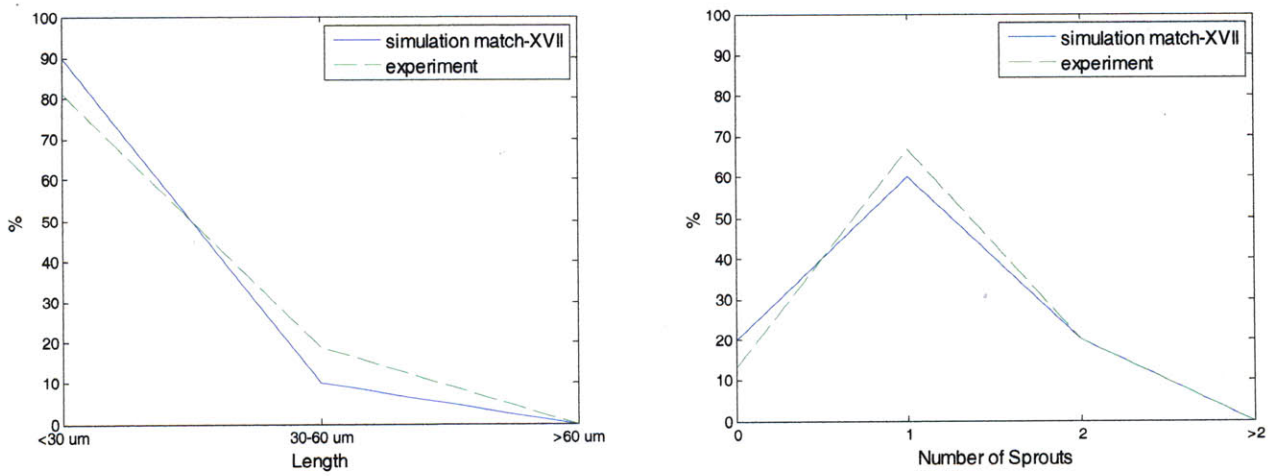

Figure 26: Best R^2 match for simulation and experiment: (a) 40 ng/ml VEGF , (b) 40 ng/ml VEGF + 100 ng/ml Ang 1; (c) 40 ng/ml VEGF + 500 ng/ml Ang 1; (d) 10 ng/ml VEGF + 100 ng/ml Ang 1; (e) 10 ng/ml VEGF + 500 ng/ml Ang 1; (f) complete media with no VEGF or Ang 1. The experimental transition probabilities are recorded as roman numerals corresponding to Q:M:P. The ones matching the morphological observations are recorded in each figure: XIII- 75:20:5; VI- 80:10:10; XII- 85:5:15; XVI- 85:5:10; XV- 90:5:5; XVII- 95:5:0.

a

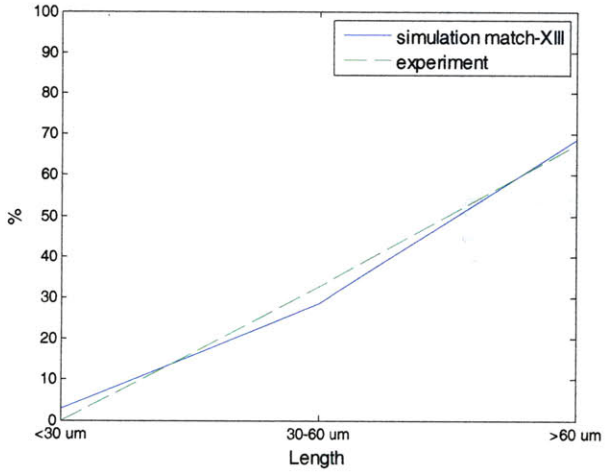

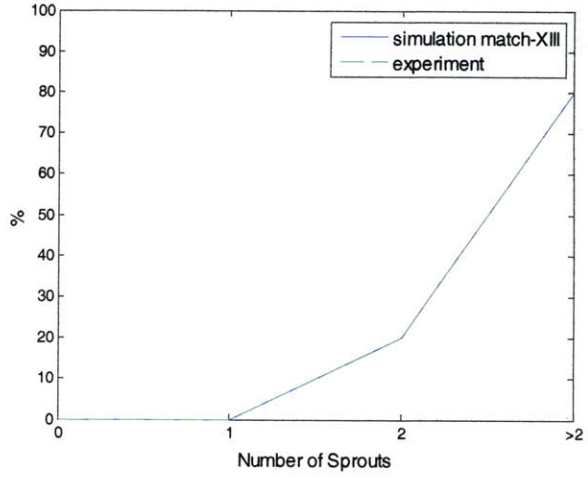

b

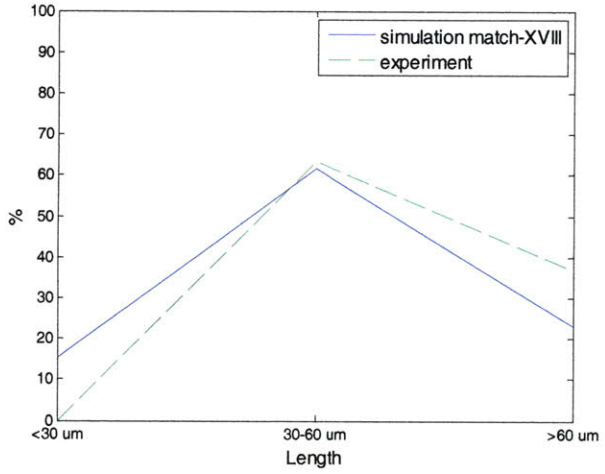

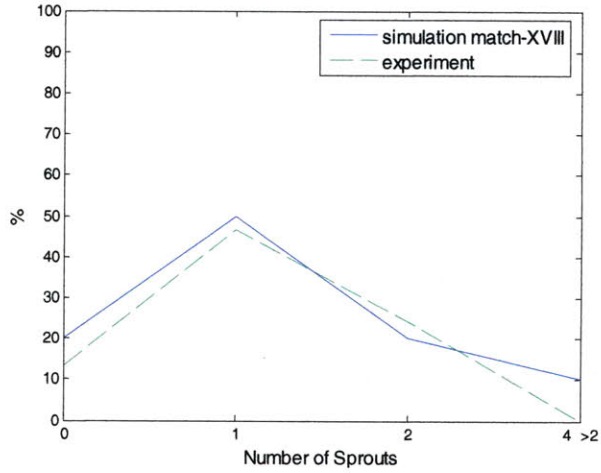

Figure 27: Best R^2 match for simulation and experiment : (a) 40 ng/ml VEGF + 10 ng/ml PF4 , (b) 40 ng/ml VEGF + 1000 ng/ml PF4. The experimental transition probabilities are recorded as roman numerals corresponding to Q:M:P. The ones matching the morphological observations are recorded in each figure: XIII- 75:20:5; XVIII- 85:10:5.

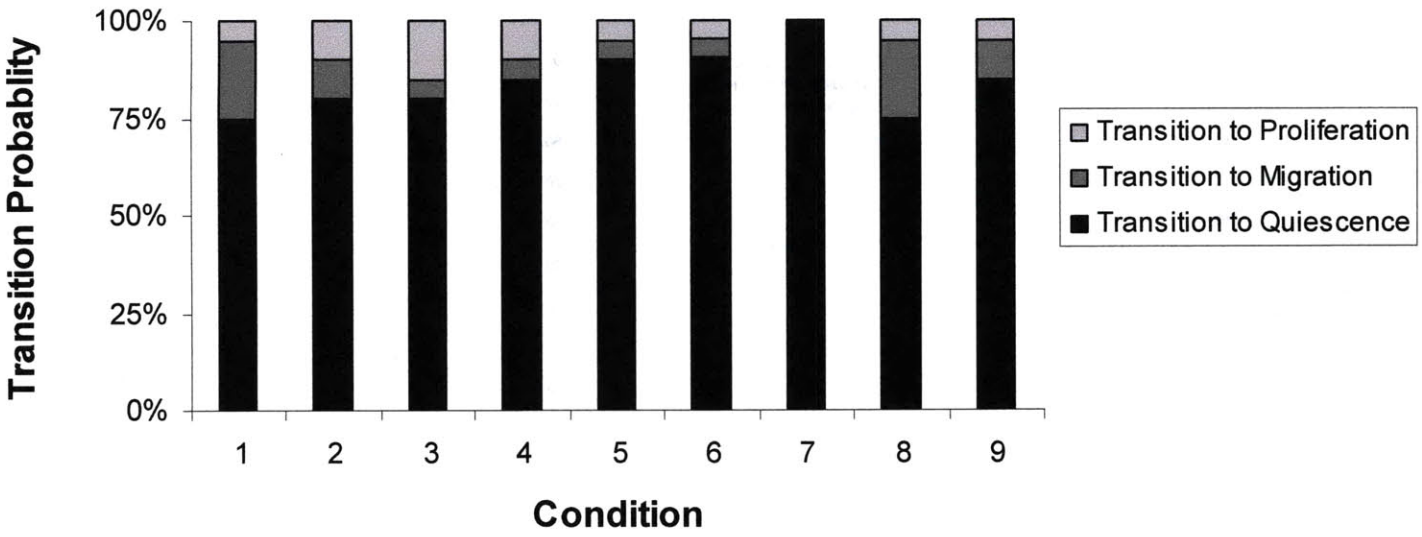

Figure 28: The distribution of transition probabilities- Q:M:P as a function of the different experimental conditions at 2.5 mg/ ml collagen gel density. The experimental conditions are- (1) 40 ng/ml VEGF , (2) 40 ng/ml VEGF + 100 ng/ml Ang 1; (3) 40 ng/ml VEGF + 500 ng/ml Ang 1; (4) 10 ng/ml VEGF + 100 ng/ml Ang 1; (5) 10 ng/ml VEGF + 500 ng/ml Ang 1; (6) complete media with no VEGF or Ang 1; (7) basic media with 500 ng/ml Ang 1; (8) 40 ng/ml VEGF + 10 ng/ ml PF4; (9) 40 ng/ml VEGF + 1000 ng/ml PF4. The experimental – simulation match has $R^2 \sim 0.82$- 0.99.

5. Conclusion

i. Summary

The accomplishments of this project can be outlined as follows:

1. We have developed a 3D hybrid stochastic model of capillary formation which can be used to replicate *in vitro* experimental data. It is a coarse-grained multi-scale hybrid model in which each cell is modeled as an individual decision-making entity and cell-cell interactions are incorporated via the combined effect of cells on the matrix and the effect of the surrounding matrix in the individual cell decision-making process. Thus, this model is unique because it demonstrates the phenomenon that when individual cells are modeled independently according to a set of rules and when cell-cell communication is embedded, the cell ensemble results in capillaries with features that can be attained experimentally in bioreactors for controlled tissue engineering purposes. It also provides a platform for bracketing these cell ensemble results into clusters with different sprout characteristics and identifying the factors that affect them. Most importantly, this study presents a model framework designed alongside experimental constraints and one that can simulate capillaries like the ones generated in an *in vitro* microfluidic system.

2. We have identified conditions which give rise to well-developed sprouts in a microfluidic device. The effect of VEGF and Ang 1 on sprout morphology has been documented in current literature with experiments conducted on a macro scale. However, their relative impact on endothelial cells cultured in a microfluidic device on a collagen I gel has not been documented before. Additionally, the optimal concentrations of VEGF and Ang 1 that would result in well developed capillaries under controlled *in vitro* conditions were

not well established. The experiments we conducted resulted in obtaining these criteria. With 40 ng/ml VEGF and 500 ng/ml Ang 1, we observed well developed capillaries in the collagen 1 gel regions (2.5 mg/ml) after 48 hours. This information provided us with starting condition around which perturbations in concentrations would result in capillaries with different characteristics.

3. We have identified the effect of varying concentrations of VEGF and Ang 1 on sprout morphology (sprout number, length, branch number, anastomoses, sprout angle) by using adapted decision tree analysis. The concentrations we used were VEGF: 0 ng/ml, 10 ng/ml and 40 ng/ml and Ang 1: 0 ng/ml, 100 ng/ml and 500 ng/ml. Through these experiments we identified the relative effects of different concentrations of VEGF and Ang 1 in a 2.5 mg/ml collagen gel on sprout characteristics after 48 hours. By using adapted DTA, we were able to match experimental imprints to simulation ones, and relate transition probabilities to sprout behavior like sprout number and sprout lengths. This information provided us with a mechanistic insight into the effect of VEGF and Ang 1 on the sub processes of angiogenesis- migration and proliferation as their relative effect on these transition probabilities were identified.

4. Based in previous literature, we formulated a hypothesis that we could use the model to determine the relative effect of PF4 on the sub-processes of angiogenesis: migration and proliferation. Literature has shown that it impacts both migration and proliferation, but its relative impact on these sub-processes at different concentrations was not well known. This study suggests that at high concentration, PF4 impacted migration more than

proliferation. As highly purified PF4 lacks chemotactic activity for neutrophils, monocytes, T cells, or any cell population tested so far, its presence during inflammation might cause a decrease in endothelial cell migration and thus affect capillary formation. This information can be used to identify the exact nodes affected in the signaling pathways of endothelial cells. Future experiments can focus on studying the extent of phosphorylation of nodes in the migratory pathways.

5. This model can be used to cluster sprout morphology as a function of various influencing factors and provide insight into the broad mechanisms (migration or proliferation) by which additional growth factors that can be added to the system will affect sprout morphology.

ii. Future Outlook

Various next steps can be pursued to extend the impact of this work:

1. The model can be extended to incorporate intracellular signals, have multiple cell types or have cells that can change size: Different intracellular signals are initiated by different cues. Addition of the cue-signal and signal-response stages to the model will enhance its use. The process of angiogenesis is very dynamic and complicated. Other cell types like smooth muscle cells and pericytes affect sprout formation by releasing various chemokines. Adding different cell types to the simulations will definitely provide a better understanding of the process.

2. Microfluidic experiments can be conducted with various other combinations of growth factors and DTA can be used to assess their effect on cell morphology: Many growth factors like PLGF, PDGF, TNFα, TGFβ, α-FGF, β-FGF, ENA/VASP can be used in the microfluidic experiments. Hypothesis can be made to test the effect of these molecules on sprout morphology via experiments and simulations.

3. The model can be incorporated into a closed loop control system, and thus can be used to control and obtain specific types of morphologies by altering the input conditions i.e. the biochemical and biomechanical influencing factors.

4. The basic layout of the computational model can be adapted for biological processes other than angiogenesis that involve cell population behavior.

APPENDIX I: REFERENCES

1) Adam B.L., Qu Y, Davis J. W., Ward M.D , Clements M.A , Cazares L.H., Semmes O.J., Schellhammer P.F., Yasui Y, Feng Z, Wright G.L. Jr. Serum protein fingerprinting coupled with a pattern-matching algorithm distinguishes prostate cancer from benign prostate hyperplasia and healthy men. Cancer Res. 2002 Jul 1;62(13):3609-14.

2) Adams, R. H, Alitalo, K. 2007. Molecular regulation of angiogenesis and lymphangiogenesis. Nature Reviews Molecular Cell Biology 8: 464-478

3) Adrienne L. G. and Matthew A. N. 2004. pH Regulates Vascular Endothelial Growth Factor Binding to Fibronectin. J. Biol. Chem. 279 (3): 2307-2315

4) Aldridge BB, Saez-Rodriguez J, Muhlich JL, Sorger PK, Lauffenburger DA. 2009. Fuzzy logic analysis of kinase pathway crosstalk in TNF/EGF/insulin-induced signaling. PLoS Comput Biol.5(4).

5) Anderson AR, Chaplain M. A. 1998. Continuous and discrete mathematical models of tumor induced angiogenesis. Bull Math Biol. 60: 857-99

6) Balding D, McElwain M. D. 1985. A mathematical model of tumor induced capillary growth. J Theor Biol. 114: 53-73

7) Bartoli, M., Platt D., Lemtalsi T., Gu Xiaolin., Brooks, S.E., Marrero M.B., Caldwell, R.B., 2003. VEGF differentially activates STAT3 in microvascular endothelial cells. The FASEB Journal. 17:1562-1564

8) Bogdanovic E, N. V., Dumont DJ. 2006. Activation of Tie2 by angiopoietin-1 and angiopoietin-2 results in their release and receptor internalization. J Cell Sci. 119, 3551-60

9) Brekken RA, Thorpe PE. 2001. Vascular endothelial growth factor and vascular targeting of solid tumors. Anticancer Res. 21(6B):4221-9

10) Cebe Suarez S, Pieren M, Cariolato L, Arn S, Hoffmann U, Bogucki A, Manlius C, Wood J, Ballmer-Hofer K. 2006. A VEGF-A splice variant defective for heparan sulfate and neuropilin-1 binding shows attenuated signaling through VEGFR-2. Cell Mol Life Sci. 63(17):2067-77

11) Celik, I, Sürücü1 O, Dietz C, Heymach JV, Force J, Höschele I, Becker CM, Folkman J, Kisker O. 2005. Therapeutic Efficacy of Endostatin Exhibits a Biphasic Dose-Response Curve. Cancer Res. 65; 11044

12) Chaplain M, Anderson A. 2004. Mathematical modelling of tumour-induced angiogenesis: network growth and structure. Cancer Treat Res.117: 51-75

13) Chaplain M. A., McDougall S. R., Anderson A. R. 2006. Mathematical modeling of tumor indused angiogenesis. Annual Rev Biomed Eng. 8: 233-57

14) Chaturvedi RH. C., Kazmierczak B., Schneider T., Izaguirre J. A., Glimm T., Hentschel H.G., Glazier J.A., Newman S.A., Alber M.S. 2005. On multiscale approaches to three-dimensional modeling of morphogenesis. J R Soc Interface. 2: 237- 53

15) Chung, L. Flanagan, S. Rhee, P. Schwarz, A. Lee, E. Monuki and N. Jeon. 2005. Human neural stem cell growth and differentiation in a gradient-generating microfluidic device. Lab Chip. 5(4), 401-06

16) Chung S, Sudo R, Mack PJ, Wan CR, Vickerman V, Kamm RD. 2009. Cell migration into scaffolds under co-culture conditions in a microfluidic platform. Lab Chip. 9(2):269-275

17) Cickovski T.M., Huang C., Chaturvedi R., Glimm T., Hentschel H.G., Alber M.S., Glazier J.A., Newman S.A., Izaguirre J. A. 2005. A framework of three-dimensional model of morphogenesis. IEEE/ ACM Trans Comput Biol Bioinform. 2(4)273-88

18) Dallon J.C., Othmer .H. G. 1997. A discrete cell model with adaptive signaling for aggregation of dictyostelium discoideum. Philos Trans R Soc Lond B Biol Sci. 352(1351):391- 417

19) Das A., Asada H., Lauffenburger D., Kamm RD. 2010. A hybrid continuum-discrete modeling approach to predict and control angiogenesis: analysis of combinatorial growth factor and matrix effects on vessel sprouting morphology. Phil. Trans. R. Soc. A 368, 2937-2960

20) Davis S, Aldrich TH, Jones PF, Acheson A, Compton DL, Jain V, Ryan TE, Bruno J, Radziejewski C, Maisonpierre PC, Yancopoulos GD. 1996. Isolation of angiopoietin-1, a ligand for the TIE2 receptor, by secretion-trap expression cloning. Cell. 87(7):1161-9

21) Eriksson K, Magnusson P, Dixelius J, Claesson-Welsh L, Cross MJ. 2003. Angiostatin and endostatin inhibit endothelial cell migration in response to FGF and VEGF without interfering with specific intracellular signal transduction pathways. *FEBS Lett. 536*: *19*–24.

22) Flegg J.A. , McElwain D.L.S., Byrne, H. M. Turner I.W. 2009. A Three Species Model to Simulate Application of Hyperbaric Oxygen Therapy to Chronic Wounds. PLoS Comput Biol. 5(7):e1000451

23) Folkman J, Shing Y. 1992. Angiogenesis. J Biol Chem. 267(16):10931-4

24) Frisk, S. Rydholm, T. Liebmann, H. Svahn, G. Stemme and H. Brismar. 2007. A microfluidic device for parallel 3-D cell cultures in asymmetric environments. Electrophoresis. 28, 4705:4712

25) Gengrinovitch S, Greenberg SM, Cohen T, et al. 1995. Platelet factor-4 inhibits the mitogenic activity of VEGF121 and VEGF165 using several concurrent mechanisms. J Biol Chem. 270: 15059–15065

26) Gomez-Sjoberg, A. Leyrat, D. Pirone, C. Chen and S. Quake. 2007. Versatile, Fully Automated, Microfluidic Cell Culture System. Anal Chem. 79, 8557:8563

27) Gu, X. Zhu, N. Futai, B. Cho and S. Takayama. 2004. Computerized microfluidic cell culture using elastomeric channels and Braille displays. *Proc Natl Acad Sci USA.* 101(45):15861-15866

28) Hayes AJ, Huang WQ, Mallah J, Yang D, Lippman ME, Li LY. 1999. Angiopoietin-1 and its receptor Tie-2 participate in the regulation of capillary-like tubule formation and survival of endothelial cells. Microvasc Res.; 58(3):224-37

29) Helm C. L., Fleury M. E., Zisch A. H., Boschetti F., Swartz M. A. 2005. Synergy between interstitial flow and VEGF directs capillary morphogenesis in vitro through a gradient amplification mechanism. Proc Natl Acad Sci U S A. 102(44):15779-84

30) Hernández Vera R, Genové E, Alvarez L, Borrós S, Kamm R, Lauffenburger D, Semino CE. 2009. Interstitial fluid flow intensity modulates endothelial sprouting in restricted Src-activated cell clusters during capillary morphogenesis. Tissue Eng Part A. (1):175-85

31) Hua F, Hautaniemi S, Yokoo R, Lauffenburger DA. 2006. Integrated mechanistic and data-driven modelling for multivariate analysis of signaling pathways. J R Soc Interface. 22; 3(9):515-26

32) Huang S, Ingber D. Shape-dependent control of cell growth, differentiation, and apoptosis: switching between attractors in cell regulatory networks. Exp Cell Res. 261, 91-103 (2000)

33) Hundelshausen, Philipp von, Petersen, Frank, Brandt, Ernst. 2007. Platelet-derived chemokines in vascular biology Thromb Haemost. 97: 704–713

34) Jackson T, Zheng X. 2010. A Cell-based Model of Endothelial Cell Migration, Proliferation and Maturation During Corneal Angiogenesis. Bull Math Biol. Epub.

35) Jeon, H. Baskaran, S. Dertinger, G. Whitesides, L. Van De Water and M. Toner. 2002. 9(5):627-35. *Nat Biotechnol.* 9(5):627-635

36) Ji J. W., Tsoukias N. M., Goldman D., Popel A. S. 2005. A computational model of oxygen transport in skeletal muscle for sprouting and splitting modes of angiogenesis. J Theor Biol. 241(1):94-108

37) Jones MK, Tomikawa M, Mohajer B, Tarnawski AS. 1999. Gastrointestinal mucosal regeneration: role of growth factors. Front Biosci. 15; 4:D303-9

38) Jośko J, Gwóźdź B, Jedrzejowska-Szypułka H, Hendryk S. 2000. Vascular endothelial growth factor (VEGF) and its effect on angiogenesis. Med Sci Monit. 6(5):1047-52

39) Kanzawa S., Endo H., Shioya N. 1993. Improved in vitro angiogenesis model by collagen density reduction and the use of type III collagen. Ann. Plast. Surg. 30, 244–251.

40) Karagiannis ED, Popel AS. 2004. A theoretical model of type I collagen proteolysis by matrix metalloproteinase (MMP) 2 and membrane type 1 MMP in the presence of tissue inhibitor of metalloproteinase 2. J Biol Chem. 279(37):39105-14

41) Koblizek TI, Weiss C, Yancopoulos GD, Deutsch U, Risau W. 1998. Angiopoietin-1 induces sprouting angiogenesis in vitro. Curr Biol. 23;8(9):529-32

42) Kothapalli CR , de Valence S, Van Veen JE, Chung S, Gertler FB, Kamm RD. A high-throughput microfluidic assay to study axonal response to growth factor gradients. Lab on a Chip. In review.

43) Kumar N, Wolf-Yadlin A, White FM, Lauffenburger DA. 2007. Modeling HER2 effects on cell behavior from mass spectrometry phosphotyrosine data. PLoS Comput Biol. 3 (1):e4.

44) Kwak HJ, So JN, Lee SJ, Kim I, Koh GY. 1999. Angiopoietin-1 is an apoptosis survival factor for endothelial cells. FEBS Lett. 448(2-3):249-53

45) Lawley T.J. & Kubota Y. 1989. Induction of morphologic differentiation of endothelial cells in culture. J. Invest. Dermatol. 93, 59S–61S.

46) Levine H. A., Sleeman B. D., Nilsen-Hamilton M. 2000. A mathematical model for the roles of pericytes and macrophages in the initiation of angiogenesis. I. The role of protease inhibitors in preventing angiogenesis. Math Biosci. 168(1):77-115

47) Levine HA, Tucker AL, Nilsen-Hamilton M. 2002. A mathematical model for the role of cell signal transduction in the initiation and inhibition of angiogenesis. Growth Factors. 20(4):155-75

48) Mac Gabhann F, Popel AS. 2007. Interactions of VEGF isoforms with VEGFR-1, VEGFR-2, and neuropilin in vivo: a computational model of human skeletal muscle. Am J Physiol Heart Circ Physiol.

49) Maione TE, Gray GS, Petro J. 1990. Inhibition of angiogenesis by recombinant human platelet factor-4 and related peptides. Science. 247: 77–79

50) Mantzaris N. V., Webb S., Othmer H. G. 2004. Mathematical modeling of tumor-induced angiogenesis. J Math Biol. 49(2):111-87

51) McDougall S. R., Anderson A.R., Chaplain M. A., Sherratt J. A. 2002. Mathematical modelling of flow through vascular networks: implications for tumour-induced angiogenesis and chemotherapy strategies. Bull Math Biol. 64(4):673-702

52) Murray J., Oster G., Harris A. 1983. A mechanical model for mesenchymal morphogenesis. Journal of Mathematical Biology 17: 125–129

53) Murray J., Maini P., Tranquillo R. 1983. Mechanochemical models for generating biological pattern and form in development. Physics Reports 171: 59–84

54) Nakatsu M., Richard C.A. Sainson, Jason N. Aoto, Kevin L. Taylor, Mark Aitkenhead, Sofi´a Pe´rez-del-Pulgar, Philip M. Carpenter and Christopher C.W. Hughesa. 2003. Angiogenic sprouting and capillary lumen formation modeled by human umbilical vein endothelial cells (HUVEC) in fibrin gels: the role of fibroblasts and Angiopoietin-1. Microvascular Research 66: 102–112

55) O'Reilly MS, Boehm T, Shing Y, et al. 1997. Endostatin: an endogenous inhibitor of angiogenesis and tumor growth. *Cell. 88: 277–*85

56) Peirce S. M., Van Gieson E. J., Skalak T.C. 2004. Multicellular simulation predicts microvascular patterning and in silico tissue assembly. FASEB J. 18(6):731-3.

57) Plank M. J., Sleeman B. D. 2004. Lattice and non-lattice models of tumour angiogenesis. Bull Math Biol. 66(6):1785-819

58) Plank M. J., Sleeman B. D. 2004. A reinforced random walk model of tumour angiogenesis and anti-angiogenic strategies. Math Med Biol. 20(2):135-81

59) Qutub A., Gabhann F., Karagiannis E., Vempati P., Popel A. 2009. Multiscale models of angiogenesis. IEEE Eng Med Biol Mag. 28(2):14-31

60) Qutub AA, Popel AS. 2009. Elongation, proliferation & migration differentiate endothelial cell phenotypes and determine capillary sprouting. BMC Syst Biol. 3:13

61) Saadi, S. Rhee, F. Lin, B. Vahidi, B. Chung and N. Jeon. 2007. Generation of stable concentration gradients in 2D and 3D environments using a microfluidic ladder chamber. *Biomed Microdevices*. 9(5):627-635

62) Slungaard A. 2005. Platelet factor 4: A Chemokine Enigma. Int J Biochem Cell Biol. 37(6):1162-7

63) Stokes C.L., Lauffenburger D.A. 1991. Analysis of the roles of microvessel endothelial cell random motility and chemotaxis in angiogenesis. J Theor Biol. 152(3):377-403

64) Sudo R, Chung S, Zervantonakis IK, Vickerman V, Toshimitsu Y, Griffith LG, Kamm RD. 2009. Transport-mediated angiogenesis in 3D epithelial coculture. FASEB J. 23(7): 2155-64

65) Takahashi K, Saishin Y, Saishin Y, et al. 2003. Intraocular expression of endostatin reduces VEGF-induced retinal vascular permeability, neovascularization, and retinal detachment. *FASEB J. 17*: *896*–8.

66) Tourovskaia, X. Figueroa-Masot and A. Folch. 2005. Differentiation-on-a-chip: a microfluidic platform for long-term cell culture studies. *Lab Chip*. 5(1):14-19

67) Teichert-Kuliszewska K, Maisonpierre PC, Jones N, Campbell AI, Master Z, Bendeck MP, Alitalo K, Dumont DJ, Yancopoulos GD, Stewart DJ. 2001. Biological action of angiopoietin-2 in a fibrin matrix model of angiogenesis is associated with activation of Tie2. Cardiovasc Res. 16;49(3):659-70

68) Tranquillo R., Murray J. 1992. Continuum model of fibroblast-driven wound contraction: inflammation-mediation. J Theor Biol 158: 135–172

69) Tsoukias NM, Goldman D, Vadapalli A, Pittman RN, Popel AS. 2007. A scomputational model of oxygen delivery by hemoglobin-based oxygen carriers in three-dimensional microvascular networks. J Theor Biol. 248(4):657-74

70) Turner S, Sherratt JA. (2002). Intercellular adhesion and cancer invasion: a discrete simulation using the extended Potts model. J Theor Biol. 216(1):85-100

71) Vickerman V., Blundo J., Chung S., Kamm R. 2008. Design, fabrication and implementation of a novel multi-parameter control microfluidic platform for three-dimensional cell culture and real-time imaging. Lab Chip. 8(9):1468-77

72) Wittmann DM, Krumsiek J, Saez-Rodriguez J, Lauffenburger DA, Klamt S, Theis FJ. 2009. Transforming Boolean models to continuous models: methodology and application to T-cell receptor signaling. BMC Syst Biol. 3:98.

73) Wickström SA, Alitalo K, Keski-Oja J. 2004. An Endostatin-derived Peptide Interacts with Integrins and Regulates Actin Cytoskeleton and Migration of Endothelial Cells. J Biol Chem. 279(19):20178-85

74) Witzenbichler B, Maisonpierre PC, Jones P, Yancopoulos GD, Isner JM. 1998. Chemotactic properties of angiopoietin-1 and -2, ligands for the endothelial-specific receptor tyrosine kinase Tie2. J Biol Chem. 17;273(29):18514-21

75) Wood L., Das A., Kamm R., Asada H. 2009. A Stochastic Broadcast Feedback Approach to Regulating Cell Population Morphology for Microfluidic Angiogenesis Platforms. IEEE Trans Biomed Eng. 6(9): 2299-303

76) Yamamura N, Sudo R, Ikeda M, Tanishita K. 2007. Effects of the mechanical properties of collagen gel on the in vitro formation of microvessel networks by endothelial cells. Tissue Eng. 13(7):1443-53

77) Yoon J, Deisboeck TS. 2009. Investigating differential dynamics of the MAPK signaling cascade using a multi-parametric global sensitivity analysis. PLoS One. 4(2).

78) Zhu WH, MacIntyre A, Nicosia RF. 2002. Regulation of angiogenesis by vascular endothelial growth factor and angiopoietin-1 in the rat aorta model: distinct temporal patterns of intracellular signaling correlate with induction of angiogenic sprouting. Am J Pathol. 161(3):823-30

APPENDIX II: PHASE CONTRAST IMAGES

Representative phase contrast images for all conditions used in the characterizing study detailed in chapter 3 are shown here. All images were taken 48 hours after seeding endothelial cells in 2.5 mg/ml collagen I gel. The images were not focused on one plane in order to get a better 2D perspective of all sprouts.

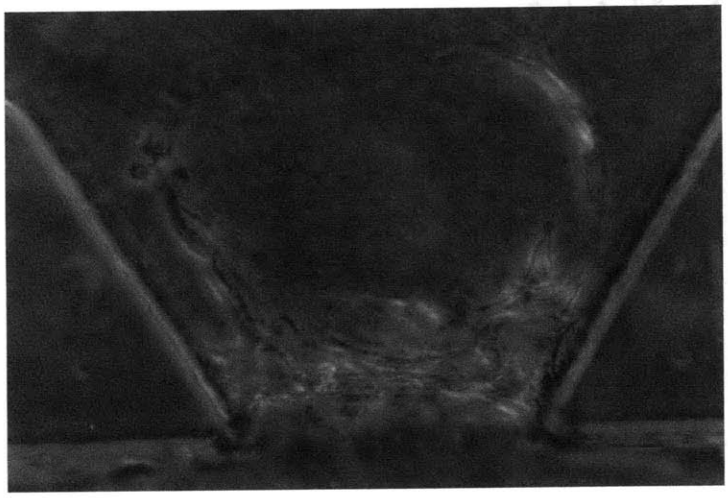

a

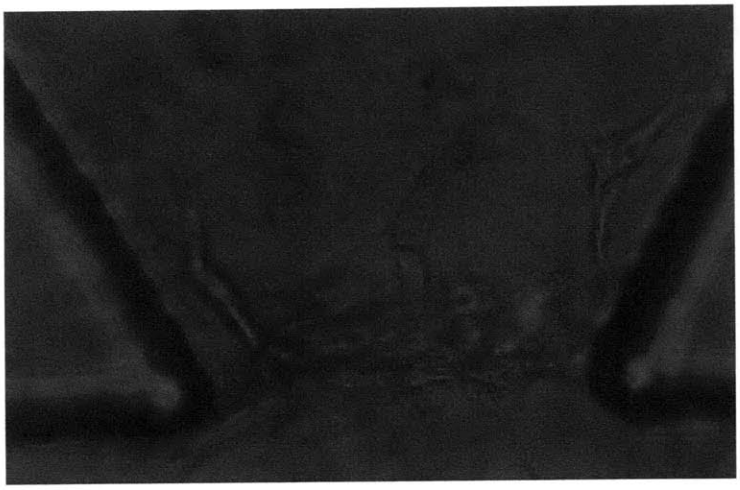

b

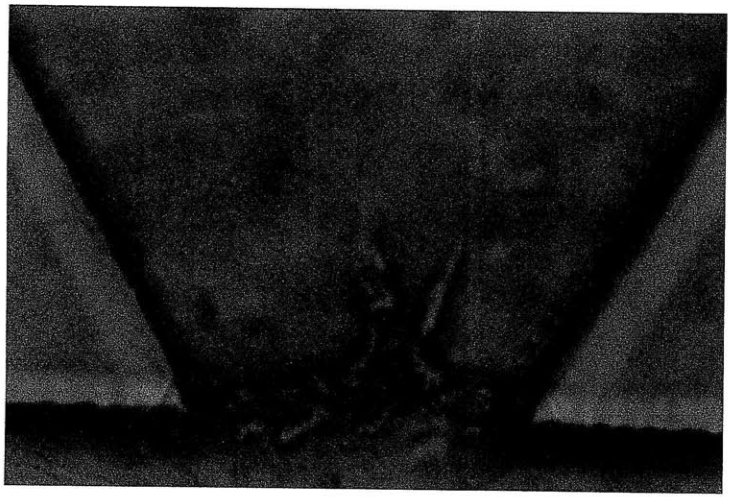

c

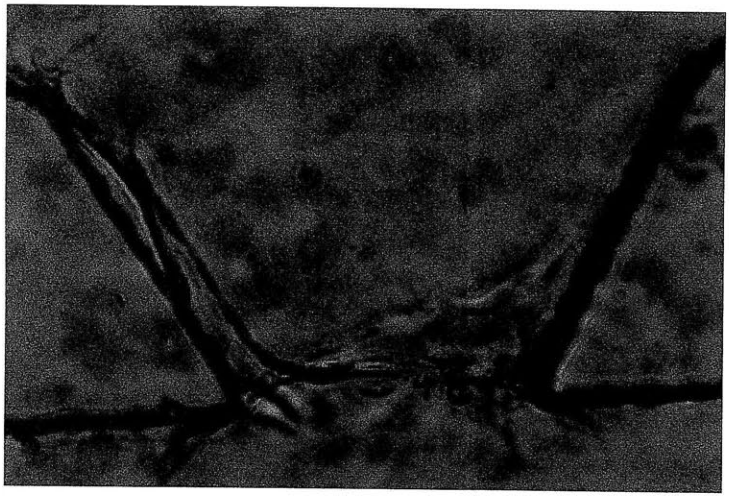

d

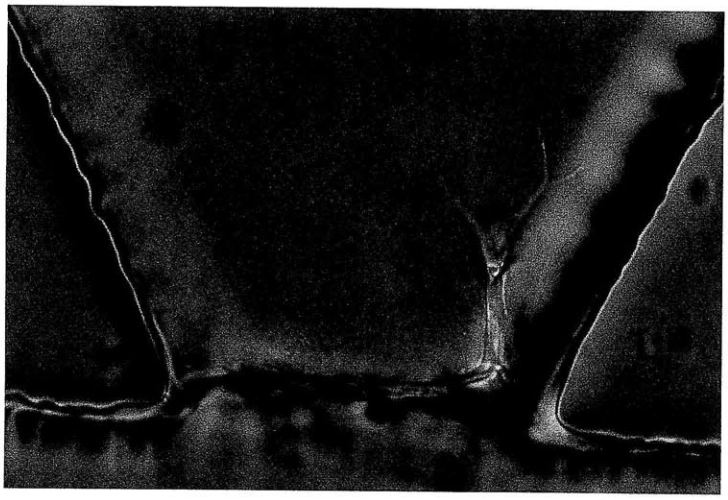

e

f

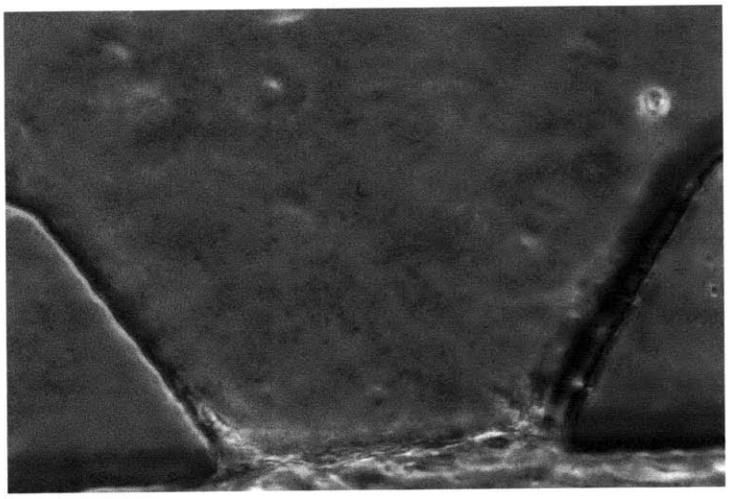

g

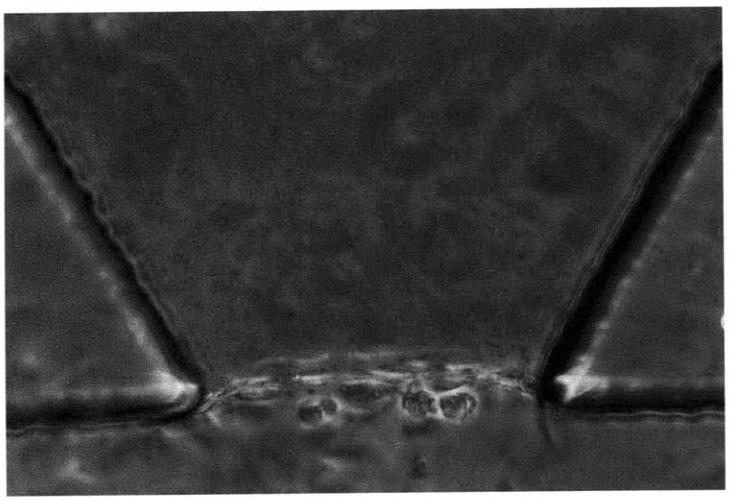

Figure 29: Representative phase contrast images taken 48 hours after seeding cells on a 2.5 mg/ml collagen I gel. For experimental conditions - (a) 40 ng/ml VEGF, (b) 40 ng/ml VEGF + 100 ng/ml Ang 1, (c) 40 ng/ml VEGF + 500 ng/ml Ang 1, (d) 10 ng/ml VEGF + 100 ng/ml Ang 1, (e) 10 ng/ml VEGF + 500 ng/ml Ang 1, (f) no VEGF and no Ang 1, (g) 500 ng/ml Ang 1.

APPENDIX III: EFFECT OF ANTI-PROLIFERATING AGENT

Several anti-proliferating agents that affect different aspect of cell cycle are known and have been used over time. We used mitomycin C at three different concentrations and then evaluated its impact on capillary formation. The experiments were conducted as before, the only change being the addition of mitomycin C along with 40 ng/ ml VEGF to the condition media. We chose three different mitomycin C concentrations: 0.2 M, 1 M and 10 M. Capillary number, capillary length and the general health of the cellular monolayer were assessed after 48 hours. The results obtained are shown in figure 30.

At the lowest concentration of mitomycin C (0.2 M), the monolayer seemed relatively healthy and the sprouts were about the same length as those obtained with just the VEGF added to the media. However, the number of sprouts per gel region was significantly lower. Most gel regions had either one or two sprouts. When the mitomycin C concentration was increased to 1 M, both the number and length of the sprouts was decreased significantly. At the highest concentration of 10 M, no sprouts were observed in any gel region and the cells in the monolayer did not appear to be very healthy. The imprints for the distribution of the number and lengths of sprouts for devices with 0.2 M mitomycin C and 1 M mitomycin C are shown in figure 31.

When we tried to match simulation results, we did not get a very good alignment with the predictions in all cases. When mitomycin C was used with 40 ng/ml VEGF, the hypothesis was that the only transition probability that would be affected would be the Q:P ratio and even that may not be affected at low mitomycin concentrations. In the first instance, when we used 0.2 M mitomycin C, it was expected that the best transition probability match would be the same as that

for the condition with 40 ng/ml VEGF i.e. Q:M:P = 75:20:5. While the imprints of the lengths of the sprouts aligned very well (R^2 = 0.94), the imprints of the number of number of sprouts per gel region did not (R^2<0). One of the reasons could be that the while the anti-proliferating agent affects proliferation and puts the cells in a quiescent state, it also indirectly impacts the cell's migration capabilities. The transition probability 80:15:5 was a better match with R^2 = 0.84 for the number of sprouts and R^2 = 0.91 for sprout length. It is also possible that the model in insensitive to small changes in transitions. In the second instance when 1 M mitomycin C was used, the best transition match was achieved with the Q:M:P ratio of 80:20:0 (R^2 for sprout number = 0.97 and R^2 for sprout length = 0.87). In this instance a change in the transition to proliferation is noted as expected. At the highest concentration of 10 M mitomycin C, no cell sprouting was observed and the cells did not appear healthy. Hence, no simulation matching was done.

The primary goal of this experiment was to determine if the impact on one of the transition states of the cell as designed in the model would result in the same trends observed in the simulations. While it can be stated that the effect of an anti-proliferating agent resulted in a decrease in the number of sprouts, as shown in the simulations, the exact trends were not obtained i.e. the hypothesis that only the Q:P ration would be affected was not completely correct. One of the causes of this could be the fact that in the model, the transition probabilities of individual cells are changed when the ratio of transitions is changed and in the experiments a certain population of the cells at the monolayer is impacted by the anti-proliferating agent. It is not possible to determine this percentage. The model is incapable of capturing this behavior because in the current form, all cells are modeled as part of the same population. Different cell

types do not exist. If the model is altered to account for different cell populations, we would be able to model populations that have a differential effect of the anti-proliferating agent depending on the concentration used in the experiments. Hence, while these results show the impact of mitomycin C on sprout formation in the microfluidic device, they don't exactly mimic the simulation trends.

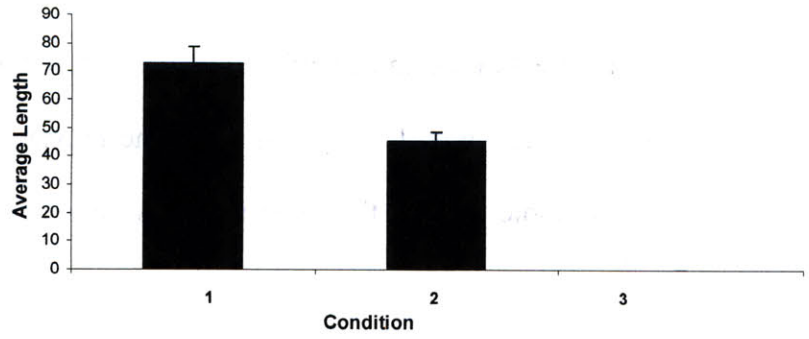

Figure 30: Average sprout lengths observed in microfluidic device under different experimental conditions. The experimental conditions are (1) 0.2 M mitomycin C (2) 1 M mitomycin C; (3) 10 M mitomycin C.

a

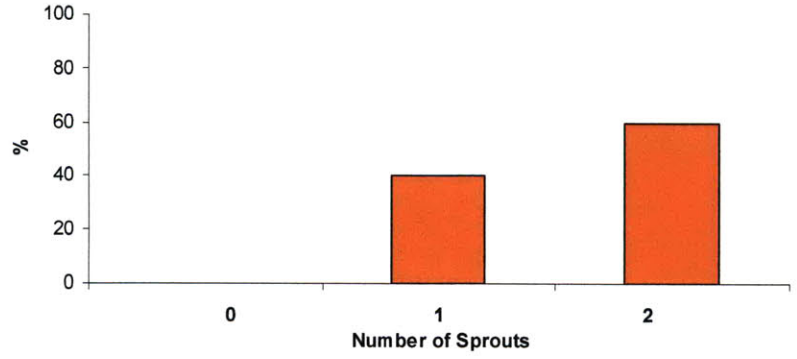

b

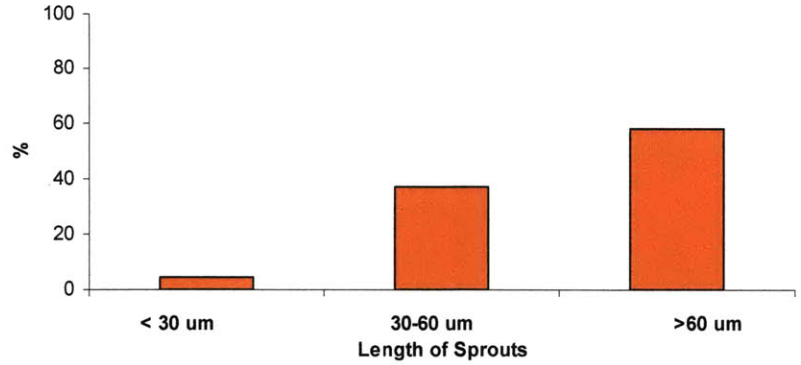

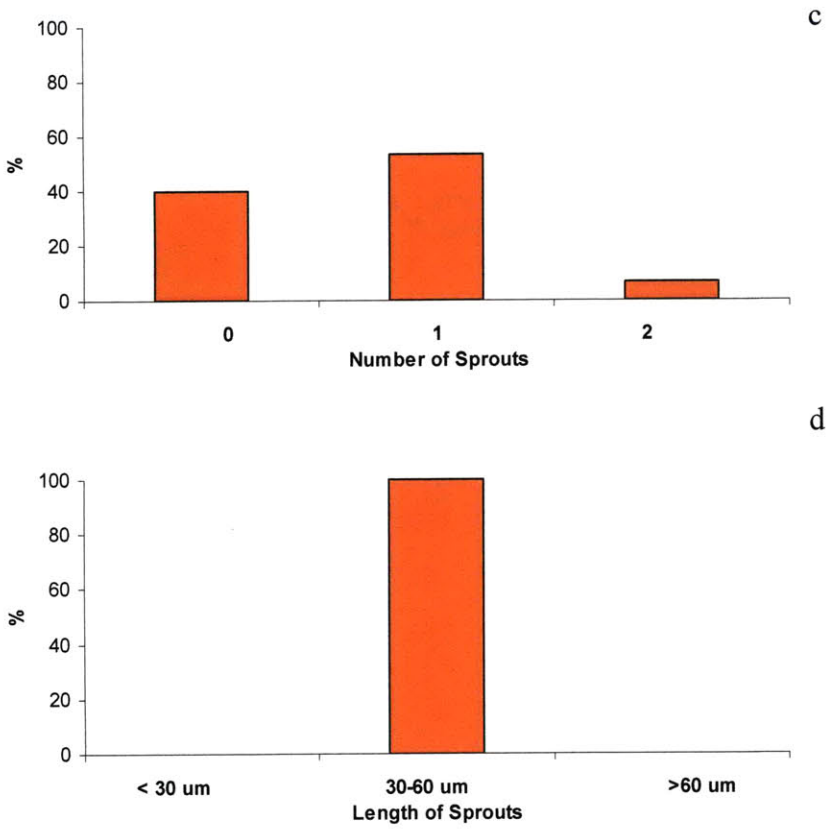

Figure 31: Imprints of the distribution of sprout number per gel region and sprout length as a function of different concetrations of mitomycin C. (a) Imprint of sprout number per gel region with 0.2 M mitomycin C. (b) Imprint of sprout lengths with 0.2 M mitomycin C. (c) Imprint of sprout number per gel region with 1 M mitomycin C. (d) Imprint of sprout length with 1 M mitomycin C.

APPENDIX IV: RUNNING THE SIMULATION FOR LONGER TIME PERIODS

We ran the computational simulation for five days and obtained well developed, branches sprouts as shown in figure 32. These show a range of different geometries the sprouts were allowed to grow under high probabilities to migrate and proliferate.

Long term experiments in the devices were conducted by other members in the lab (by verbal communication). In many cases sprout regression in devices was observed five days after seeding. Such regression is not observed when the experiments were conducted for only two days. Possible explanations could be a change in the nature of the gel or lack of nutrient perfusion over a long period of time. It is also possible that some other factors are needed to maintain sprouts over a period of five days.

A slight difference between the devices and simulations after five days is the fact that the regression of sprouts as observed in the devices, does not occur in the simulations. If the cause is the last of the above mentioned reasons, and additional factors are indeed required, then the simulation needs to be altered to account for this. The simulation needs to be changed to account for the sprout regression in the absence of these additional factors. Thus, any comparison after 48 hours will not be accurate due to this difference. The simulations tend to have developed a lot more branches over five days. In order to obtain better experiment – simulation matching, methods to stabilize the vessels long term in the devices have to be developed. One method could be the addition of sphingosine -1P to the basal media for all conditions (Vickerman, verbal

communication). Another method could be increasing the number of posts in the gel region in the devices.

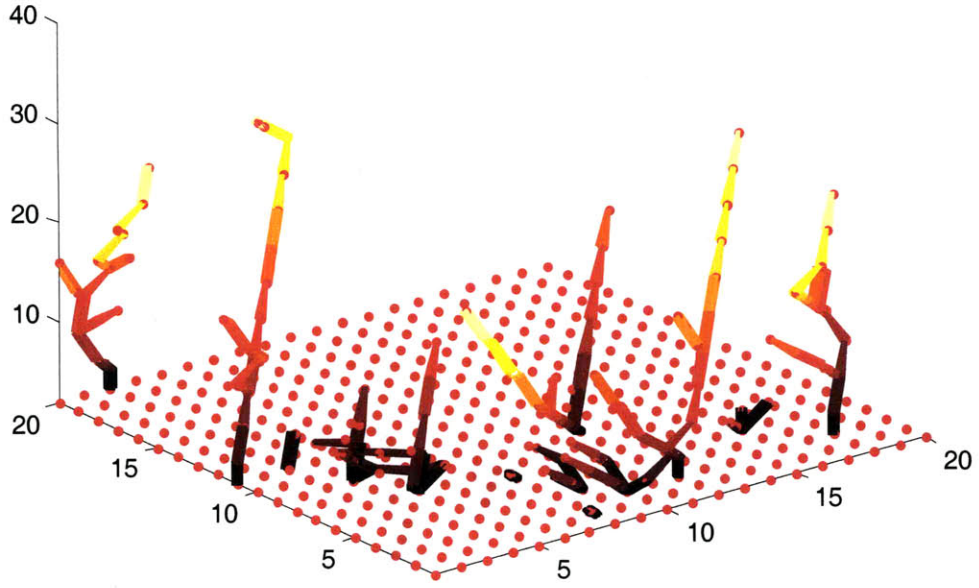
40
30
20
10
20
15
10
5
5
10
15
20

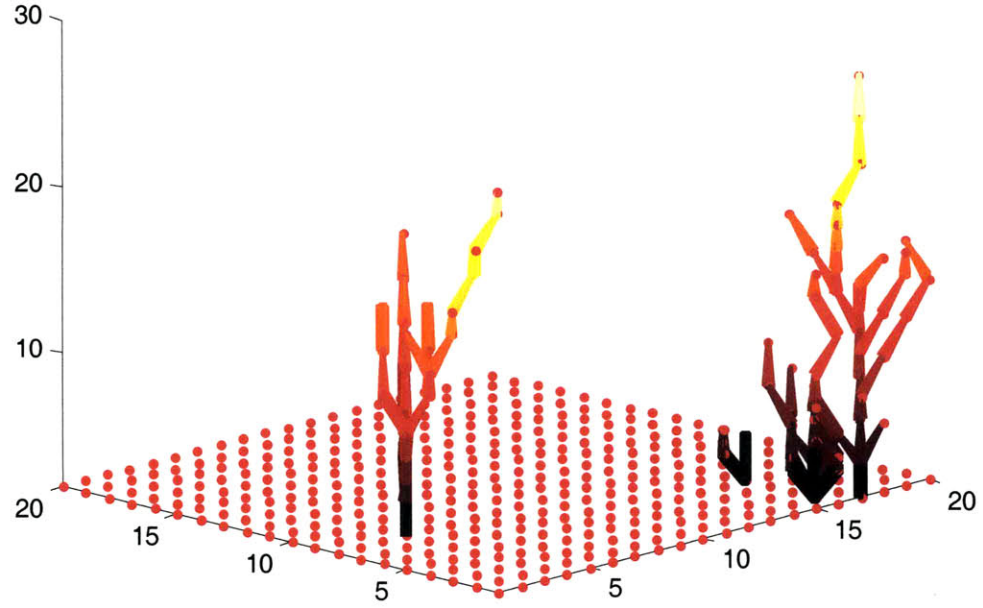
30
20
10
20
15
10
5
5
10
15
20

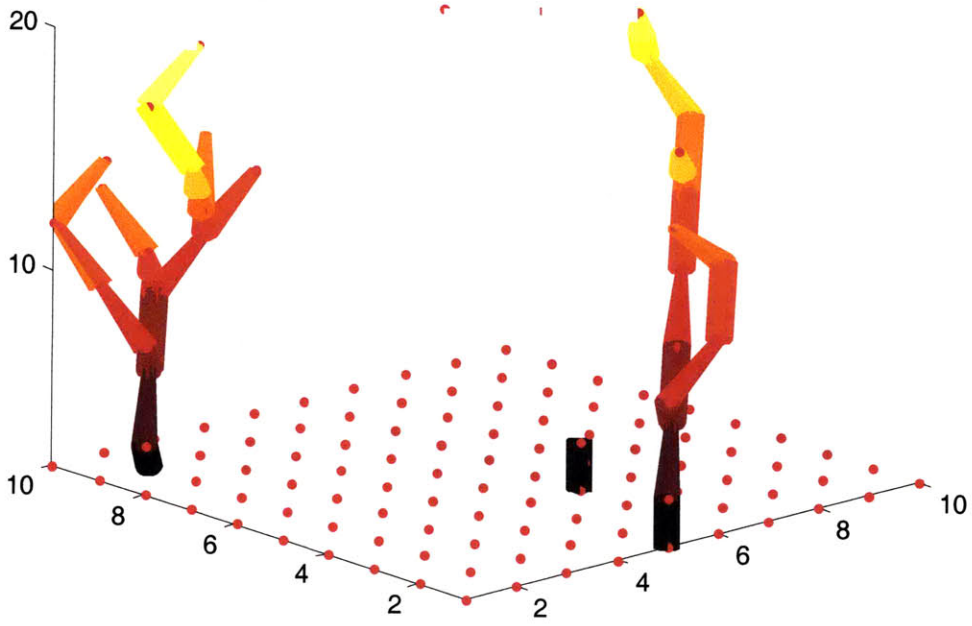

Figure 32: Simulations obtained after five days for different geometries.